UNIVERSIDADE DE BRASÍLIA
INSTITUTO DE CIÊNCIAS HUMANAS
DEPARTAMENTO DE GEOGRAFIA
PROGRAMA DE PÓS-GRADUAÇÃO EM GEOGRAFIA

DINÂMICA DE INCÊNDIOS FLORESTAIS E ALTERAÇÕES BIOFÍSICAS NA AMAZÔNIA E CERRADO BRASILEIROS A PARTIR DE SÉRIES TEMPORAIS DE SENSORIAMENTO REMOTO

Níckolas Castro Santana

Tese de Doutorado

Brasília-DF: abril / 2019

UNIVERSIDADE DE BRASÍLIA
INSTITUTO DE CIÊNCIAS HUMANAS
DEPARTAMENTO DE GEOGRAFIA
PROGRAMA DE PÓS-GRADUAÇÃO EM GEOGRAFIA

DINÂMICA DE INCÊNDIOS FLORESTAIS E ALTERAÇÕES BIOFÍSICAS NA AMAZÔNIA E CERRADO BRASILEIROS A PARTIR DE SÉRIES TEMPORAIS DE SENSORIAMENTO REMOTO

Níckolas Castro Santana

Orientador: Osmar Abílio de Carvalho Júnior

Tese de Doutorado

Brasília-DF: abril / 2019

UNIVERSIDADE DE BRASÍLIA
INSTITUTO DE CIÊNCIAS HUMANAS
DEPARTAMENTO DE GEOGRAFIA
PROGRAMA DE PÓS-GRADUAÇÃO EM GEOGRAFIA

DINÂMICA DE INCÊNDIOS FLORESTAIS E ALTERAÇÕES BIOFÍSICAS NA AMAZÔNIA E CERRADO BRASILEIROS A PARTIR DE SÉRIES TEMPORAIS DE SENSORIAMENTO REMOTO

Níckolas Castro Santana

Tese de Doutorado submetida ao Departamento de Geografia da Universidade de Brasília, como parte dos requisitos para a obtenção do Grau de Doutor em Geografia, área de concentração Gestão Ambiental e Territorial, opção Acadêmica.

Aprovado por:

_____

Prof. Dr. Osmar Abílio de Carvalho Júnior (UnB)
(Orientador)

_____

Prof. Dr. Eraldo Aparecido Trondoli Matricardi (UnB)
(Examinador Externo)

_____

Prof. Dr. Manoel do Couto Fernandes (UFRJ)
(Examinador Externo)

_____

Prof. Dr. Roberto Rosa (UFU)
(Examinador Externo)

_____

Prof. Dr. Roberto Arnaldo Trancoso Gomes (UnB)
(Suplente)

Brasília – DF, abril de 2019.

FICHA CATALOGRÁFICA

REFERÊNCIA BIBLIOGRÁFICA

SANTANA, N. C. **Dinâmica de incêndios florestais e alterações biofísicas na Amazônia e Cerrado brasileiros a partir de séries temporais de sensoriamento remoto**. 2019.94 p. Tese (Doutorado em Geografia) – Universidade de Brasília, Brasília.

DEDICATÓRIA

Dedico este trabalho aos jovens cientistas.
Não desistam dos seus sonhos.

AGRADECIMENTOS

Nessa jornada do doutorado não faltam pessoas para agradecer que contribuíram imensamente para o meu crescimento científico e pessoal:

Agradeço a Deus por me conceder força nos momentos em que pensei em desistir.

Agradeço ao meu professor orientador Osmar Abílio de Carvalho Júnior por todo o apoio nesta empreitada, pela paciência, e tanto pelos conhecimentos científicos partilhados quanto pelos conselhos que levarei para a vida.

Agradeço aos professores da UnB que tive o prazer de conhecer e foram incríveis no compartilhamento dos seus conhecimentos, em especial os professores Roberto, Renato, Helen e Gustavo.

Os amigos conquistados no Laboratório de Sistemas e Informações Espaciais merecem um agradecimento especial e mesmo já estando distante de alguns, não os esquecerei jamais! Especialmente aos amigos, na ordem em que nos conhecemos, Marcus Fábio, Sandro, Verônica, Cristiane, Miriam, Marcos Pereira e Núbia, muito obrigado por tudo!

Agradeço a minha família por todo o apoio e por ouvirem minhas angustias! Passamos por muitas dificuldades, mas nos mantemos unidos contra as adversidades! Mãe e PA vocês são incríveis! A minha querida avó Maria, que mesmo não estando mais ao meu lado, me fortalece todos os dias...

Agradeço aos colegas e professores do CEP-EMB que foram um refúgio nesses anos e me fizeram ter uma nova paixão na vida. Sem vocês talvez essa tese não tivesse sido concluída!

Agradeço a Coordenação de Aperfeiçoamento de Pessoal de Nível Superior pela bolsa de estudos que foi essencial para manter a dedicação neste projeto. A Universidade de Brasília e ao Conselho Nacional de Desenvolvimento Científico e Tecnológico pelo apoio financeiro em campo e para publicações.

Sou grato também as agências brasileiras, americanas e europeias cuja política de distribuição gratuita dos seus milhares de dados da superfície terrestre permite que tantos cientistas possam colaborar para um melhor conhecimento do nosso planeta!

Por fim agradeço a todos que me ajudaram nessa jornada (não foram poucos!), desde as graduações, estágios e no mestrado. Vocês fazem parte da minha história!

RESUMO

Os biomas brasileiros se adaptaram a diferentes padrões de presença ou ausência do fogo. Dados derivados de sensoriamento remoto têm sido uma das principais bases para a detecção de incêndios florestais e os danos na estrutura da vegetação, especialmente com o desenvolvimento de sensores com alta resolução temporal e espectral, e o estabelecimento de longas séries contínuas. Nesse sentido, esta tese buscou aprofundamento em três pontos: (1) Qual a potencialidade de produtos de sensoriamento remoto para a descrição da dinâmica do fogo no Brasil? (2) Como detectar cicatrizes de queimadas a partir de séries temporais em ambientes amazônicos?; e por fim (3) Quais os danos na vegetação resultantes da alteração do regime histórico do fogo e como podem ser quantificados por sensoriamento remoto? Para ampliar o conhecimento sobre essas questões foram utilizados diversos produtos derivados dos sensores *Moderate Resolution Imaging Spectroradiometer* (MODIS), *Thematic Mapper* (TM), *Enhanced Thematic Mapper Plus* (ETM+) e *Operational Land Imager* (OLI), além de diversos dados espaciais, em três escalas: uma para todo o território nacional, uma área específica do Cerrado e duas áreas específicas da Amazônia. A metodologia básica consistiu na análise de séries temporais MODIS para detecção e quantificação dos efeitos do fogo. Os resultados permitiram concluir que: (1) Os produtos globais MODIS de detecção de cicatrizes de queimadas apresentaram altas taxas de erros de omissão no Brasil, superiores a 78% em média no território nacional, sendo seu uso recomendado apenas para análises regionais ou globais. Os produtos de queimadas apresentaram as menores acurácias nos biomas dos Pampas, Amazônia e Mata Atlântica e as maiores acurácias nos biomas do Cerrado e da Caatinga. Apesar desta limitação, o produto MCD64 permitiu descrever o regime do fogo no país, as principais regiões de ocorrência e a influência da umidade e classe de vegetação neste padrão. Foram estabelecidas como limite para a ação do fogo, as zonas sem estiagem, como o Oeste da Amazônia e litoral leste do Brasil, assim como as áreas do semiárido nordestino. (2) Dentre os métodos analisados de diferença sazonal e normalização temporal, a normalização pela média da banda espectral do Infravermelho Próximo foi responsável pela maior acurácia na detecção de cicatrizes de queimadas na Amazônia, retificando a utilização de alguns índices especializados originalmente para vegetações temperadas, como o Normalized Burn Ratio (NBR). Outros métodos analisados, como a diferença sazonal e normalização por z-score, apresentaram melhor acurácia que imagens originais, mas inferior em comparação com a normalização pela

média. (3) A alteração da recorrência do fogo teve influência direta no padrão biofísico e fenológico da vegetação nas áreas de estudo na Amazônia e no Cerrado. As variáveis de produtividade primária bruta e albedo apresentaram baixa representatividade espacial. As mudanças com maior inclinação da tendência, do Enhanced Vegetation Index (EVI) e temperatura superficial, foram tanto relacionadas com a recorrência do fogo, quanto com a classe de uso da vegetação, como nas terras indígenas. A inclinação da tendência, no EVI e temperatura superficial, foi maior na área do Cerrado, reforçando a necessidade urgente de conservação deste bioma. A pesquisa atestou a importância de dados de sensoriamento remoto para avaliação da dinâmica do fogo e dos seus efeitos na vegetação. A utilização de séries temporais do sensor MODIS permitiu tanto identificar as áreas queimadas com maior acurácia que outros produtos disponíveis, quanto quantificar as fragilidades da vegetação relacionadas ao padrão de fogo atual.

Palavras-Chave: Incêndios florestais, Sensoriamento remoto, Séries temporais, MODIS

ABSTRACT

Brazilian biomes have adapted to different patterns of presence or absence of fire. Data derived from remote sensing have been one of the main techniques for the detection of forest fires and damage to vegetation structure, especially with the development of high temporal and spectral resolution sensors and the establishment of long continuous series. Thus, we intend to focus on three points in this thesis: (1) What is the potential of remote sensing products for the description of fire dynamics in Brazil? (2) How to detect burn scars from remote sensing time series in Amazonian environments? And finally (3) What damages in the vegetation resulting from the alteration of the historical fire regime and how can they be quantified by remote sensing? In order to increase the knowledge about these issues, several products derived from the Moderate Resolution Imaging Spectroradiometer (MODIS), Thematic Mapper (TM), Enhanced Thematic Mapper Plus (ETM+) and Operational Land Imager (OLI) sensors were used, in addition to diverse spatial data, in three scales: one for the whole national territory, one specific area of the Cerrado and two specific areas of the Amazon. The basic methodology consisted of the analysis of MODIS time series for the detection and quantification of fire effects. The results allowed to conclude that: (1) MODIS global burned area products presented high omission errors rates in Brazil, higher than 78% on average in the national territory, and their use is recommended only for regional or global analyzes. The burned area products showed the lowest value in the biomes of the Pampas, Amazon Forest and Atlantic Forest, and the highest values in the biomes of the Cerrado and Caatinga. In spite of this limitation, the product MCD64 allowed to describe the fire regime in the country, the main regions of occurrence and the influence of moisture and vegetation class in this pattern. Were established as a limit for the action of the fire the areas without drought, such as the Western Amazon and the east coast of Brazil, as well as areas with low availability of rainfall and fuel, such as the semi-arid in the Northeast. (2) Among the analyzed methods of seasonal difference and temporal normalization, the normalization of the Near Infrared spectral band by the zero-mean, was responsible for the greater accuracy in the detection of burn scars in the Amazon region, rectifying the use of some indices originally specialized for temperate vegetation, such as the Normalized Burn Ratio (NBR). Other methods analyzed, such as the seasonal difference and z-score normalization, showed better accuracy than original images, but lower than normalization by the zero-mean. (3) The alteration of fire recurrence had a direct influence on the

biophysical and phenological pattern of vegetation the study areas of Amazon and Cerrado. The variables of gross primary productivity and albedo showed low spatial representativeness. The changes with higher trend slope, of Enhanced Vegetation Index (EVI) and surface temperature, were related both to fire recurrence and to the vegetation use class, as in indigenous lands. The slope of the trend in EVI and surface temperature was higher in the Cerrado area, reinforcing the urgent need for conservation of this biome. The research attested the importance of remote sensing data for the evaluation of fire dynamics and its effects on vegetation. The use of MODIS time series allowed both identifying the burned areas with greater accuracy than other available products, and quantifying the fragilities of the vegetation related to the current fire pattern.

Keywords: Forest fires; Remote sensing; Time series; MODIS

SUMÁRIO

LISTA DE FIGURAS

LISTA DE TABELAS

LISTA DE ABREVIATURAS E SIGLAS

Δ – Diferença Sazonal

μm – Micrômetro

AAT – Annual Aggregated Time Series

ANP – Araguaia National Park

BAIM – Burnt Area Index

CE – Comission Error

CSP – Cantão State Park

DC – Dice Coefficient

ESA – European Space Agency

ETM+ - Enhanced Thematic Mapper Plus

EVI – Enhanced Vegetation Index

GEMI – Global Environmental Monitoring Index

GPP – Gross Primary Productivity

IBGE – Instituto Brasileiro de Geografia e Estatística

JPRB – Ji-Paraná River Basin

KC – Kappa Coefficient

Km - Quilômetro

LANDSAT – Land Remote Sensing Satellite

m - Metros

MERIS – Medium Resolution Imaging Spectrometer

MFI – Mean Fire Interval

MIRBI – Mid Infrared Burn Index

MMA – Ministério do Meio Ambiente

MODIS – Moderate Resolution Imaging Spectroradiometer

MPA –Monthly Percentage of Affected Area

NASA – National Aeronautics and Space Administration

NBR – Normalized Burn Ratio

NBR2 – Normalized Burn Ratio variation

NDVI – Normalized Difference Vegetation Index

NIR – Near-Infrared

OA – Overall Accuracy

OE – Omission Error

OLI – Operational Land Imager

PROBIO - Projeto de Conservação e Utilização Sustentável da Diversidade Biológica Brasileira

SIVAM – Sistema de Vigilância da Amazônia

SPOT – Satellite Pour l'Observation de la Terre

SWIR – Short-wave infrared

TM – Thematic Mapper

USGS – United States Geological Survey

UTM – Universal Transversa de Mercator

WGS84 – 1984 World Geodetic System

WRS – Worldwide Reference System

CAPÍTULO 1: APRESENTAÇÃO

Introdução

A presença ou ausência do fogo é um dos principais fatores determinantes da estrutura e composição da vegetação terrestre. Muitos biomas se desenvolveram dependentes do fogo, com a redução de espécies arbóreas em detrimento do desenvolvimento de espécies rasteiras (EVA; LAMBIN, 2000; BOND; WOODWARD; MIDGLEY, 2005; MURPHY; BOWMAN, 2012). O regime do fogo global é um dos principais parâmetros definidores da diversidade vegetal, e da estrutura ecológica dos biomas de savanas, atrasando a exclusão competitiva, possibilitando a maior diversidade ecológica da paisagem e permitindo o surgimento de diversas espécies (BOWMAN et al., 2009; MARLON et al., 2013; PAUSAS; RIBEIRO, 2017).

O fogo tem sido um importante distúrbio ecológico em todo o continente da América do Sul, queimando em média 18,7 milhões de hectares anualmente (GIGLIO; RANDERSON; van der WERF, 2013), sendo os biomas brasileiros do Cerrado e da Amazônia, os com maior total de área proporcionalmente queimada (de ARAÚJO; FERREIRA; ARANTES, 2012). Fatores climáticos e humanos são os principais agentes na dinâmica do regime do fogo na região, que tanto podem intensificar quanto atenuar este regime (DI BELLA et al., 2006).

As áreas do Brasil central são compostas majoritariamente por vegetações típicas de savana (Cerrado). Estas áreas são caracterizadas por altas temperaturas e secas sazonais (ALVARADO et al., 2017), tendo no fogo um elemento fundamental para a manutenção da sua fisionomia e estrutura, limitando o crescimento da vegetação (SCHOLES; ARCHER, 1997; BOND; WOODWARD; MIDGLEY, 2005).

As savanas globais, incluindo-se o Cerrado, têm apresentado alterações na estação e intensidade nas quais o fogo ocorre, principalmente por práticas de manutenção agropecuária ou indiretamente por mudanças no clima global (GOVENDER; TROLLOPE; VAN WILGEN, 2006; ARCHIBALD, 2016). Apesar dessas mudanças ocasionarem a diminuição no total de área queimada (ANDELA et al., 2017), houve aumento no número de pequenos incêndios com o crescimento de atividades agrícolas, densidade populacional e fragmentação da vegetação comprovando a fragilidade das savanas frente ao novo padrão de incêndios (ARCHIBALD, 2016).

Em contraste com as áreas de Cerrado, o restante do país é classificado em um grupo de biomas altamente vulneráveis ao fogo (CHUVIECO et al., 2014). Nas áreas de florestas tropicais, Amazônia e Mata Atlântica, devido às condições climáticas que favorecem a alta umidade dos combustíveis, dificultando a propagação dos raros incêndios ocasionados por raios (BOWMAN et al., 2011). No caso da vegetação de semiárido, no Nordeste do país, ou nas pastagens ao Sul, a baixa incidência natural do fogo está relacionada principalmente com a baixa disponibilidade de combustíveis (MARLON et al., 2013).

A introdução atual do fogo na Amazônia ocorre basicamente nas regiões onde há intenso desmatamento e mudanças no uso e cobertura do solo. Em 2005, por exemplo, mais de 90% das queimadas na Amazônia se localizaram em áreas desmatadas, indicando a utilização do fogo para manutenção agropecuária (LIMA et al., 2012). Mesmo aquelas áreas onde a floresta ainda não foi completamente desmatada, mas é afetada por práticas de corte seletivo, já são intensamente vulneráveis ao fogo devido à fragmentação e degradação (COCHRANE; SCHULZE, 1999), com o aumento de madeira morta no sub-bosque e a diminuição do dossel (FANIN; VAN DER WERF, 2015).

A alteração do regime do fogo, quando combinada entre os diferentes ecossistemas, tem profunda influência no ciclo do planeta. Com efeitos globais no ciclo climático, com alterações na absorção de radiação solar pelas emissões de aerossóis. Regionalmente na formação de nuvens e no regime pluviométrico. Além de localmente com impactos ambientais, sociais e econômicos, como consumo de combustível, produção e dispersão de gases nocivos à saúde, mortalidade de plantas, alteração no albedo superficial, erosão, ciclagem de nutrientes e sucessão vegetal (REINHARDT; KEANE; BROWN, 2001; BOWMAN et al., 2009, 2017).

Dadas as diversas alterações que o fogo pode ocasionar nos ciclos biogeoquímicos do planeta, e da fragilidade atual dos biomas frente ao novo regime do fogo e da sua alta degradação, há a necessidade do seu monitoramento para maior compreensão destes fenômenos na superfície terrestre. Uma das possibilidades de análises atuais é com a utilização de dados derivados de sensoriamento remoto, que têm se tornado fontes de informações essenciais para a análise da dinâmica terrestre (LENTILE et al., 2006).

A análise da influência do fogo, na estrutura da vegetação, em áreas extensas da Terra, pode ser realizada tanto por sensores com alta resolução temporal, espacial e espectral. A alta resolução temporal permite acompanhar os estágios de evolução da vegetação, e o seu padrão espaço-temporal de maturidade, senescência, dormência e

crescimento (ZHANG et al., 2003; SILVA et al., 2013). Sensores com alta resolução espacial e espectral permitem acompanhar com maior detalhe as condições biofísicas da superfície (ANDERSON, 2012).

A detecção de fogo a partir de sensoriamento remoto, em geral, é realizada de duas formas específicas. A primeira se utiliza do padrão térmico dos alvos para detectar anomalias termais, como por exemplo o fogo ativo. A observação é realizada por sensores capazes de obter informações nos canais espectrais do infravermelho médio e termal (SAN-MIGUEL-AYANZ et al., 2005). A segunda tem o objetivo de mapear as cicatrizes de queimadas, e é realizada levando-se em conta as alterações espectrais da vegetação, principalmente nos canais do visível e infravermelho próximo, relacionadas ao total de cinzas e carvão, solo exposto e à recuperação da vegetação (PEREIRA, 2003; GITAS et al., 2012).

As pesquisas relacionadas ao mapeamento de áreas queimadas ou a avaliação dos danos totais a vegetação se baseiam em sua maioria em: Aplicação de índices espectrais nos canais sensíveis a alterações ocasionadas pelo fogo (HOLDEN et al., 2005; LENTILE et al., 2006; QUINTANO et al., 2011; LIBONATI et al., 2015); Detecção de mudança a partir da comparação de séries temporais de imagens (ROY et al., 2005; VAN LEEUWEN et al., 2010; CARVALHO JÚNIOR et al., 2015); ou Aplicação de modelos de mistura espectral para separação de membros puros e os pixels derivados (COCHRANE; SOUZA, 1998; GITAS et al., 2012; QUINTANO; FERNANDEZ-MANSO; ROBERTS, 2017). A opção de utilização de mais de um método para melhor identificação dos alvos também é indicada, além da inclusão das alterações temporais de temperatura de superfície observadas no infravermelho termal (HOLDEN et al., 2005; GIGLIO et al., 2009; MORTON et al., 2011; STILL; PAU; EDWARDS, 2014).

O aprimoramento de técnicas de detecção do fogo assim como o conhecimento das suas características e efeitos relacionados na vegetação, principalmente nas regiões de florestas tropicais, pode auxiliar no entendimento de fatores condicionantes, tanto para o seu manejo sustentável, como para as possíveis adaptações com as mudanças globais em curso (MURPHY et al., 2013; ALENCAR et al., 2015).

As diferentes alterações dos biomas ocasionadas pelo fogo, assim como a influência da sua estrutura e dimensão espacial na disseminação de grandes incêndios, permanecem áreas de importância para o estudo do fogo. Uma visão integrada entre padrões espaciais, estruturais e antrópicos é a principal alternativa para responder

algumas das principais questões atuais sobre este regime e como defini-lo (BOWMAN et al., 2009):

Questões de Pesquisa

- Qual a aplicabilidade de produtos globais de mapeamento de áreas queimadas nos diferentes biomas brasileiros?
- Qual a potencialidade de produtos globais de mapeamento de áreas queimadas para a descrição do regime do fogo no Brasil?
- Qual é um método eficaz de mapeamento de áreas queimadas em séries temporais que suporte a detecção de cicatrizes em áreas de floresta tropical?
- Qual a potencialidade de dados orbitais na quantificação dos efeitos do fogo sobre parâmetros biofísicos da vegetação de savana e de floresta tropical?

Justificativa

O mapeamento de cicatrizes de queimadas é essencial para estudos de emissões de gases, regime do fogo e manejo ambiental (LENTILE et al., 2006; MOUILLOT et al., 2014). Os métodos atuais têm avançado na detecção do fogo e cicatrizes em diversos biomas mundiais, porém ainda se observa dificuldades na aquisição de informações para áreas florestais, como na Amazônia (GIGLIO et al., 2009; PADILLA; STEHMAN; CHUVIECO, 2014). Além disso os produtos atuais apresentam lacunas quanto a sua acurácia nos diferentes biomas brasileiros, sendo que estudos que se preocuparam com o Brasil, o fizeram em abordagens globais, com baixo detalhamento.

Diversos estudos propõem a utilização de dados de sensoriamento remoto para estimar variáveis da vegetação, dentre elas há inferências, por exemplo, sobre densidade da madeira, biomassa, altura da copa, produtividade, fenologia, temperatura de superfície, balanço de radiação, albedo, evapotranspiração e umidade (ANDERSON, 2012; OLIVEIRA et al., 2016), sendo importante identificar a aplicabilidade destes dados para compreender os processos biogeoquímicos alterados pelo fogo. Deste modo, esta pesquisa buscou avaliar séries temporais do sensor MODIS, em diversos produtos relacionados à vegetação, como área queimada, reflectância, temperatura e produtividade

primária bruta, em uma combinação de dados espaciais locais para avaliação da dinâmica do fogo no Brasil.

Objetivos

Buscando responder as questões prioritárias identificadas, o objetivo geral desta tese é analisar a dinâmica temporal de incêndios florestais nos biomas brasileiros, com enfoque na Amazônia e no Cerrado, a partir de um conjunto de dados de sensoriamento remoto e espaciais. Com a identificação da potencialidade de diferentes produtos, índices e métodos na delimitação de áreas queimadas e na quantificação das alterações biofísicas e fenológicas decorrentes de diferentes frequências de fogo, além do impacto dos diferentes cenários de conservação.

Os objetivos específicos desta tese, elucidados nos capítulos 2, 3 e 4, são:
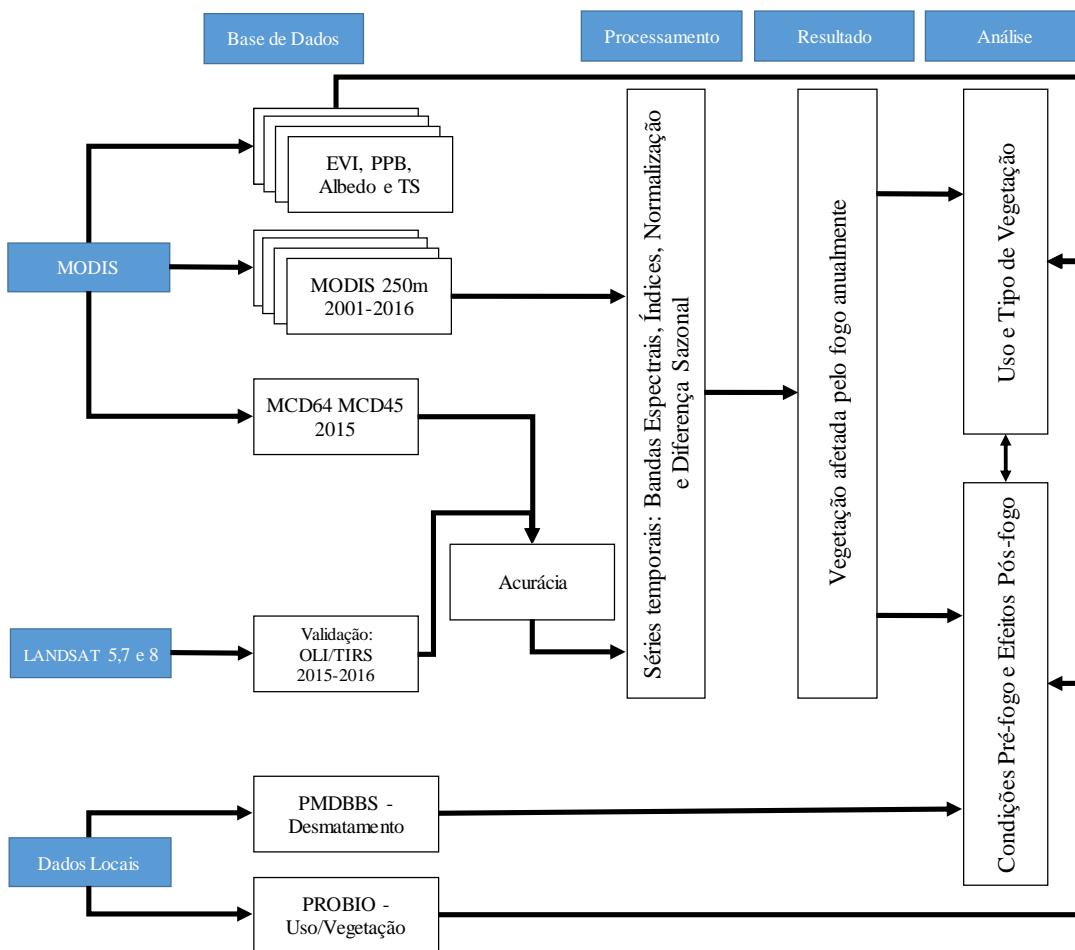
- Avaliar a aplicabilidade de produtos de mapeamento de queimadas a nível global para a descrição da distribuição do fogo no Brasil.
- Identificar áreas afetadas pelo fogo em ambientes de Floresta Amazônica, a partir da utilização de métodos de diferença sazonal e normalização temporal, em diferentes índices espectrais.
- Quantificar as alterações biofísicas e fenológicas ocasionadas por incêndios na vegetação de áreas da Amazônia e Cerrado com diferentes cenários de recorrência do fogo, a partir de dados orbitais.

Estrutura da Tese

Este trabalho está subdividido em quatro capítulos, com a utilização de diferentes produtos derivados de sensoriamento remoto e dados espaciais diversos. A figura 1 detalha as etapas realizadas nesta pesquisa.

O capítulo 1 apresenta a revisão dos principais aspectos relacionados aos incêndios florestais no Brasil, a introdução de técnicas de sensoriamento remoto para detecção de cicatrizes de queimadas e a potencialidade na estimativa de parâmetros biofísicas da vegetação. Por fim traçamos as principais questões aprofundadas nesta tese.

O capítulo 2 buscou avaliar a eficácia de produtos de mapeamento de cicatrizes de queimadas e focos de incêndio no Brasil. A acurácia dos produtos MODIS foi avaliada por matrizes de confusão a partir de dados produzidos por inspeção visual em imagens Landsat. A acurácia do produto de focos de incêndio foi avaliada por meio de regressão linear. A partir da combinação de produtos MODIS com dados climáticos e de uso do solo foi definida a distribuição do fogo nos diferentes ambientes em uma série histórica de 15 anos.
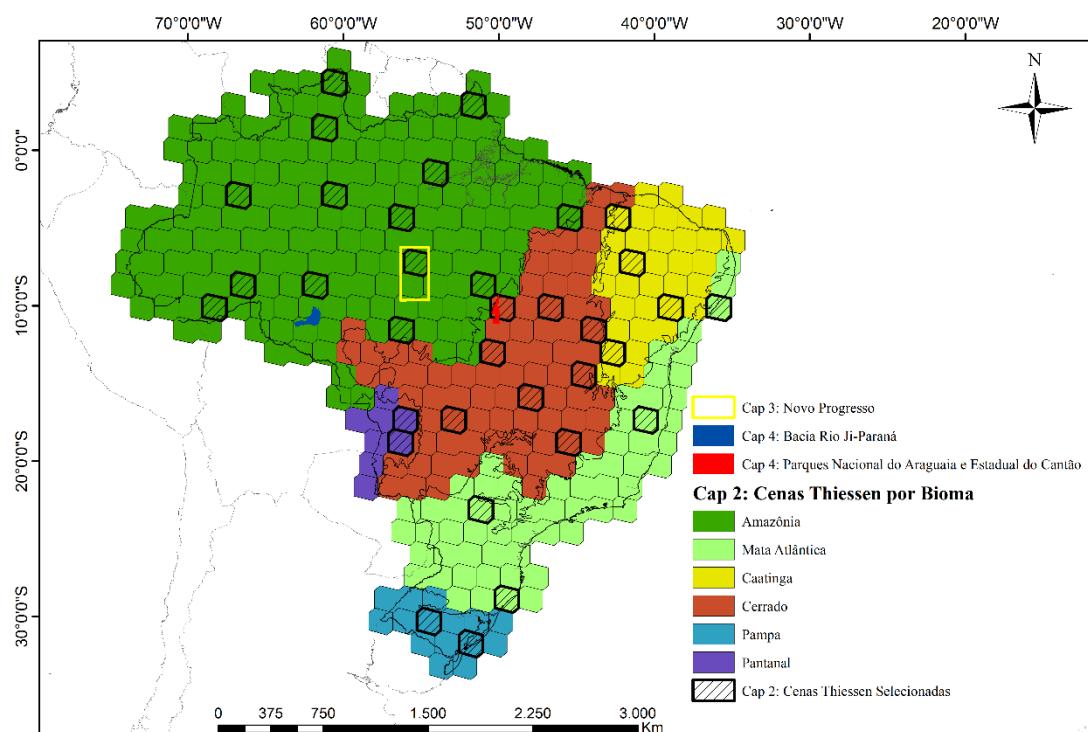
Figura 1.1. Fluxograma da Pesquisa.

No capítulo 3 foram examinados diferentes métodos de detecção de áreas queimadas a partir dos métodos de normalização de séries temporais e de diferença sazonal, dos índices espectrais BAIM, GEMI, MIRBI, NBR, NBR2 e NDVI, além da banda do Infravermelho Próximo. Foi avaliada a capacidade de mapeamento nos diferentes usos do solo na região de Novo Progresso – PA, que variam desde florestas ombrófilas a áreas de savanas.

No capítulo 4, foram quantificadas as tendências temporais de alterações biofísicas, do albedo, da produtividade primária bruta e da temperatura superficial, e as mudanças fenológicas no índice de vegetação. Foram utilizadas séries temporais MODIS, no período de 2001 a 2016, em áreas com diferentes recorrências do fogo e detectadas como queimadas a partir da metodologia definida no capítulo 3, na bacia do rio Ji-Paraná, em Rondônia e nos Parques Nacional do Araguaia e Estadual do Cantão, no Tocantins.

As áreas de estudo específicas de cada capítulo estão destacadas na figura 1.2: todo os biomas brasileiros e 34 amostras de cenas Landsat no primeiro capítulo; para o capítulo 2 a região do entorno do município de Novo Progresso no Pará; e para o capítulo 4 a bacia do rio Ji-Paraná, em Rondônia, e os Parques Nacional do Araguaia e Estadual do Cantão, no Tocantins.

Figura 1.2. Localização das Áreas de Estudo da Tese.

Referências

ALENCAR, A. A.; BRANDO, P. M.; ASNER, G. P.; PUTZ, F. E. Landscape fragmentation, severe drought, and the new Amazon forest fire regime. **Ecological Applications**, v. 25, n. 6, p. 1493–1505, 2015.

ALVARADO, S. T.; FORNAZARI, T.; CÓSTOLA, A.; MORELLATO, L. P. C.;

SILVA, T. S. F. Drivers of fire occurrence in a mountainous Brazilian cerrado savanna: tracking long-term fire regimes using remote sensing. **Ecological Indicators**, v. 78, p. 270–281, 2017.

ANDELA, N.; MORTON, D. C.; GIGLIO, L.; CHEN, Y.; VAN DER WERF, G. R.; KASIBHATLA, P. S.; DEFRIES, R. S.; COLLATZ, G. J.; HANTSON, S.; KLOSTER, S.; BACHELET, D.; FORREST, M.; LASSLOP, G.; LI, F.; MANGEON, S.; MELTON, J. R.; YUE, C.; RANDERSON, J. T. A human-driven decline in global burned area. **Science**, v. 356, n. 6345, p. 1356–1362, 2017.

ANDERSON, L. O. Biome-scale forest properties in Amazonia based on field and satellite observations. **Remote Sensing**, v. 4, n. 5, p. 1245–1271, 2012.

ARAÚJO, F. M. de; FERREIRA, L. G.; ARANTES, A. E. Distribution Patterns of Burned Areas in the Brazilian Biomes: An Analysis Based on Satellite Data for the 2002-2010 Period. **Remote Sensing**, v. 4, n. 7, p. 1929–1946, 2012.

ARCHIBALD, S. Managing the human component of fire regimes: lessons from Africa. **Philosophical Transactions of the Royal Society B: Biological Sciences**, v. 371, n. 1696, p. 20150346, 2016.

BOND, W. J.; WOODWARD, F. . I.; MIDGLEY, G. F. The Global Distribtuion of Ecosystems in a world without Fire. **New Phytologist**, v. 165, n. 2, p. 525–538, 2005.

BOWMAN, D. M. J. S.; BALCH, J.; ARTAXO, P.; BOND, W. J.; COCHRANE, M. A.; D'ANTONIO, C. M.; DEFRIES, R.; JOHNSTON, F. H.; KEELEY, J. E.; KRAWCHUK, M. A.; KULL, C. A.; MACK, M.; MORITZ, M. A.; PYNE, S.; ROOS, C. I.; SCOTT, A. C.; SODHI, N. S.; SWETNAM, T. W. The human dimension of fire regimes on Earth. **Journal of Biogeography**, v. 38, n. 12, p. 2223–2236, 2011.

BOWMAN, D. M. J. S.; BALCH, J. K.; ARTAXO, P.; BOND, W. J.; CARLSON, J. M.; COCHRANE, M. A.; D'ANTONIO, C. M. A.; DEFRIES, R. S.; DOYLE, J. C.; HARRISON, S. P.; JOHNSTON, F. H.; KEELEY, J. E.; KRAWCHUK, M. A.; KULL, C. a; MARSTON, J. B.; MORITZ, M. a; PRENTICE, I. C.; ROOS, C. I.; SCOTT, A. C.; SWETNAM, T. W.; VAN DER WERF, G. R.; BOWMAN, D. M. J. S.; S.J., P.; D'ANTONIO, C. M.; PYNE, S. J. Fire in the Earth System. **Science**, v. 324, n. 5926, p. 481–484, 2009.

BOWMAN, D. M. J. S.; WILLIAMSON, G. J.; ABATZOGLOU, J. T.; KOLDEN, C.

A.; COCHRANE, M. A.; SMITH, A. M. S. Human exposure and sensitivity to globally extreme wildfire events. **Nature Ecology and Evolution**, v. 1, n. 3, p. 1–6, 2017.

CARVALHO JÚNIOR, O. A. de; GUIMARÃES, R. F.; SILVA, C.; GOMES, R. A. T. Standardized Time-Series and Interannual Phenological Deviation: New Techniques for Burned-Area Detection Using Long-Term MODIS-NBR Dataset. **Remote Sensing**, v. 7, n. 6, p. 6950–6985, 2015.

CHUVIECO, E.; MARTÍNEZ, S.; ROMÁN, M. V.; HANTSON, S.; PETTINARI, M. L. Integration of ecological and socio-economic factors to assess global vulnerability to wildfire. **Global Ecology and Biogeography**, v. 23, n. 2, p. 245–258, 2014.

COCHRANE, M. A.; SCHULZE, M. D. Fire as a recurrent event in tropical forests of the eastern Amazon: effects on forest structure, biomass, and species composition. **Biotropica**, v. 31, n. 1, p. 2–16, 1999.

COCHRANE, M. A.; SOUZA, C. M. Linear mixture model classification of burned forests in the Eastern Amazon. **International Journal of Remote Sensing**, v. 19, n. 17, p. 3433–3440, 1998.

DI BELLA, C. M.; JOBBÁGY, E. G.; PARUELO, J. M.; PINNOCK, S. Continental fire density patterns in South America. **Global Ecology and Biogeography**, v. 15, n. 2, p. 192–199, 2006.

EVA, H.; LAMBIN, E. F. Fires and land-cover change in the tropics:a remote sensing analysis at the landscape scale. **Journal of Biogeography**, v. 27, n. 3, p. 765–776, 2000.

FANIN, T.; VAN DER WERF, G. R. Relationships between burned area, forest cover loss, and land cover change in the Brazilian Amazon based on satellite data. **Biogeosciences**, v. 12, n. 20, p. 6033–6043, 2015.

GIGLIO, L.; LOBODA, T.; ROY, D. P.; QUAYLE, B.; JUSTICE, C. O. An active-fire based burned area mapping algorithm for the MODIS sensor. **Remote Sensing of Environment**, v. 113, n. 2, p. 408–420, 2009.

GIGLIO, L.; RANDERSON, J. T.; VAN DER WERF, G. R. Analysis of daily, monthly, and annual burned area using the fourth-generation global fire emissions database (GFED4). **Journal of Geophysical Research: Biogeosciences**, v. 118, n. 1, p. 317–328, 2013.

GITAS, I.; MITRI, G.; VERAVERBEKE, S.; POLYCHRONAKI, A. Advances in

Remote Sensing of Post-Fire Vegetation Recovery Monitoring - A Review. In: FATOYINBO, L. (Ed.). **Remote Sensing of Biomass - Principles and Applications**. 1. ed. InTech, 2012.

GOVENDER, N.; TROLLOPE, W. S. W.; VAN WILGEN, B. W. The effect of fire season, fire frequency, rainfall and management on fire intensity in savanna vegetation in South Africa. **Journal of Applied Ecology**, v. 43, n. 4, p. 748–758, 2006.

HOLDEN, Z. A.; SMITH, A. M. S.; MORGAN, P.; ROLLINS, M. G.; GESSLER, P. E. Evaluation of novel thermally enhanced spectral indices for mapping fire perimeters and comparisons with fire atlas data. **International Journal of Remote Sensing**, v. 26, n. 21, p. 4801–4808, 2005.

LENTILE, L. B.; HOLDEN A, Z. A.; SMITH, A. M. S.; FALKOWSKI, M. J.; HUDAK, A. T.; MORGAN, P.; LEWIS, S. A.; GESSLER, P. E.; BENSON, N. C. Remote sensing techniques to assess active fire characteristics and post-fire effects. **International Journal of Wildland Fire**, v. 15, p. 319–345, 2006.

LIBONATI, R.; DACAMARA, C. C.; SETZER, A. W.; MORELLI, F.; MELCHIORI, A. E. An algorithm for burned area detection in the Brazilian Cerrado using 4 μm MODIS imagery. **Remote Sensing**, v. 7, n. 11, p. 15782–15803, 2015.

LIMA, A.; SILVA, T. S. F.; DE ARAGÃO, L. E. O. e C.; DE FEITAS, R. M.; ADAMI, M.; FORMAGGIO, A. R.; SHIMABUKURO, Y. E. Land use and land cover changes determine the spatial relationship between fire and deforestation in the Brazilian Amazon. **Applied Geography**, v. 34, p. 239–246, 2012.

MARLON, J. R.; BARTLEIN, P. J.; DANIAU, A. L.; HARRISON, S. P.; MAEZUMI, S. Y.; POWER, M. J.; TINNER, W.; VANNIÉRE, B. Global biomass burning: A synthesis and review of Holocene paleofire records and their controls. **Quaternary Science Reviews**, v. 65, p. 5–25, 2013.

MORTON, D. C.; DEFRIES, R. S.; NAGOL, J.; SOUZA, C. M.; KASISCHKE, E. S.; HURTT, G. C.; DUBAYAH, R. Mapping canopy damage from understory fires in Amazon forests using annual time series of Landsat and MODIS data. **Remote Sensing of Environment**, v. 115, n. 7, p. 1706–1720, 2011.

MOUILLOT, F.; SCHULTZ, M. G.; YUE, C.; CADULE, P.; TANSEY, K.; CIAIS, P.; CHUVIECO, E. Ten years of global burned area products from spaceborne remote

sensing-A review: Analysis of user needs and recommendations for future developments. **International Journal of Applied Earth Observation and Geoinformation**, v. 26, n. 1, p. 64–79, 2014.

MURPHY, B. P.; BOWMAN, D. M. J. S. What controls the distribution of tropical forest and savanna? **Ecology Letters**, v. 15, n. 7, p. 748–758, 2012.

MURPHY, B. P.; BRADSTOCK, R. A.; BOER, M. M.; CARTER, J.; CARY, G. J.; COCHRANE, M. A.; FENSHAM, R. J.; RUSSELL-SMITH, J.; WILLIAMSON, G. J.; BOWMAN, D. M. J. S. Fire regimes of Australia: A pyrogeographic model system. **Journal of Biogeography**, v. 40, n. 6, p. 1048–1058, 2013.

OLIVEIRA, G. de; BRUNSELL, N. A.; MORAES, E. C.; BERTANI, G.; DOS SANTOS, T. V.; SHIMABUKURO, Y. E.; ARAGÃO, L. E. O. C. Use of MODIS sensor images combined with reanalysis products to retrieve net radiation in Amazonia. **Sensors (Switzerland)**, v. 16, n. 7, 2016.

PADILLA, M.; STEHMAN, S. V.; CHUVIECO, E. Validation of the 2008 MODIS-MCD45 global burned area product using stratified random sampling. **Remote Sensing of Environment**, v. 144, p. 187–196, 2014.

PAUSAS, J. G.; RIBEIRO, E. Fire and plant diversity at the global scale. **Global Ecology and Biogeography**, v. 26, n. 8, p. 889–897, 2017.

PEREIRA, J. M. C. Remote sensing of burned areas in tropical savannas. **International Journal of Wildland Fire**, v. 12, n. 4, p. 259, 2003.

QUINTANO, C.; FERNANDEZ-MANSO, A.; ROBERTS, D. A. Burn severity mapping from Landsat MESMA fraction images and Land Surface Temperature. **Remote Sensing of Environment**, v. 190, p. 83–95, 2017.

QUINTANO, C.; FERNÁNDEZ-MANSO, A.; STEIN, A.; BIJKER, W. Estimation of area burned by forest fires in Mediterranean countries: A remote sensing data mining perspective. **Forest Ecology and Management**, v. 262, n. 8, p. 1597–1607, 2011.

REINHARDT, E. D.; KEANE, R. E.; BROWN, J. K. Modeling fire effects. **International Journal of Wildland Fire**, v. 10, n. 4, p. 373–380, 2001.

ROY, D. P.; JIN, Y.; LEWIS, P. E.; JUSTICE, C. O. Prototyping a global algorithm for systematic fire-affected area mapping using MODIS time series data. **Remote Sensing of Environment**, v. 97, n. 2, p. 137–162, 2005.

SAN-MIGUEL-AYANZ, J.; RAVAIL, N.; KELHA, V.; OLLERO, A. Active fire detection for fire emergency management: Potential and limitations for the operational use of remote sensing. **Natural Hazards**, v. 35, n. 3, p. 361–376, 2005.

SCHOLES, R. J.; ARCHER, S. R. Tree-grass interactions in savannas. Annual Review of Ecology and Systematics, v. 28, p. 517–544, 1997.

SILVA, F. B.; SHIMABUKURO, Y. E.; ARAGÃO, L. E. O. C.; ANDERSON, L. O.; PEREIRA, G.; CARDOZO, F. da S.; ARAI, E. Large-scale heterogeneity of Amazonian phenology revealed from 26-year long AVHRR / NDVI time-series. **Environmental Research Letters**, v. 8, p. 12, 2013.

STILL, C. J.; PAU, S.; EDWARDS, E. J. Land surface skin temperature captures thermal environments of C3 and C4 grasses. **Global Ecology and Biogeography**, v. 23, n. 3, p. 286–296, 2014.

VAN LEEUWEN, W. J. D.; CASADY, G. M.; NEARY, D. G.; BAUTISTA, S.; ALLOZA, J. A.; CARMEL, Y.; WITTENBERG, L.; MALKINSON, D.; ORR, B. J. Monitoring post-wildfire vegetation response with remotely sensed time-series data in Spain, USA and Israel. **International Journal of Wildland Fire**, v. 19, n. 1, p. 75–93, 2010.

ZHANG, X.; FRIEDL, M. A.; SCHAAF, C. B.; STRAHLER, A. H.; HODGES, J. C. F.; GAO, F.; REED, B. C.; HUETE, A. Monitoring vegetation phenology using MODIS. **Remote Sensing of Environment**, v. 84, n. 3, p. 471–475, 2003.

CAPÍTULO 2 – Accuracy and Spatiotemporal Distribution of Fire in the Brazilian Biomes from the MODIS Burned Area Products[1]

Nickolas Castro Santana[*], Osmar Abílio de Carvalho Júnior[*], Roberto Arnaldo Trancoso Gomes[*], Renato Fontes Guimarães[*]

[*]Department of Geography, University of Brasília, Brasília, Brazil

Abstract

Remote sensing derived databases are the primary sources of regional and global information on fire events, being the MODIS products the most used by the scientific community in the burned area monitoring on regional and global scales. This research aimed to assess the accuracy of MODIS burned and hotspots products and their ability to describe fire patterns in Brazil. The accuracy was estimated by comparing the MODIS products and the burned areas detected by the visual interpretation of the LANDSAT / OLI images using a confusion matrix method. The fire regime analysis used the best accuracy product in conjunction with environmental variables during the period 2001-2015. The MCD45 product showed low accuracy to detected burned areas due to a high error of commission (>36.69%) and omission (>77.04%) for the whole country dataset. The MCD64 product showed lower errors of omission (64.05%) and high errors of commission (45.85%). The fire distribution in Brazilian biomes and its spatiotemporal variations in the period 2001-2015 indicated three domains of fire in the country conditioned by the humidity level. The grasslands and savannas located in semi-humid zones are the most fire prone areas, burning up to 25% of its total area annually

Keywords: validation; fire scars; wildfire; Brazil; multitemporal.

Introduction

Wildfires are change vectors in terrestrial ecosystems, which may accelerate modifications in forest formations or limiting the development of savannas (Eva and Lambin 2000; Bond *et al.* 2005). In fire management, spatial extent and recurrence are key factors to determine the fire regime (Murphy *et al.* 2013). The database of regional fire studies has generally been derived from remote sensing products (Archibald *et al.* 2013).

---

[1] Artigo submetido ao periódico *International Journal of Wildland Fire.*

The accuracy of these products may vary, with commission errors greater than 40% and omission errors greater than 60% in products derived from MODIS and SPOT (Padilla *et al.* 2015). The MODIS sensor products named MCD45 (Roy *et al.* 2005) and its successor MCD64 (Giglio *et al.* 2009) have been the most used due to the high temporal resolution and lower error rates (Mouillot *et al.* 2014). Those products are able to detect the location of the burned area, with a spatial resolution of 500 meters and approximate date of occurrence. The MCD45 uses a bi-directional model to detect persistent changes in a sequence of days, while the MCD64 uses the identification of persistent changes in vegetation index time series with the inclusion of the location of active fires to delimit the burned area. **Table 2.1** lists the surveys that evaluate the accuracy of MODIS burned area products. Several studies have used Landsat images and confusion matrix approach to assess accuracy of MODIS MCD45 and MCD64 products, using matrices of confusion, errors of commission and omission. The global studies had few samples in Brazil, besides not indicate the accuracy in the different Brazilian biomes.

Table 2.1. Validation research for MCD45 and MCD64 products.

Reference	Product	Validation Area	Method	Validation	Accuracy
(Roy And Boschetti., 2009)	MCD45	South Africa	Landsat interpretation	Confusion Matrix	CE: 0,0860 to 0,6549 OE: 0,0470 to 0,9428
(Giglio *et al.* 2009)	MCD64	Central Siberia, Western United States and Southern Africa	Landsat interpretation	Confusion Matrix and Correlation	Kappa Coefficient: 0,49 to 0,82
(Padilla *et al.* 2014)	MCD45	Global Samples	Semi-Automatic Algorithm and Visual Interpretation	Confusion Matrix	CE: 43% to 95% OE: 65% to 99%
(Tsela *et al.* 2014)	MCD45	South Africa	Landsat Interpretation	Error Matrix	CE: 11,53% to 40,35% OE: 38,50% to 90,48%
(Tsela *et al.* 2014)	MCD64	South Africa	Landsat Interpretation	Error Matrix	CE: 0,62% to 56,03% OE: 4,05% to 79,98%
(Padilla *et al.* 2015)	MCD45	Global Samples	Semi-Automatic Algorithm and Landsat Interpretation	Error Matrix	CE: 46% OE: 72% Dice Coefficient: 37%

(Padilla *et al.* 2015)	MCD64	Global Samples	Semi-Automatic Algorithm and Landsat Interpretation	Error Matrix	CE: 42% OE: 68% Dice Coefficient: 42%
(Mohler and Goodin 2016)	MCD45	Kansas, United States	Supervised Classification in MODIS images	Confusion Matrix	Kappa Coefficient: 0,14 to 0,58
(Giglio *et al.* 2018)	MCD45	Global Samples	Landsat Interpretation	Confusion Matrix	CE: 23% OE: 45%
(Giglio *et al.* 2018)	MCD64	Global Samples	Landsat Interpretation	Confusion Matrix	CE: 22% OE: 40%

CE: Comission Errors; OE: Omission Errors.

South America has one of the lowest rates of burned-area detection using the MCD45 product (Roy *et al.* 2005). The burn mapping in Brazil using satellite images does not detail the error according to the biomes (Schroeder *et al.* 2005; Araújo *et al.* 2012; Caúla *et al.* 2015). The fire regime studies in the country are fragmented in specific areas of the Cerrado (Daldegan *et al.* 2014; Alvarado *et al.* 2017) and Amazonian biomes (Aragão *et al.* 2008; Cardozo *et al.* 2014; Alves and Pérez-Cabello 2017). The critical variables of the fire regime at the regional scale are poorly understood, based on local or global scale studies only (Bond and Keeley 2005; Di Bella *et al.* 2006; Bowman *et al.* 2009; Krawchuk *et al.* 2009; Alvarado *et al.* 2017).
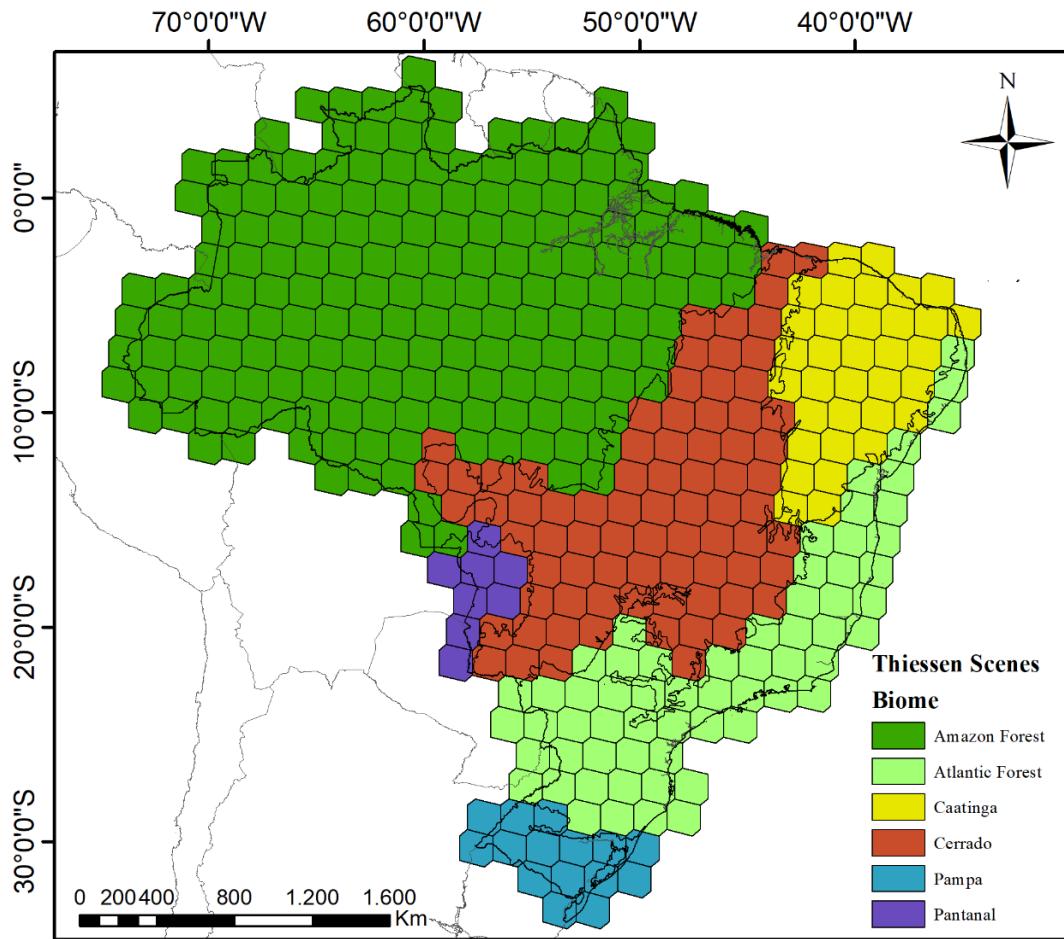
This research intended to: (a) validate the global products of burned area mapping MCD45 and its successor MCD64 for the year 2015 in the different Brazilian biomes; and (b) assess the fire distribution in Brazil from the MCD64 product during the period 2001-2015, and the climatic and vegetation factors that may characterize the pyrogeographic regions of Brazil.

Material and Methods

Accuracy Analysis

This study adopted 16 tiles of MODIS products (MCD45 and MCD64) for the period 2001-2015. The methodology includes: (a) accuracy analysis of the MODIS burned area products for 34 areas in the year 2015, which encompassed approximately 24,000 km² each area; (b) analysis of the fire recurrence for the entire Brazilian territory over the period 2001-2015; and (c) assess effects of vegetation and moisture on fire regime.
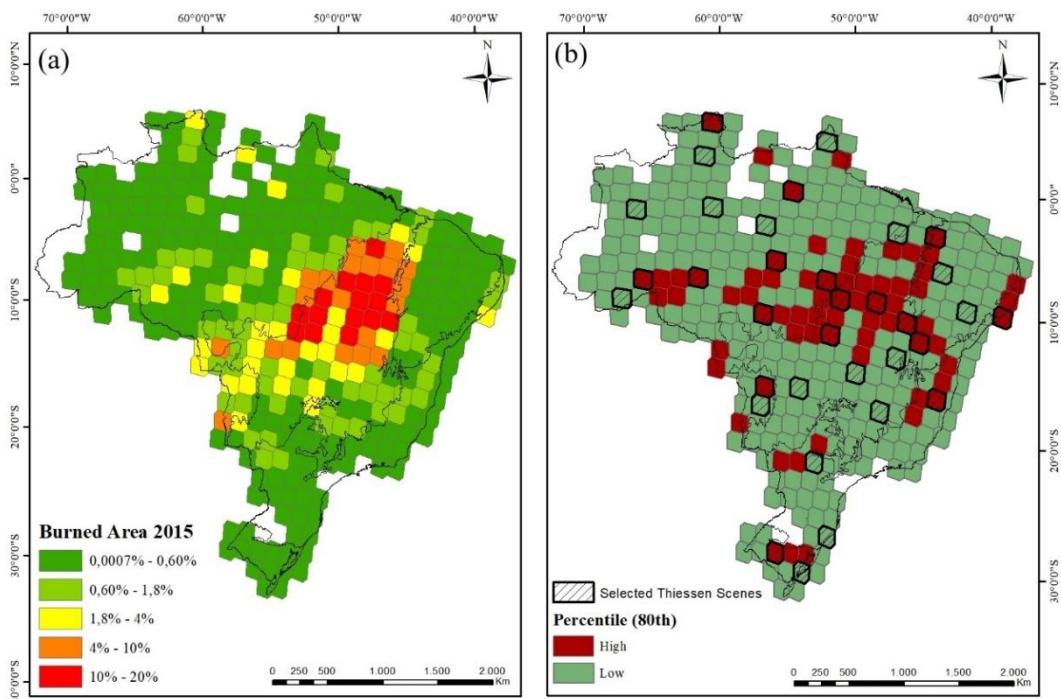
We used the methodological approach based on stratified random samples, proposed by Boschetti *et al*. (2016), to assess accuracy of MODIS burned area products. The validation reference data were extracted from the Landsat 8 images (WRS-II) (Padilla *et al*. 2014; Boschetti *et al*. 2016), by creating non-overlapping polygons from the latitude and longitude coordinates of the center of the Landsat scene, which encompassed an area of 24,000 km² spatially distributed in the six Brazilian biomes (**Figure 2.1**).

Figure 2.1. Thiessen scenes per Brazilian biome.

The total burned area detected using the MCD64 product in the year 2015 in each scene included the following classes: (a) low occurrence of fire represented by the quartile of 80%; and (b) high fire occurrence represented by the 20% quartile. The exclusion of non-fire scenes resulted in 365 scenes in the Brazilian territory (**Figure 2.2a**). This step is essential because the simple random selection can include areas of low fire-occurrence. The random selection adopted an equal number of low and high fire activity scenes by the Equal Allocation method (Boschetti *et al*. 2016), resulting in 34 scenes divided into proportional sizes areas by biomes: Amazon (49.29% of the territory); Cerrado (23.92%);

Atlantic Forest (13.04%); Caatinga (9.92%); Pampa (2.07%), and Pantanal (1.76%) (**Figure 2.2b**).

Figure 2.2. Burned area by Thiessen Scenes (a) and selected Thiessen Scenes by Brazilian biomes (b).

The reference burned area data was prepared by applying visual interpretation on Landsat OLI images. This methodological approach used a set of three images to eliminate false fire events, including one scene before and one scene after the date of the fire. The adoption of three scenes for each studied area resulted in 102 Landsat OLI images. The selection of images considered the end of the dry period and a cloud cover of up to 15%. The accuracy analysis compared the burn and unburned classes between the MODIS products and the reference mapping by calculating the confusion matrix (**Table 2.2**) and its metrics (Congalton 1991): overall accuracy ($OA = p_{11} + p_{22}$); commission errors ($CE = p_{12} / p_{1.}$); omission errors ($OE = p_{21} / p_{.1}$), and Kappa coefficient (KC= ((p11+p12)-pe)/(1-pe), where pe =(p1.*p.1)+(p2.*p.2)).

KC has limitations in the accuracy analysis by both the randomness as the potential to overestimate the success (Pontius and Millones 2011). Therefore, Olofsson *et al*. (2014) consider that the OA can replace KC without prejudice to accuracy analysis. However, the unburned area in the fire accuracy analyzes is generally more representative and shows high OA values. So we also used the Dice Coefficient (DC) (Fleiss *et al*. 2003)

that combines the results of omission and commission errors into a single category according to the equation (3).

$$DC = \frac{2*a}{2*a+b+c} \tag{1}$$

Where "a" refers to the burned area mapped correctly in both methods, "b" the commission errors, and "c" the omission errors. This coefficient also presents limitations by adding the differences between errors of commission and omission, being recommended its use only in cases where these values are not important individually (Padilla *et al*. 2014).

Table 2.2. Confusion matrix with the total of agreement or disagreement between MODIS and Reference data.

		Reference Data		
		Burned	Unburned	Total
MODIS Data	Burned	p_{11}	p_{12}	$p_{1.}$
	Unburned	p_{21}	p_{22}	$p_{2.}$
	Total	$p_{.1}$	$p_{.2}$	1

Furthermore, we assess the linear regression relationships between: (a) the burned pixel density present in the MODIS thermal bands (MOD14/MYD14 fire products - collection 6) (Giglio *et al.* 2016) and the burned area detected using Landsat interpretation in the 34 Thiessen Scenes; (b) the burned pixel density estimated using the MODIS thermal bands and the burned area from MCD45 and MCD64 for all the 336 Thiessen scenes with presence of fire in Brazil in 2015. This procedure adapted the methodology developed by (Hantson *et al.* 2013), which compared MODIS hotspots and burned areas in Landsat images in nine regions of the Earth with high fire presence.

Fire Regime

The fire recurrence analysis in Brazil using the product MCD64 for the period 2001-2015 considered: (a) the total number of annual burnings in the period 2001-2015; (b) mean fire return interval (Wittkuhn and Hamilton 2010); and (c) seasonality of the fire defined as the average period of occurrence in each region.

Furthermore, we assess the influence of vegetation and moisture in the spatial distribution of fire by adapting the method developed by Murphy *et al*. (2013) and

Archibald *et al*. (2010b). This method compares spatial information of the burned area, frequency, range, seasonality, fire intensity, as well as environmental and human gradients to describe the fire regime in Australia and South Africa. The following secondary data was used: (a) MODIS Land Cover Type product (MCD12Q1) for the year 2013, this product is based on the classification of the annual time series (Friedl *et al*. 2010), and (b) climatic map prepared by the Brazilian Institute of Geography and Statistics (IBGE, 2002).

Results

Accuracy of the MCD45 and MCD64 products

Table 2.3 lists Overall Accuracy (OA), Comission Errors (CE), Omission Errors (OE), Kappa Coefficient (KC), and Dice Coefficient (DC) for the different Brazilian biomes. The MCD45 product showed the following mean values: CE of 42.01%, OE of 78.03%, OA of 97.20%, KC of 0.27 and DC of 0.26. The MCD64 product showed a higher accuraccy (CE (50.45%), OA (98.72%), KC (0.39) and DC (0.39), and lower OE (63.99%)). The OA tends to present high values due to the higher proportion of unburned area in all scenes, so its interpretation must be performed in conjunction with other accuracy parameters (Padilla *et al*. 2014). The spatial resolution is an important factor in the precision measurements between images of different sensors, that can generate errors regardless of the mapping method (Boschetti *et al*. 2016).
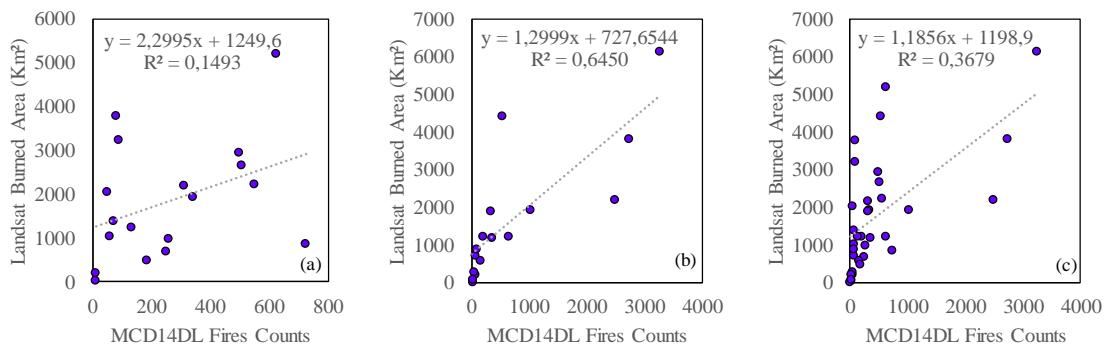
The MCD45 and MCD64 products have lower detection capacity of burn scars in the Amazon Forest, Atlantic Forest, and Pampa biomes, which resulted in higher CE and OE rates, resulting in KC and DC between 0.07 and 0.30. In the Cerrado and Caatinga biomes, OE is the lowest in the two products, resulting in the highest DC values ranging from 0.48 for the MCD45 in the Caatinga and 0.60 for the MCD64 in the Cerrado. The Pantanal biome showed high OE for the product MCD45. The product MCD64, however, improved the mapping with reduction of the CE and OE, resulting in the second-best KC and DC for the studied biomes.

The regression analysis evaluated the distribution of the 34 Thiessen scenes in the scatterplot, considering the reference burned areas from the OLI Landsat 8 images and the active fire pixels from the MODIS thermal bands. The results indicated a lack of correlation in tropical forest biomes ($R^2 = 0.1493$), the low correlation in the other biomes ($R^2 = 0.6450$), and for all Brazilian biomes ($R^2 = 0.3679$) (**Fig. 2.3**). The regression

analysis between the active fire pixels (MCD14DL) and the burned area products MCD45 e MCD64, by considering the 336 Thiessen scenes in the year 2015, indicated a low R^2 value for the MCD64 (R^2 = 0.3823) (**Fig. 2.4b**) and MCD45 (R^2 = 0.25) products (**Fig. 2.4a**).
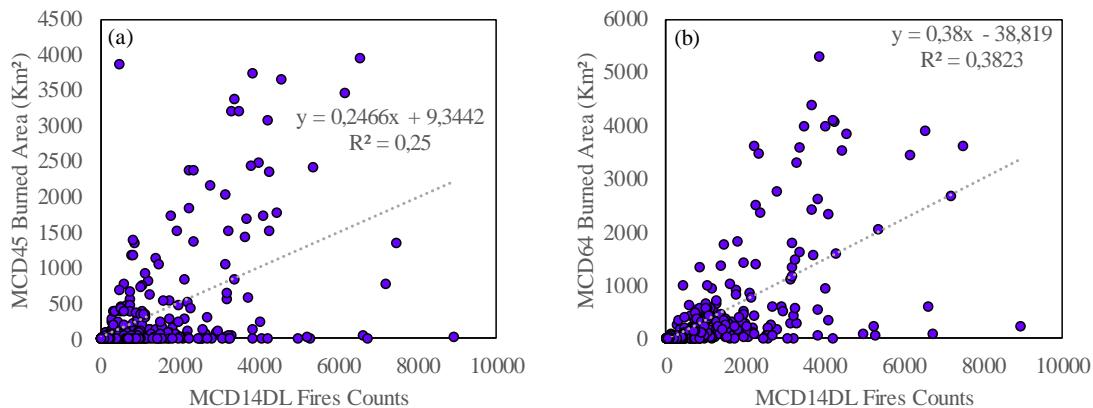
Table 2.3. Accuracy analysis of the MODIS MCD45A1 / MCD64A1 products of burned area mapping and reference data elaborated from Landsat OLI images in the different Brazilian biomes.

Biome	Product	Commission Errors	Omission Errors	Overall Accuracy	Kappa Coefficient	Dice Coefficient
Amazon	MCD45	23.36%	92.69%	90.33%	0.1133	0.0986
Forest	MCD64	51.45%	72.56%	98.54%	0.3059	0.2960
Caatinga	MCD45	29.62%	61.05%	98.63%	0.4759	0.4803
(Semi-Arid)	MCD64	37.65%	52.74%	98.64%	0.5118	0.5176
Cerrado	MCD45	38.99%	53.95%	96.54%	0.4805	0.4972
(Savanna)	MCD64	33.29%	44.03%	97.45%	0.5888	0.6028
Atlantic	MCD45	55.00%	77.77%	99.37%	0.2570	0.2593
Forest	MCD64	66.46%	77.06%	99.03%	0.2286	0.2546
Pampa	MCD45	54.87%	95.09%	99.93%	0.0789	0.0789
(Grasslands)	MCD64	75.57%	83.93%	99.93%	0.1930	0.1932
Pantanal	MCD45	50.23%	87.63%	98.40%	0.1854	0.1887
(Wetlands)	MCD64	38.31%	53.64%	98.80%	0.5150	0.5211

Figure 2.3. Regression analysis between MODIS TERRA/AQUA active fire pixels (MCD14DL) and LANDSAT 8 OLI burned area in 2015, where each point represents
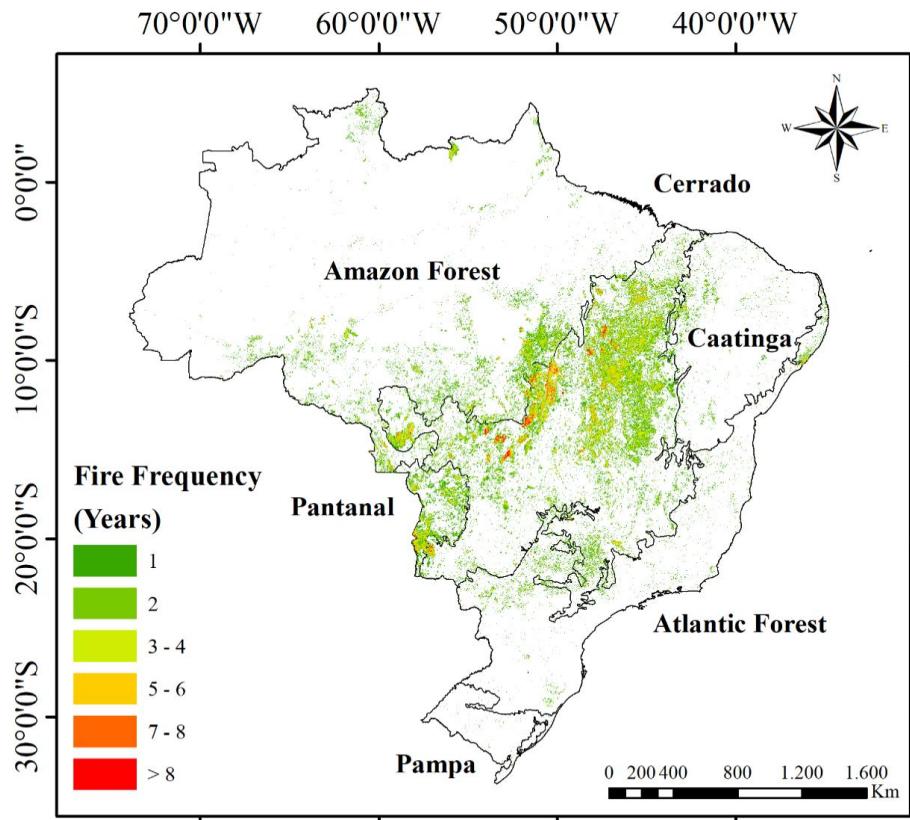
one Thiessen Scene in Tropical Forest (Amazon and Atlantic Forest biomes) (a); Caatinga, Cerrado, Pampa and Pantanal biomes (b); and all the Brazilian biomes (c).

Figure 2.4. Regression analysis between MODIS TERRA/AQUA active fire pixels – MCD14DL and the MCD45 (a) and MCD64 (b) burned area products. Each point represents one Thiessen Scene in 2015, totaling 336 points distributed in the scatterplot.
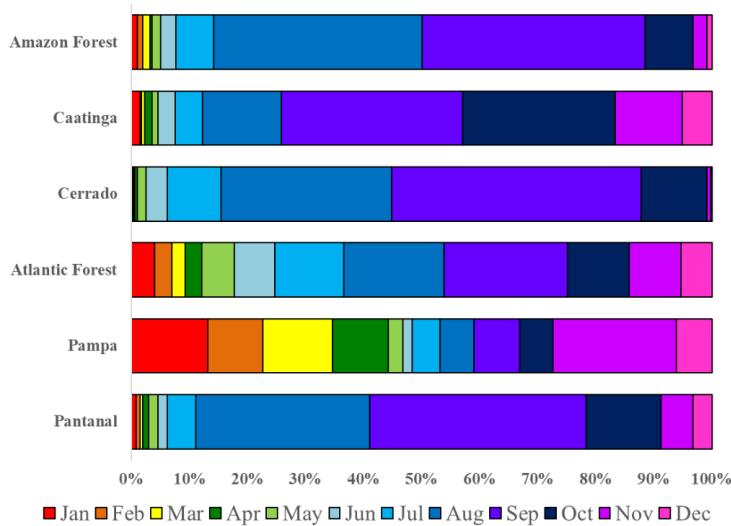
Burned Area and fire frequency

The MCD64 product shows that 850,000 km² was burned in Brazil in the period 2001-2015, which corresponds to 120,111.2 km² of annual average burning of. By evaluating the observed OE and CE, this area may be 20% larger. More than 10% of the country's area burned in the last 14 years, with more than 70% of fire events occurring between 1 and 2 years (**Figure. 2.5**). The highest fire frequency group was observed in the savanna region with low fragmentation similar to those observed in the South African savannas (Archibald 2016) and in the transition zones of the Cerrado to Amazon Forest.

Figure 2.5. Fire recurrence based on the MODIS MCD64 product for a period of 14 years.
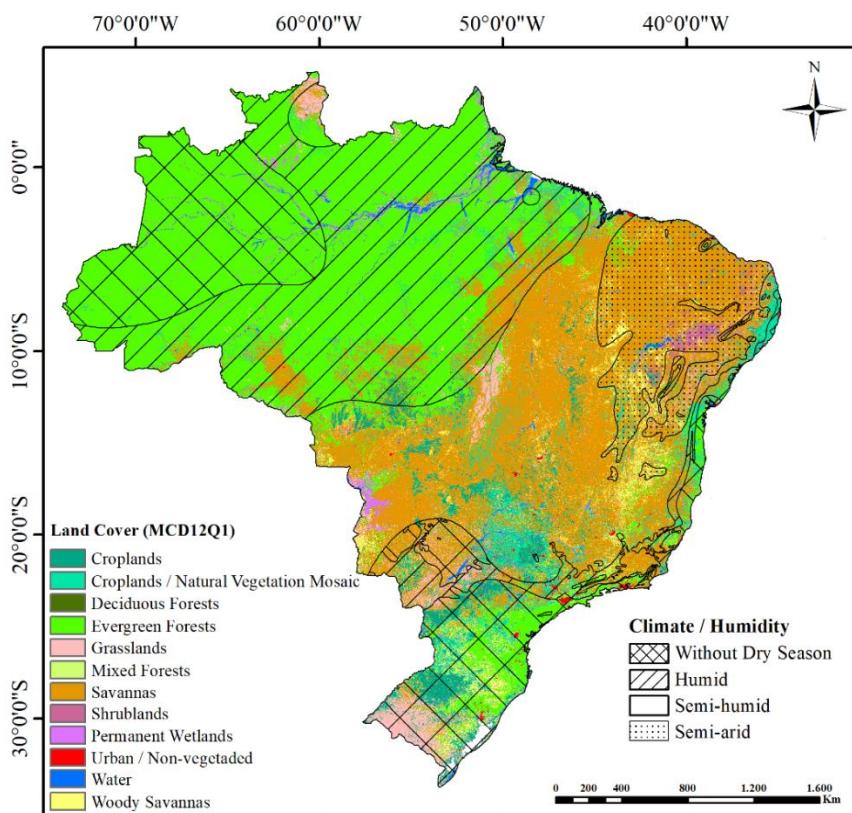
Figure 2.6 shows the seasonal burning pattern for the Brazilian biomes. Between August and September, we observed more events in the Amazon Forest, Cerrado, Atlantic Forest, and Pantanal biomes. The vegetation of the semi-arid region (Caatinga) showed a fire peak one month behind the other biomes, while Pampa biome (southern Brazil) showed the peak from November to January.

Figure 2.6. Monthly burned area by Brazilian biomes.

Environmental Regional Context

The main environmental characteristics that define the fire regime in Brazil are rainfall distribution; vegetation and land use. **Figure 2.7** shows the distribution of the different regions analyzed by soil cover type and humidity. Pluviometry regimes can be grouped into the categories: (a) regions without dry period, which basically occur in the western Amazon region, east coast of the country and the South, being mainly covered by tropical forests and croplands; (b) humid regions with a drought period of 1 to 3 months, occurring in most of the Amazon region and in the transition of the super-humid areas of the Southeast and South of the country. These regions are mainly composed of tropical forests, but are also characterized by areas of intense livestock use, with the conversion of forest areas to pasture; (c) semi-humid regions with up to 6 months of drought occurring in the central, northeastern and extreme north regions of the country, being composed especially of mosaics of savannas and agriculture; and (d) semi-arid regions occupying much of the Northeast region, composed of semi-arid savannas with little agricultural use.

Figure 2.7. Brazilian fire regime zones derived from the MODIS Land Cover Type product (MCD12Q1) and Climate Map from the Brazilian Institute of Geography and Statistics.

Fire distribution from vegetation and humid

Table 2.4 lists the proportion of burned areas under different land cover conditions and humidity. The influence factors of the fire regime were rainfall and soil type. The data subdivide into three groups: (1) very humid regions with lower occurrence of fires and high fire interval in all vegetation types and land cover; (2) regions of seasonal droughts with enough wet season for biomass growth and drought periods that allow the ignition of the fire, being the region more burned and with the lower mean fire interval; and (3) semi-arid areas with fuel deficiencies that prevent the occurrence of fires, having the lowest percentage of burned area and higher mean fire interval than the semi-humid zones in most of the land cover. The temporal distribution of vegetation fire along the land-cover types showed two periods of highest occurrence: July-September or August-October.

Discussion

This study assessed the MODIS burned area products in the different Brazilian biomes. An accuracy analysis adopted a random sampling stratified by zones of high and low fire presence (Padilla *et al*. 2015; Boschetti *et al*. 2016). The MCD64 product is superior in all accuracy metrics in the Cerrado and Pantanal biomes, as well as having smaller OE in all biomes. The MCD45 product has lower CE in the biomes of Atlantic Forest, Amazon Forest, Caatinga, and Pampa. Products with lower CE rates are more indicated for burned area studies (Mouillot *et al.* 2014). The low detection of burned areas in the tropical forests from the MCD64 product may be due to the use of active fires in their algorithm (Giglio *et al.* 2009), which has a lower capacity to identify hotspots in these regions. In addition, the burn algorithms are not specific to each class of land cover.

The values of CE and OE were compatible with the other validation studies (**Table 2.1**), presenting the lowest CE in the savanna (Cerrado), tropical forest (Amazon) and semi-arid (Caatinga) biomes, in addition to presenting higher OE in relation to CE. The results were similar to those Padilla *et al*. (2014) where the detail of errors in the different global biomes indicates a smaller DC in tropical forests compared to savannas, and the global study of Giglio *et al*. (2018) in which the mean CE was 22% and OE 40% in the product MCD64, while CE was 23% and OE 45% in the product MCD45.

Table 2.4. Area and period of fire occurrence in the Brazilian fire regime zones, considering the following attributes: land cover, humidity, average monthly percentage of affected area (MPA), dominant period, and mean fire interval in years (MFI).

Land Cover	Humidity	MPA (%)	Dominant period	MFI (years)
Grasslands	Without dry season	0.7%	July-September	12
	Humid / Semi-humid	26%	July-September	5
	Semi-arid	0.6%	July-September	6
Permanent Wetlands	Without dry season	0.3%	No domain	13
	Humid / Semi-humid	8.6%	August-October	10
Croplands	Without dry season	1.2%	July-September	8
	Humid / Semi-humid	10.7%	July-September	5
	Semi-arid	2.5%	July-September	5
Croplands/Natural Vegetation Mosaic	Without dry season	1.5%	July-September	7
	Humid / Semi-humid	6.9%	July-September	5
	Semi-arid	2.3%	August-October	5
Evergreen Forests	Without dry season	0.9%	July-September	14
	Humid / Semi-humid	0.6%	August-October	11
Deciduous Forests	Humid / Semi-humid	5.2%	August-October	6
	Semi-arid	9.9%	July-September	8
Mixed Forests	Any	14.8%	July-September	6
Shrublands	Humid / Semi-humid	21.7%	July-September	8
	Semi-arid	0.4%	August-October	11
Woody Savannas	Without dry season	0.9%	July-September	9
	Humid / Semi-humid	24.7%	August-October	5
	Semi-arid	5.8%	August-October	6
Savannas	Without dry season	1.4%	July-September	9
	Humid / Semi-humid	15.2%	July-September	6
	Semi-arid	4%	August-October	6

However, the patterns were different from those observed by Tsela *et al*. (2014) in South African savannas, where CE varied between 0.62% to 30%, and OE between 25% to 55%, this better accuracy is a result of the different validation methodology employed by the authors.

The underestimated results of the burned area in all biomes confirm the studies of Padilla *et al*. (2014) and Roy and Boschetti (2009). The high underestimation of burned

area in mainly related to the low spatial resolution of MODIS sensor, where small fragments of burned area cannot be detected (Giglio *et al.* 2009). In Brazil, the Pampa and Atlantic Forest biomes are the most fragmented (Overbeck *et al.* 2015), with greater fire detection difficulty due to the spectral mixture in the MODIS resolution.

Although the limitations of the Kappa coefficient (Pontius and Millones 2011, Olofsson *et al.* 2014), it showed results similar to the Dice coefficient. Besides, we did not observe the redundancy between overall accuracy and Kappa coefficient indicated by Olofsson *et al*. (2014), since the comparison between burned and unburned areas generally results in a higher overall accuracy due to the more significant proportion of unburned area.

The comparison between MODIS hotspots, the burned area from Landsat images and MODIS burned area products indicated the low correlation between methods, especially for tropical forest biomes, one of the relevant factors for this low relation is the low spatial resolution of the thermal bands, with a pixel of about 1km. The MODIS hotspots in the Cerrado biome also showed limitations with a low rate of CE and high rates of OE by considering several scenarios (Hantson *et al.* 2013).

The regional distribution of rainfall is one of the main explanatory variables of the fire regime in Brazil, in addition to factors such as vegetation and its ignition. The minimum rainfall that favors the occurrence of fires occurs during September in the Caatinga, while in the Cerrado, Atlantic Rainforest and Pantanal happen in August (Araújo *et al.*2012). Rainfall regions, with high or low rainfall, have a small percentage of the burned area and low fire recurrence. In contrast, regions with intermediate rainfall regimes of central Brazil have a high percentage of burned area and a shorter period of fire recurrence. This pattern occurs in several tropical regions of Africa and Oceania (Archibald *et al.* 2010b, 2010a; Murphy *et al.* 2013).

The knowledge of the fire regime in Brazil and the characteristics of each vegetation region can help in the establishment of a new fire management policy in the country, topic widely covered by several authors, especially in the Cerrado biome (Moreira, 2000; Durigan; Ratter, 2016; Alvarado *et al.* 2018). Due to high omission error rates of burned area products in the Brazilian biomes of tropical forest and pampa, there is a prioritization of studies of fire management techniques directed toward the Cerrado, such as the implementation of a new policy in Cerrado protected areas, that is based on ancestral knowledge of the fire regime and the use of controlled fires to prevent high severity events (Schmidt *et al.* 2016). Despite this initiative, most areas of Cerrado still

use the exclusion of fire as a form of management, the same practice that is also used in the rest of the country.

Conclusions

This research assessed the accuracy of the MODIS burned area products (MCD45 and MCD64) in different Brazilian biomes by applying a stratified random sampling method. Both analyzed products presented large omission errors, mainly in tropical forest areas, underestimating an area burned by about 40% for the MCD45 product and 20% for the MCD64 product. Among the main factors for this result are the resolution difference between the evaluated sensors, and the mapping method. Methods developed for specific vegetation, climate and soil classes tend to present superior results compared to generalist methods.

Grassland, woodland savannas, and shrublands were the regions most affected by the fire, with an average of more than 20% of their total area burned annually, while environments with high rainfall and evergreen forests had an incidence of less than 10%. The semi-humid areas present greater fire presence. The validation of MODIS products was compatible with other studies in different regions of the world, but it shows that in Brazilian forests there is greater difficulty in detecting fires.

In this scenario, the description of the fire regime using remote sensing and environmental data is one of the most widely used forms in regional studies as a basis for decision making by fire managers, however, it should be noted the various limitations that these data present especially regarding the high omission of burned areas.

References

Alvarado ST, Fornazari T, Cóstola A, Morellato LPC, Silva TSF (2017) Drivers of fire occurrence in a mountainous Brazilian cerrado savanna: tracking long-term fire regimes using remote sensing. Ecological Indicators 78, 270–281. doi:10.1016/j.ecolind.2017.02.037.

Alvarado ST, Silva TSF, Archibald S (2018) Management impacts on fire occurrence: A comparison of fire regimes of African and South American tropical savannas in different protected areas. Journal of Environmental Management 218, 79–87. doi:10.1016/j.jenvman.2018.04.004.

Alves DB, Pérez-Cabello F (2017) Multiple remote sensing data sources to assess spatio-temporal patterns of fire incidence over Campos Amazônicos Savanna Vegetation

Enclave (Brazilian Amazon). Science of the Total Environment 601–602, 142–158. doi:10.1016/j.scitotenv.2017.05.194.

Aragão LEOC, Malhi Y, Barbier N, Lima AA, Shimabukuro Y, Anderson L, Saatchi S (2008) Interactions between rainfall, deforestation and fires during recent years in the Brazilian Amazonia. Philosophical Transactions of the Royal Society of London Series B, Biological Sciences 363, 1779–85. doi:10.1098/rstb.2007.0026.

Araújo FM de, Ferreira LG, Arantes AE (2012) Distribution Patterns of Burned Areas in the Brazilian Biomes: An Analysis Based on Satellite Data for the 2002-2010 Period. Remote Sensing 4, 1929–1946. doi:10.3390/rs4071929.

Archibald S (2016) Managing the human component of fire regimes: lessons from Africa. Philosophical Transactions of the Royal Society B: Biological Sciences 371, 20150346. doi:10.1098/rstb.2015.0346.

Archibald S, Lehmann CER, Gómez-dans JL, Bradstock RA (2013) Defining pyromes and global syndromes of fire regimes. doi:10.1073/pnas.1211466110/.

Archibald S, Nickless A, Scholes RJ, Schulze R (2010) Methods to determine the impact of rainfall on fuels and burned area in southern African savannas. International Journal of Wildland Fire 19, 774–782. doi:10.1071/WF08207.

Archibald S, Scholes RJ, Roy DP, Roberts G, Boschetti L (2010) Southern African fire regimes as revealed by remote sensing. International Journal of Wildland Fire 19, 861–878. doi:10.1071/WF10008.

Di Bella CM, Jobbágy EG, Paruelo JM, Pinnock S (2006) Continental fire density patterns in South America. Global Ecology and Biogeography 15, 192–199. doi:10.1111/j.1466-822X.2006.00225.x.

Bond WJ, Keeley JE (2005) Fire as a global 'herbivore': The ecology and evolution of flammable ecosystems. Trends in Ecology and Evolution 20, 387–394. doi:10.1016/j.tree.2005.04.025.

Bond WJ, Woodward F. I, Midgley GF (2005) The Global Distribtuion of Ecosystems in a world without Fire. New Phytologist 165, 525–538. doi:10.1111/j.1469-8137.2004.01252.x.

Boschetti L, Stehman S V., Roy DP (2016) A stratified random sampling design in space and time for regional to global scale burned area product validation. Remote Sensing of Environment 186, 465–478. doi:10.1016/j.rse.2016.09.016.

Bowman DMJS, Balch JK, Artaxo P, Bond WJ, Carlson JM, Cochrane MA, D'Antonio CMA, DeFries RS, Doyle JC, Harrison SP, Johnston FH, Keeley JE, Krawchuk MA,

Kull C a, Marston JB, Moritz M a, Prentice IC, Roos CI, Scott AC, Swetnam TW, van der Werf GR, Bowman DMJS, S.J. P, D'Antonio CM, Pyne SJ (2009) Fire in the Earth System. Science 324, 481–484. doi:10.1126/science.1163886.

Cardozo S, Pereira G, Shimabukuro YE, Moraes EC (2014) Avaliação Das Áreas Queimadas No Estado De Rondônia. Revista Brasileira de Cartografia v.66/3, p.705-716.

Caúla RH, Oliveira-Júnior JF, Lyra GB, Delgado RC, Heilbron Filho PFL (2015) Overview of fire foci causes and locations in Brazil based on meteorological satellite data from 1998 to 2011. Environmental Earth Sciences 74, 1497–1508. doi:10.1007/s12665-015-4142-z.

Congalton RG (1991) A review of assessing the accuracy of classifications of remotely sensed data. Remote Sensing of Environment 37, 35–46. doi:10.1016/0034-4257(91)90048-B.

Daldegan GA, de Carvalho Júnior OA, Guimarães RF, Gomes RAT, Ribeiro F de F, McManus C (2014) Spatial patterns of fire recurrence using remote sensing and GIS in the Brazilian savanna: Serra do Tombador Nature Reserve, Brazil. Remote Sensing 6, 9873–9894. doi:10.3390/rs6109873.

Durigan G, Ratter JA (2016) The need for a consistent fire policy for Cerrado conservation. Journal of Applied Ecology 53, 11–15. doi:10.1111/1365-2664.12559.

Eva H, Lambin EF (2000) Fires and land-cover change in the tropics:a remote sensing analysis at the landscape scale. Journal of Biogeography 27, 765–776. doi:10.1046/j.1365-2699.2000.00441.x.

Fleiss JL, Levin B, Paik MC (2003) 'Statistical Methods for Rates and Proportions.' (John Wiley & Sons, Inc.: Hoboken, NJ, USA, NJ, USA) doi:10.1002/0471445428.

Friedl MA, Sulla-Menashe D, Tan B, Schneider A, Ramankutty N, Sibley A, Huang X (2010) MODIS Collection 5 global land cover: Algorithm refinements and characterization of new datasets. Remote Sensing of Environment 114, 168–182. doi:10.1016/j.rse.2009.08.016.

Giglio L, Boschetti L, Roy DP, Humber ML, Justice CO (2018) The Collection 6 MODIS burned area mapping algorithm and product. Remote Sensing of Environment 217, 72–85. doi:10.1016/j.rse.2018.08.005.

Giglio L, Loboda T, Roy DP, Quayle B, Justice CO (2009) An active-fire based burned area mapping algorithm for the MODIS sensor. Remote Sensing of Environment 113, 408–420. doi:10.1016/j.rse.2008.10.006.

Giglio L, Schroeder W, Justice CO (2016) The collection 6 MODIS active fire detection algorithm and fire products. Remote Sensing of Environment 178, 31–41. doi:10.1016/j.rse.2016.02.054.

Hantson S, Padilla M, Corti D, Chuvieco E (2013) Strengths and weaknesses of MODIS hotspots to characterize global fire occurrence. Remote Sensing of Environment 131, 152–159. doi:10.1016/j.rse.2012.12.004.

Instituto Brasileiro de Geografia e Estatística (IBGE) (2002) Mapa de Climas do Brasil. http://portaldemapas.ibge.gov.br.

Krawchuk MA, Moritz MA, Parisien MA, Van Dorn J, Hayhoe K (2009) Global pyrogeography: The current and future distribution of wildfire. PLoS ONE 4,. doi:10.1371/journal.pone.0005102.

Mohler R, Goodin D (2016) An Assessment of the Accuracy of the MCA45A1 Burned Area Product in Tallgrass Prairie. Papers in Applied Geography 2, 253–260. doi:10.1080/23754931.2015.1115368.

Moreira AG (2000) Effects of fire protection on savanna structure in central Brazil. Journal of Biogeography 27, 1021–1029. doi:10.1046/j.1365-2699.2000.00422.x.

Mouillot F, Schultz MG, Yue C, Cadule P, Tansey K, Ciais P, Chuvieco E (2014) Ten years of global burned area products from spaceborne remote sensing-A review: Analysis of user needs and recommendations for future developments. International Journal of Applied Earth Observation and Geoinformation 26, 64–79. doi:10.1016/j.jag.2013.05.014.

Murphy BP, Bradstock RA, Boer MM, Carter J, Cary GJ, Cochrane MA, Fensham RJ, Russell-Smith J, Williamson GJ, Bowman DMJS (2013) Fire regimes of Australia: A pyrogeographic model system. Journal of Biogeography 40, 1048–1058. doi:10.1111/jbi.12065.

Olofsson P, Foody GM, Herold M, Stehman S V., Woodcock CE, Wulder MA (2014) Good practices for estimating area and assessing accuracy of land change. Remote Sensing of Environment 148, 42–57. doi:10.1016/j.rse.2014.02.015.

Overbeck GE, Vélez-Martin E, Scarano FR, Lewinsohn TM, Fonseca CR, Meyer ST, Müller SC, Ceotto P, Dadalt L, Durigan G, Ganade G, Gossner MM, Guadagnin DL, Lorenzen K, Jacobi CM, Weisser WW, Pillar VD (2015) Conservation in Brazil needs to include non-forest ecosystems. Diversity and Distributions 21, 1455–1460. doi:10.1111/ddi.12380.

Padilla M, Stehman S V., Chuvieco E (2014) Validation of the 2008 MODIS-MCD45

global burned area product using stratified random sampling. Remote Sensing of Environment 144, 187–196. doi:10.1016/j.rse.2014.01.008.

Padilla M, Stehman S V., Ramo R, Corti D, Hantson S, Oliva P, Alonso-Canas I, Bradley A V., Tansey K, Mota B, Pereira JM, Chuvieco E (2015) Comparing the accuracies of remote sensing global burned area products using stratified random sampling and estimation. Remote Sensing of Environment 160, 114–121. doi:10.1016/j.rse.2015.01.005.

Pontius RG, Millones M (2011) Death to Kappa: Birth of quantity disagreement and allocation disagreement for accuracy assessment. International Journal of Remote Sensing 32, 4407–4429. doi:10.1080/01431161.2011.552923.

Roy DP, Boschetti L (2009) Southern Africa validation of the MODIS, L3JRC, and GlobCarbon burned-area products. IEEE Transactions on Geoscience and Remote Sensing 47, 1032–1044. doi:10.1109/TGRS.2008.2009000.

Roy DP, Jin Y, Lewis PE, Justice CO (2005) Prototyping a global algorithm for systematic fire-affected area mapping using MODIS time series data. Remote Sensing of Environment 97, 137–162. doi:10.1016/j.rse.2005.04.007.

Schmidt IS, Fonseca CB, Ferreira MC, Sato MN (2016) Implementação do Programa Piloto de Manejo Integrado do Fogo em três Unidades de Conservação do Cerrado. Biodiversidade Brasileira 6, 55–70.

Schroeder W, Morisette JT, Csiszar I, Giglio L, Morton D, Justice CO (2005) Characterizing vegetation fire dynamics in Brazil through multisatellite data: Common trends and practical issues. Earth Interactions 9,. doi:10.1175/EI120.1.

Tsela P, Wessels K, Botai J, Archibald S, Swanepoel D, Steenkamp K, Frost P (2014) Validation of the two standard MODIS satellite burned-area products and an empirically-derived merged product in South Africa. Remote Sensing 6, 1275–1293. doi:10.3390/rs6021275.

Wittkuhn RS, Hamilton T (2010) Using fire history data to map temporal sequences of fire return intervals and seasons. Fire Ecology 6, 97–114. doi:10.4996/fireecology.0602097.

remote sensing

CAPÍTULO 3 – Burned-Area Detection in Amazonian Environments Using Standardized Time Series Per Pixel in MODIS Data[2]

Níckolas Castro Santana [1], Osmar Abílio de Carvalho Júnior [1], Roberto Arnaldo Trancoso Gomes [1] and Renato Fontes Guimarães [1]

[1]   Departamento de Geografia Campus Universitário Darcy Ribeiro, Asa Norte, Universidade de Brasília (UnB), DF 70910-900, Brasília, Brazil;

Abstract: Fires associated with the expansion of cattle ranching and agriculture have become a problem in the Amazon biome, causing severe environmental damages. Remote sensing techniques have been widely used in fire monitoring on the extensive Amazon forest, but accurate automated fire detection needs improvements. The popular Moderate Resolution Imaging Spectroradiometer (MODIS) MCD64 product still has high omission errors in the region. This research aimed to evaluate MODIS time series spectral indices for mapping burned areas in the municipality of Novo Progresso (State of Pará) and to determine their accuracy in the different types of land use/land cover during the period 2000–2014. The burned area mapping from 8-day composite products, compared the following data: near-infrared (NIR) band; spectral indices (Burnt Area Index (BAIM), Global Environmental Monitoring Index (GEMI), Mid Infrared Burn Index (MIRBI), Normalized Burn Ratio (NBR), variation of Normalized Burn Ratio (NBR2), and Normalized Difference Vegetation Index (NDVI)); and the seasonal difference of spectral indices. Moreover, we compared the time series normalization methods per pixel (zero-mean normalization and Z-score) and the seasonal difference between consecutive years. Threshold-value determination for the fire occurrences was obtained from the comparison of MODIS series with visual image classification of Landsat Thematic Mapper (TM), Enhanced Thematic Mapper Plus (ETM+), and Operational Land Imager (OLI) data using the overall accuracy. The best result considered the following factors: NIR band and zero-mean normalization, obtaining the overall accuracy of 98.99%, commission errors of 32.41%, and omission errors of 31.64%. The proposed method presented better results in burned area detection in the natural fields (Campinarana) with an overall accuracy value of 99.25%, commission errors of 9.71%, and omission errors of 27.60%, as well as pasture, with overall accuracy value of 99.19%, commission errors of 27.60%, and omission errors of 34.76%. Forest areas had a lower accuracy, with an overall accuracy of 98.62%, commission errors of 23.40%, and omission errors of 49.62%. The best performance of the burned area detection in the pastures is relevant because the deforested areas are responsible for more than 70% of fire events. The results of the proposed method were better than the burned area products (MCD45, MCD64, and FIRE-CCI), but still presented limitations in the identification of burn events in the savanna formations and secondary vegetation.

Keywords: fire; forest fires; fire regime; time series; remote sensing; Amazon forest

1. Introduction

Human disturbance is the primary cause of burned events in the Amazon Forest, mainly in areas of deforestation, agriculture, and pastures [1–4]. Anthropogenic fire from farming and livestock usually escapes into neighboring forest areas, resulting in large-scale fire events [5]. Therefore, land-use determines the burning patterns of the Amazon forest, where areas with

---

[2]Artigo publicado no periódico *Remote Sensing*

intense deforestation, fragmentation, and the presence of highways have a higher number of fires, whilst Conservation Units and Indigenous Reserves are essential barriers [6–10]. The Amazon forest has a high vulnerability to fire incidences due to the following factors: most species do not tolerate recurrent fire events, floristic and structural changes, and organic matter incineration that is essential for the maintenance of ecological processes [11–13].

The concentration of Amazon forest fires is along an area called the arc of deforestation, which presents an intensification of anthropogenic actions along the eastern and southern forest edges. Compared with the central zones of the forests, the arc of deforestation has lower biomass and drier climate resulting in larger burnings [14,15]. During severe drought periods, there is an increase in tree mortality on forest edges and the accumulation of dry leaves [16,17], which favor fire events mainly in degraded forests [18–20]. Models of climate change in the Amazon rainforest provide for the expansion of fires due to more frequent droughts and land use intensification [4,21].

In the monitoring of the Amazon Forest (5.5 million km^2), the use of remote sensing data is necessary due to its synoptic view, rapidity, and high cost-effectiveness. The major impediment to optical remote sensing in the Amazon region is the high atmospheric interference from cloud cover and aerosols [22]. Therefore, high temporal resolution optical sensors are essential for the monitoring of Amazon forest fires, increasing the possibility of acquiring good quality images without atmospheric interference [23–25]. Among the high temporal resolution sensors, the Moderate Resolution Imaging Spectroradiometer (MODIS) sensor has been prominent in the mapping of fires in the different terrestrial biomes [26–28], offering global scale products of active fires [29,30] and burned areas [26,29]. Active fire detection captures the energy emission using thermal infrared imagery (3.6–12 µm range), and provides information only of burning pixels during the passage of the satellite, not allowing the burned area quantification [26,29,31]. In contrast, the post-fire mapping evidenced by ash, coal, and vegetation changes enable obtaining of the perimeter, area, and an estimate of damage caused by forest fires. Thus burned area products (MODIS-MCD45/MCD64) were extensively used in diversity studies about ecosystem structure change and biomass burning emissions [24,32–34]. Padilla *et al.* [35] performed a validation of the MCD45 and MCD64 products for several terrestrial biomes, obtaining estimated commission errors rates of 46% and 42%, and omission error rates of 72% and 68% for MCD45 and MCD64, respectively. Therefore, the burned area product tends to underestimate the extent of the burned area, where the omission errors were higher than commission errors [35–38]. Cardozo *et al.* [39] showed that the MODIS burned area product (MCD45) in the Amazon region at different dates, presents values higher than 90% of omission errors, which corresponds to low accuracy and a need for the development of new algorithms adjusted for this region.

Different remote sensing methods have been proposed for the burned area mapping. The most widely used processing using bi-temporal images combines two algebraic operations: (a) Spectral index calculation, where the most commonly used are the Normalized Burn Ratio (NBR) [40] and Normalized Difference Vegetation Index (NDVI) [41]; and (b) Seasonal differences between the pre- and post-burned indices, such as dNDVI [42] and dNBR [40]. Other indices have been proposed such as the Burned Area Index Modified (BAIM) [43], Global Environmental Monitoring Index (GEMI) [44], Mid-Infrared Burned Index (MIRBI) [45], and the variation of Normalized Burn Ratio (NBR2) [46].

The adaptation of the index differentiation method to long-term MODIS time series [47,48] considers the entire time series of one year with its antecedent, generating an image set rather than just a single difference image from a custom selection. However, the automatic difference over the time series shows a significant increase in signal-to-noise ratio, with respect to the bi-temporal images that were pre-defined by the analyst. Therefore, the application of the differencing method in continuous time series requires methodological improvements [47,48]. Lhermitte *et al.* [49] tried to solve this problem by selecting control pixels surrounding the unburned area based on time series similarity. This approach considers the spatial context
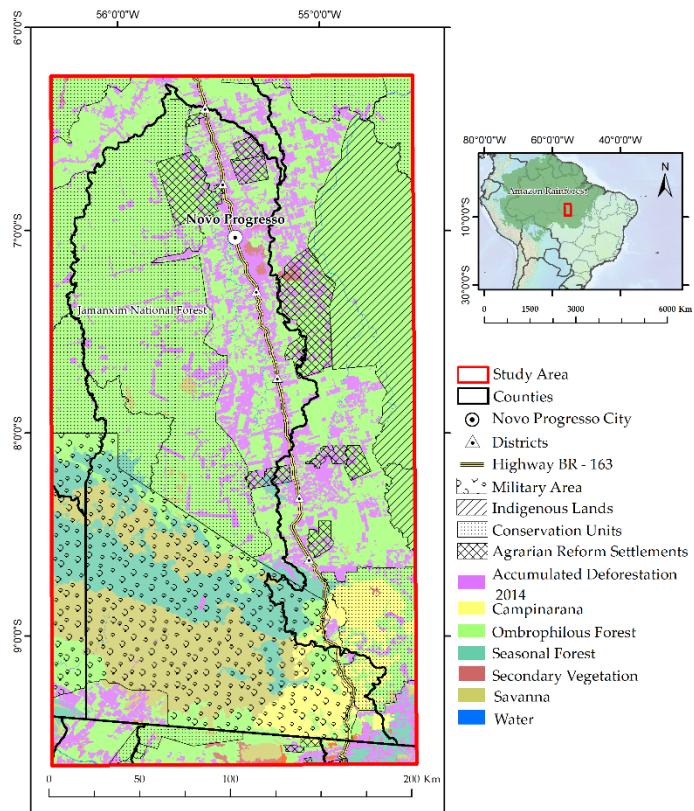
(neighboring pixels) to minimize the external influences and phenological variations [50]. However, this method has severe limitations for complete automation, requiring supervision for not including neighboring pixels with different characteristics as compared to the analyzed pixel.

A proposed alternative is the use of normalized time series using the Z-score (mean zero and standard deviation equal to 1) or means (mean zero), which allow highlighting of the burned areas without changing the signal-to-noise ratio [47]. The normalization procedure is very promising because it does not require neighboring control pixels, considering only the time series of the pixel. This method is different from that proposed by the research of Diáz-Delgado et al. [50] and Lhermitte et al. [49], because it is fast and simple data processing restricted to the pixel, which generates an image that emphasizes the burning points in different environments.

The present paper aims to evaluate and compare different methods of burned area mapping from MODIS time series (BAIM, GEMI, MIRBI, NBR, NBR2, NDVI, and the near-infrared band) and normalized time series per pixel (Mean and Z-Score) in different land covers in the municipality of Novo Progresso, belonging to the Amazon region. This research also evaluates the spatial and temporal distribution of fire in different land use types.

2. Study Area

The study area is the municipality of Novo Progresso and surroundings (74,552.1518 km²), State of Pará, Southeast Brazilian Amazon (Figure 3.1). The climate is Humid Equatorial with annual precipitation ranging from 2050 mm to 2650 mm and average temperature above 25ºC [51,52]. The rainy season is from November to May and the dry season, from June to October, when most fire events occur [53].

Figure 3.1. Location of the study area, showing the territorial units and the land-use and land-cover types derived from the following data: Land Use [54,55], Conservation Units [56], Indigenous Lands [57], Land Reform Settlements [58], and Military Area [59].
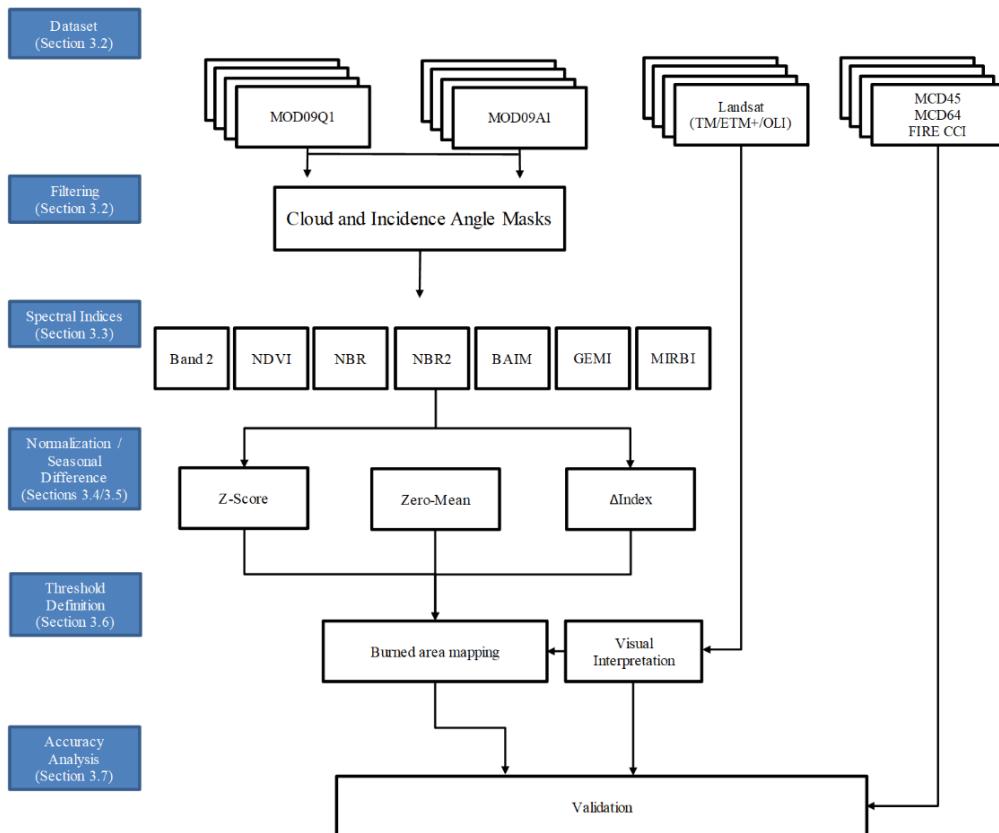
The predominant vegetation is classified as Open Ombrophilous Sub-Montane Forest, but it also contains areas of Forest Savanna and Submontane Semideciduous Seasonal Forest [55]. This

region has been inhabited by indigenous populations, currently restricted to the Baú and Menkragnoti Indigenous Reserves [60]. The construction of the federal highway BR-163 in the 1980s brought an intense migratory flow that increased the soybean cultivation, livestock, and infrastructure projects [61]. The Conservation Units curb deforestation growth within Integral Protection Units (Rio Novo National Park, Cristalino State Park, Nascentes da Serra do Cachimbo Biological Reserve, and Crystal Private Reserve Natural Heritage) and Sustainable Use Units (Jamanxim and Altamira National Forests, Iriri State Forest and Tapajós Environmental Protection Area) [56]. The Agrarian Reform Settlements and Military Areas complement the federal land types of the region [58,59]. The leading causes of fire are deforestation and pasture maintenance [2,9].

3. Materials and Methods

3.1. Methodology Flowchart

The methodology adopted the following steps, including MODIS 8-day composites data acquisition (MOD09A1 and MOD09Q1), calculation of spectral indices, filtering, time series normalization, burned area mapping, and validation (Figure 3.2). The research calculated seven spectral indices and applied in each index two types of time series normalization per pixel (Z-score and zero-mean) and the seasonal difference method, computing a total of 21 different procedures. Finally, we compared the burned areas by the different MODIS image processing with the following data: Visual interpretation of Landsat images (Thematic Mapper (TM)/ Enhanced Thematic Mapper Plus (ETM+)/Operational Land Imager (OLI)) and burned area products (MCD45 [31], MCD64 [26], and Fire CCI) [62,63].

Figure 3.2. Methodology flowchart.

3.2. MODIS Data

The MODIS sensor aboard the Terra and Aqua satellites was developed by the National Aeronautics and Space Administration (NASA) to provide continuous observations of the Earth's surface [64]. This sensor has 36 spectral bands ranging from 0.4 μm to 14.4 μm at three spatial resolutions (250, 500 meters, and 1 kilometer) according to the band. We used the following MODIS products: (a) 8-day composite surface reflectance at 250 and 500-m resolution (MOD09A1 and MOD09Q1); (b) daily burned area at 500-m resolution (MCD45A1) [31];(c) daily burned area at 500-m resolution (MCD64A1) [26], and (d) monthly burned area product at 300-m resolution derived from both MODIS and Medium Resolution Imaging Spectrometer (MERIS) sensors (FIRE CCI) [62,63]. The data download sites were the NASA Land Data Products and Services website (https://search.earthdata.nasa.gov/) and from the European Space Agency (ESA) Fire CCI website (http://www.esa-fire-cci.org/).

MODIS surface reflectance product is composed by bands 1–2 (0.6μm–0.9μm) at 250-m spatial resolution and bands 3–7 (0.4 μm–2.1μm) at 500-m spatial resolution [65]. These images are available as daily data and 8-day composite product that select the best observation within the time interval and eliminate the presence of artifacts such as cloud or cloud shadow. The traditional temporal composite based on the maximization of values can cause loss of information of burned areas, which are characterized by low albedo [66]. In contrast, daily images have more noise and atmospheric effects that can also lead to the insertion of invalid information.

The acquisition of MODIS data covered the period 2000–2014, resulting in 683 8-day composite images. We discarded the poor-quality pixels with (a) cloud coverage, (b) related to the high and medium aerosol classes, and (c) relative to frontal scattering and with zenith angles greater than 60°, because of the influence of the spectral mixing of the targets with their shadows, especially in the near-infrared (NIR) band [66,67]. We converted the MODIS images from native sinusoidal projection to the Universal Transverse Mercator (UTM, WGS 84 ellipsoid) projection. Spectral bands with the spatial resolution of 500 m were resampled at 250 m using the nearest neighbor interpolation method to make the data compatible.

3.3. Spectral Indices

The data compared to the fire detection were: (a) Only the NIR band (band 2); (b) NDVI, NBR, NBR2, BAIM, GEMI, and MIRBI index; and (c) temporal differencing (Δ) (Table 3.1). The NIR band allows a high separation of the burned areas compared to other spectral channels [68,69]. The NDVI uses the RED and NIR bands, and is widely used to highlight vegetation changes [70]. The NBR index developed to highlight burned areas adopts the normalized difference between the NIR and Short Wave Infrared (SWIR) [40]. The NBR2 and MIRBI indices are variations of the NBR and NDVI indices, considering the SWIR1 and SWIR channels to highlight the burn areas [45,46]. The BAIM index maximizes the spectral deviation between the burned area and other land covers from the NIR and SWIR channels [43]. The GEMI index was determined to evaluate the vegetation conditions, reducing the content of both the NIR and RED channels [45].

Seasonal differencing is a change detection method with extensive use in the analysis of the severity of a fire [47,48,71–73]. This method consists of subtracting the values of spectral indices or bands acquired before and after a fire event (pre-fire minus post-fire) to emphasize the changes related to the fire. The advantage of the method is the possibility of defining the fire severity, apart from indicating the areas with vegetation regeneration [46]. Despite the proven utility of the technique in many different environments, there are few details about its application in the Amazon region or other areas of tropical forests. Seasonal differencing techniques have been used with different spectral indices including: ΔNBR [48,74], ΔNDVI [75], ΔNBR2 [76], ΔBAIM [74], ΔGEMI [77], and ΔMIRBI [78].

Table 3.1. Spectral indices to highlight the burned areas adopted in this research.

Index	Equation	Bibliographic reference
NBR/ΔNBR	$NBR = \dfrac{NIR - SWIR2}{NIR + SWIR2}$	[40,79]
NDVI/ΔNDVI	$NDVI = \dfrac{NIR - RED}{NIR + RED}$	[41]
NBR2/ΔNBR2	$NBR2 = \dfrac{SWIR1 - SWIR2}{SWIR1 + SWIR2}$	[46]
BAIM/ΔBAIM	$BAIM = \dfrac{1}{(0.05 - NIR)^2 + (0.2 - SWIR2)^2}$	[43]
GEMI/ΔGEMI	$GEMI = n(1 - 0.25\,n) - \dfrac{RED - 0.125}{1 - RED}$	[44]
MIRBI/ΔMIRBI	$MIRBI = (10 * SWIR2) - (9.8 * SWIR1) + 2$	[45]
Δ	$prefire - postfire$	

Notes: In GEMI $n = \dfrac{2(NIR^2 - RED^2) + 1.5_{NIR} + 0.5_{RED}}{NIR + RED + 0.5}$
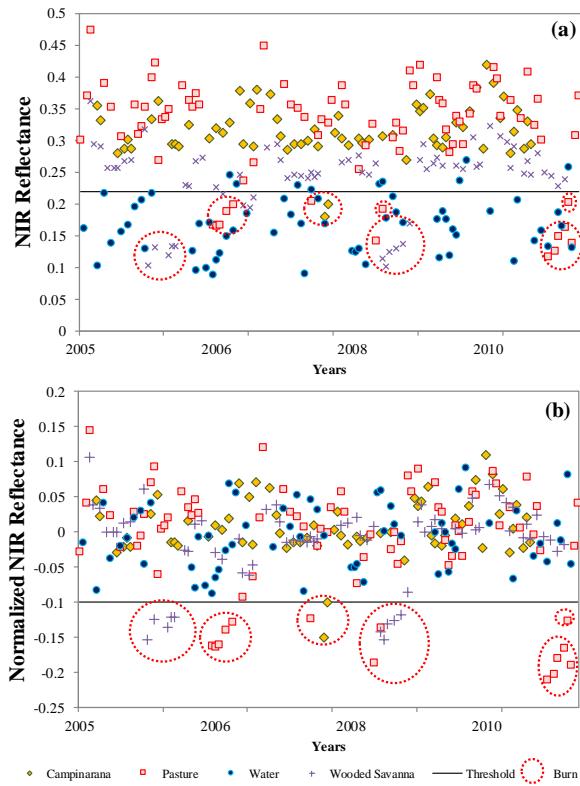
3.4. Time Series Standardization per Pixel

The burned areas show differences in spectral behavior according to the vegetation type and the period after the fire [80]. In the Amazon, burning occurs mostly in pasture and agriculture, but there are significant impacts on forest and savanna areas [81,82]. Therefore, the detection of areas burned by remote sensing should be adaptable for environmental differences. The normalized time series allows to equate the behavior of distinct vegetation and highlight the burned areas [83]. The normalization procedures consider the temporal data per pixel. The two evaluated methods of time series normalization were: Zero-mean (mean equal to 0) and Z-score (mean equal to 0 and standard deviation equal to 1) expressed by the following formulations:
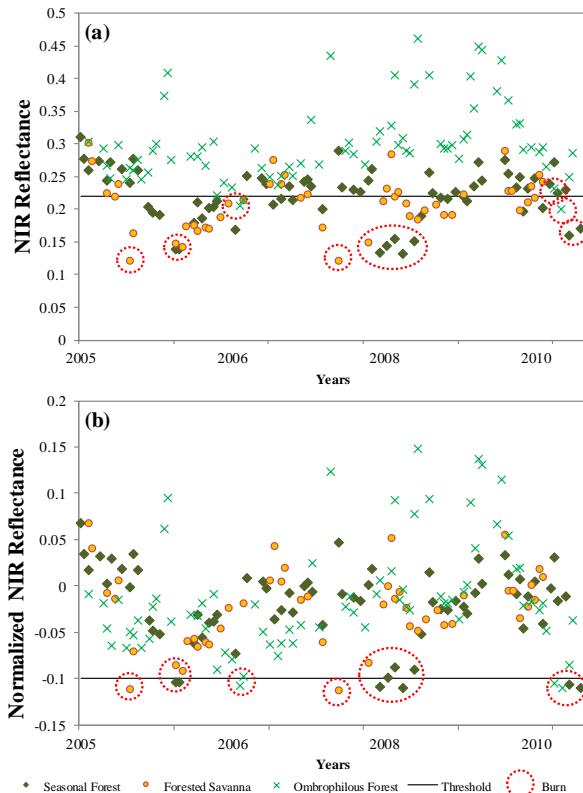
$$Zero - mean = x_t - \mu \tag{1}$$

$$Z - score = \frac{x_t - \mu}{\sigma} \tag{2}$$

where x is the pixel value, t is the time, μ is the mean of the remote sensing data over time (t) for a pixel, and σ is its standard deviation. Therefore, the two normalization methods present negative values when the remote sensing values are smaller than the temporal mean and positive values when they are above. The Z-score approach was successful for burned area detection in regions of savanna vegetation [83]. Normalization makes the burned-area features of different environments compatible and eliminates confusion with low-albedo targets (e.g., water). As an example, we compared the MODIS NIR temporal series of water bodies with burned areas in natural fields (Campinarana), grasslands, and wooded savannas, showing an overlap of values and the inability to distinguish different targets by a single threshold value (Figure 3.3a). The time series normalized by the mean allows separating the burned area and water bodies by a single threshold (Figure 3.3b). Moreover, the Ombrophilous forests have reflectance values in the NIR range that are higher than the seasonal forests and forested savannas, which remain higher even after a fire event and prevent the use of a single threshold for the detection of burning among these types of vegetation (Figure 3.4a). The method of time series normalization equalizes the fire points. Thus, forest time series normalized by the mean decrease false fire events significantly, but the omission of some points occurs mainly in the seasonal forest and forested savanna (Figure 3.4b).
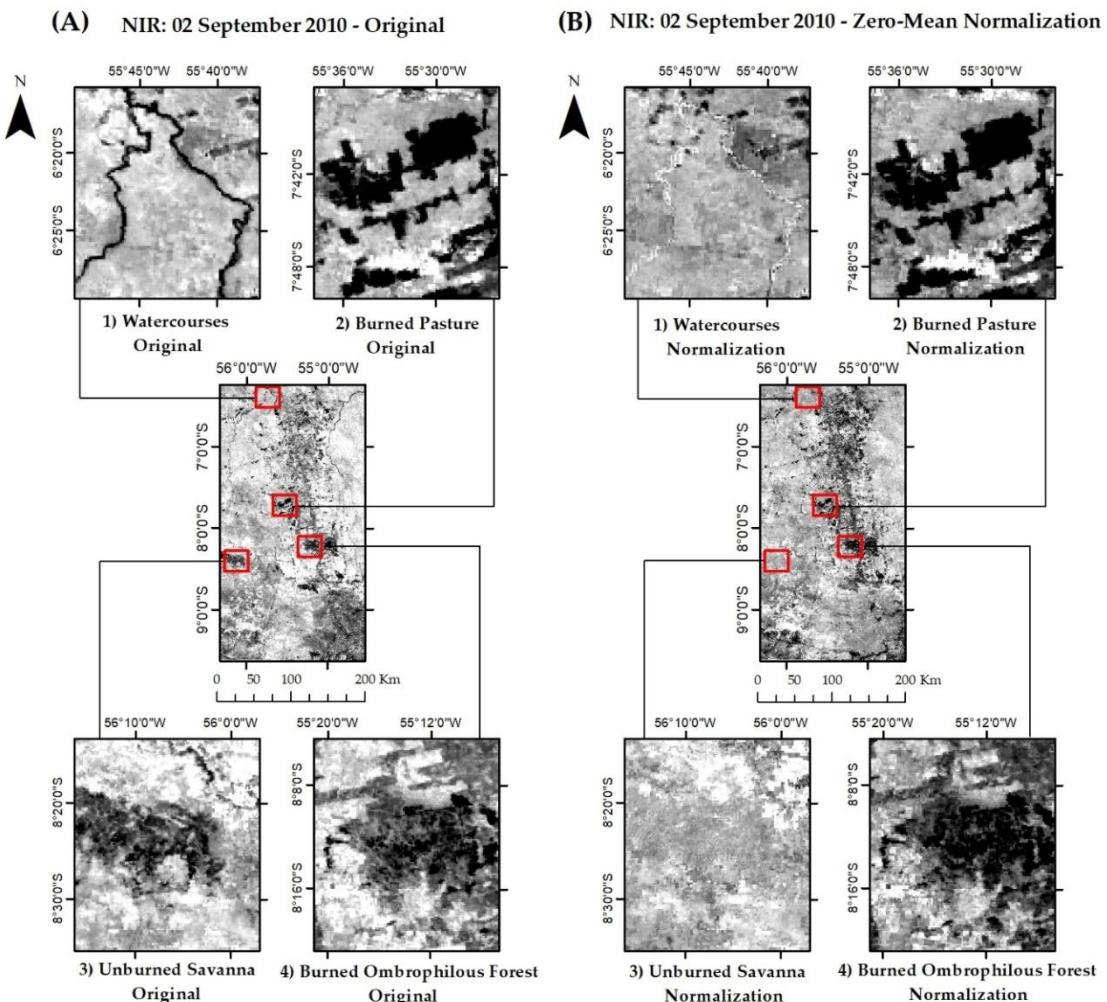
Figure 3.3. Comparison of MODIS near-infrared time series for different burned and unburned targets within Campinarana, Pasture, Water and Wooded Savanna: (a) without normalization; (b) with zero-mean normalization. Missing values are masked pixels.

Figure 3.4. Comparison of MODIS near-infrared time series for different burned and unburned targets within Seasonal Forest, Forested Savanna, and Ombrophilous Forest: (**a**) without normalization; (**b**) with zero-mean normalization. Missing values are masked pixels.

In addition to the relevant results in the time dimension, normalization per pixel also causes a significant digital enhancement of the burned areas in the spatial dimension. In images without normalization, the savanna and watercourses have similar values to the burned areas, being confused in the application of a threshold value (Figure 3.5a). The normalized image allows an apparent distinction between the burned areas compared to water bodies, since they have significantly lower values (Figure 3.5b).

Figure 3.5. Exemplification of digital enhancement using normalized time series of the near-infrared band. (A) without normalization; (B) with zero-mean normalization. The zero-mean normalization allows the distinction between burned and unburned targets.

3.5. Seasonal Differencing
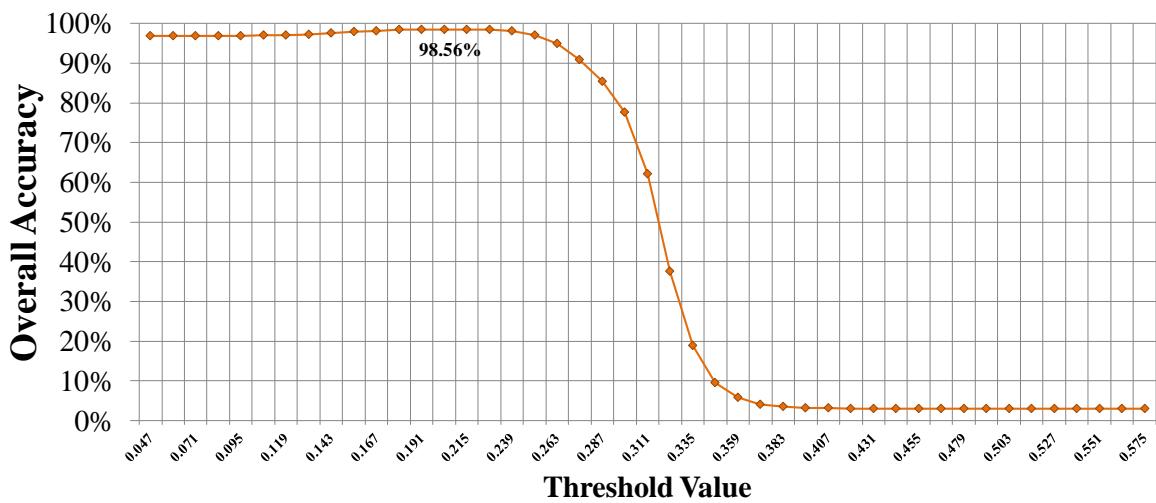
The seasonal difference is one of the most commonly used methods for the detection of burned areas, but studies focus on bi-temporal analysis based on preselected images. Therefore, most studies adopt a specific fire event, where selection by the analyst of two images near the birthday dates considers the low presence of clouds or noises. Few studies detect areas burned by seasonal differences in long-term time series of satellite images, using tens or hundreds of images. The seasonal difference algorithms in long time series assume fixed time intervals and present a certain amount of random noise, since it is impossible to get multiple cloudless and noise-free images on birthday dates in different years [47–49,83]. Thus, some proposals have been made to mitigate interference, considering spatial and temporal dimensions. A spatial approach involves selecting control pixels for pre-fire data by examining the contextual neighborhood

around the focal pixel and averaging two or more similar pixels within spatial windows [84,85]. A temporal approach involves the use of the average of the birthday data of the complete time series rather than the simple data from the previous year [47,83].

In this research, the seasonal differencing considered two strategies: (a) Automatic method with a fixed annual interval, where a pre-fire image was subtracted from the post-fire with a range of one year exactly; and (b) Method to select a good quality image closer to the anniversary date when the previous year's image had poor quality or cloud coverage. The latter option may have non-fixed subtraction intervals, performing the temporal search for a better-quality pixel within a time window.

3.6. Landsat Reference Data and Burned Area Mapping

The threshold definition for separation between burned and unburned areas used the method developed by Carvalho Júnior *et al.* [83]. This procedure compares a reference map of the burned areas, previously obtained from an image with better spatial resolution, and the burned areas acquired by a sequence of thresholds from a spectral band or spectral index. Thus, the method generates an overall accuracy curve from the comparison of the reference map and the classifications using threshold values (Figure 3.6). The fire detection in other time series images used the threshold value with the best overall accuracy. In this research, the definition of the best threshold used seven reference maps of the burned area produced by the visual interpretation of the Landsat TM and ETM+ images on the following dates: 15/08/2001, 19/09/2002, 28/07/2003, 30/07/2004, 03/09/2005, 10/08/2008, and 01/09/2010 (Table 3.2, Figure 3.7). The acquisition of Landsat data came from the United States Geological Survey (USGS) website (https://earthexplorer.usgs.gov/). The visual image interpretation methodology [35,86] used at least two different dates to identify burned areas and exclude false positives. The fires in the region occur mainly during the dry season, where there is more availability of cloudless images and Landsat/MODIS pairs with matching dates, avoiding the possible omission of fires due to different dates.
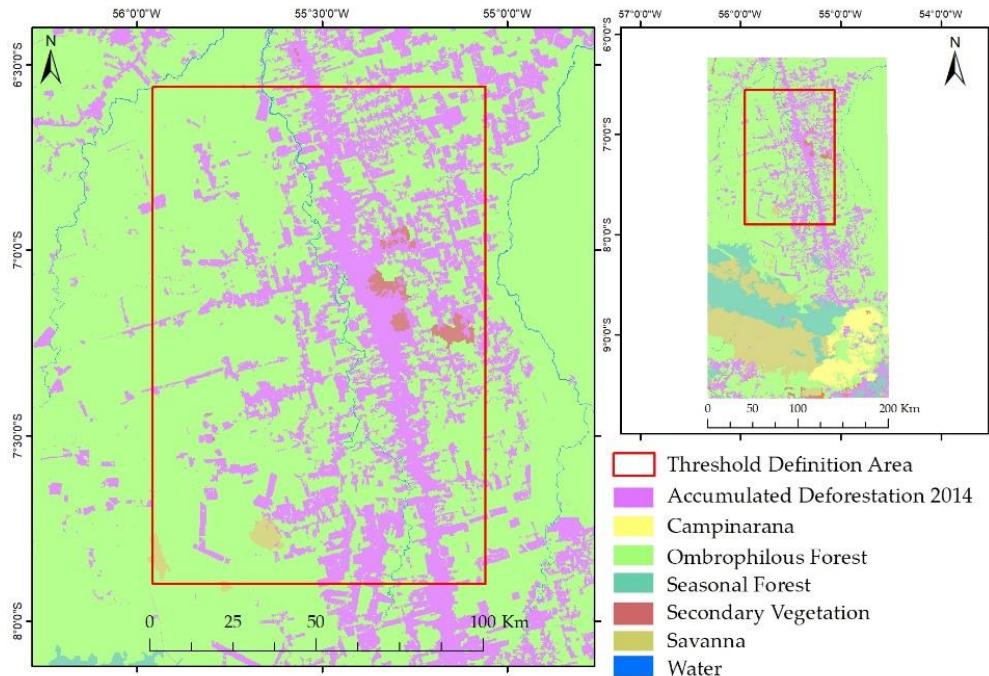
Figure 3.6. Example of the overall accuracy curve between the burned areas from the visual interpretation of Landsat-5 TM image (30/07/2004) and the results from the classifications using different thresholds in the MODIS near-infrared band. The optimal threshold is 0.215 in the band 2 image (overall accuracy of 98.56%).

The tests covered an area corresponding to 20% of the study area (14,689.638 km²), containing the highest rate of deforestation and burning in the analyzed image set. The images included three classes: burned area, unburned area, and low-quality pixels (clouds and noise) from the quality mask available with Landsat images on the EarthExplorer site (Table 3.2). The

seasonal difference with the fixed interval presupposes the image selection with exactly one previous year, being able to have a high percentage of pixels with atmospheric interference. The seasonal difference with the closest high-quality image selects data with the lowest cloud coverage within a user-stipulated period.

Table 3.2. Low-quality pixel percentage of Landsat scenes used to define the threshold value.

Image Date	Sensor	Percentage of low-quality pixels		
		Normalization Method	Seasonal Difference (Fixed Interval)	Seasonal Difference– (Closest High-Quality Image)
15/08/2001	ETM+	34%	-	-
19/09/2002	ETM+	25%	77%	19%
28/07/2003	TM	13%	82%	24%
30/07/2004	TM	44%	51%	13%
03/09/2005	TM	26%	51%	12%
10/08/2008	TM	47%	57%	45%
01/09/2010	TM	7%	49%	22%
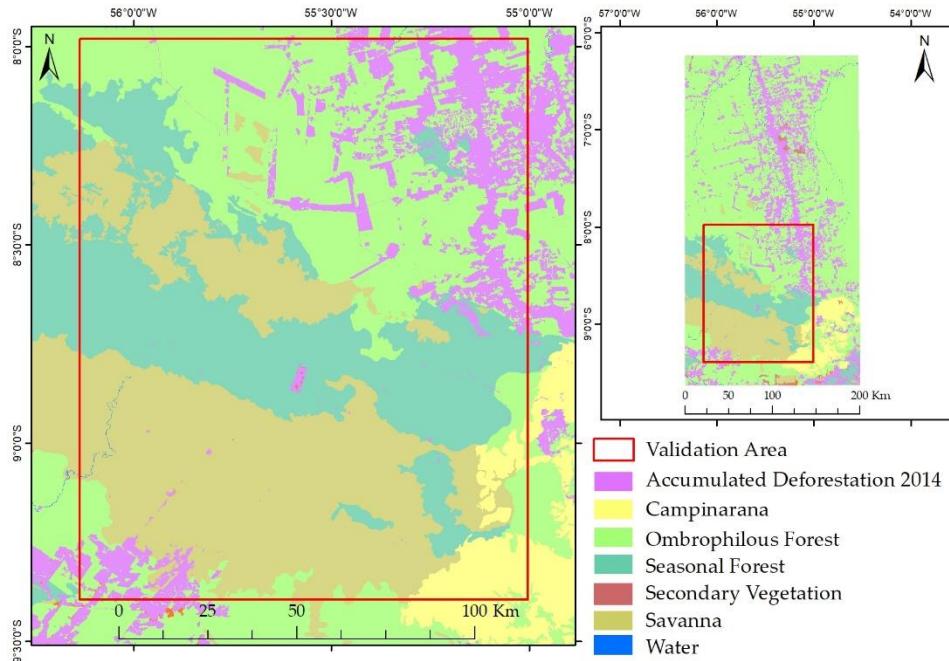
Figure 3.7. Area used to set the best threshold value.

We applied the average of the seven best thresholds in the complete time series of 14 years, generating a time series of burned area mask. The best threshold definition uses the equation $x \leq y$, where x is the value of the burned pixel and y is the threshold value for band 2, GEMI, NBR, NBR2, NDVI, ΔBAIM, and ΔMIRBI, while the equation $x \geq y$ for BAIM, MIRBI, ΔBand2, ΔGEMI, ΔNBR, ΔNBR2, and ΔNDVI.

The overlap of the same-year polygons resulted in burned areas during the year. We used an algorithm that eliminated the burned areas that did not occur on at least two consecutive dates (8-day), which were considered noises because the ash of burns in savanna and forest requires a longer time to be extinguished [69,87,88]. The errors of areas burned in water bodies were corrected from the land use/land cover mapping produced by the Amazon Surveillance System (SIVAM) [55].

3.7. Dataset Comparison and Accuracy Analysis

Accuracy analysis used visual interpretations of independent areas of those adopted in the determination of optimal threshold values (Figure 3.8). The methodology assumed was proposed by Padilla et al. [89], which considers the confusion matrices between the classification of MODIS and Landsat images (Table 3.3) and its indices: Overall Accuracy (OA) (Equation (3)), Commission Errors (CE) (Equation (4)), and Omission Errors (OE) (Equation (5)) [90].

Figure 3.8. Reference map of the study area.

Table 3.3. Confusion matrix.

		True condition (Landsat Classification)	
		Burned area	**Unburned area**
Predicted Condition	Burned area	True Positive (TP)	False Positive (FP)
(MODIS Classification)	Unburned area	False Negative (FN)	True Negative (TN)

$$OA = \frac{\sum TP + \sum TN}{Total\ Population} * 100 \tag{3}$$

$$CE = \frac{\sum FP}{\sum FP + \sum TP} * 100 \tag{4}$$

$$OE = \frac{\sum FN}{\sum FN + \sum TP} * 100 \tag{5}$$

We also used the Dice coefficient (DC), described in Reference [91]**,** which combines CE and OE into a single category according to the below Equation, as in Reference [38]:

$$DC = \frac{2 * a}{2 * a + b + c} \tag{6}$$

where "a" refers to the burned area mapped correctly in both methods, "b" the commission errors, and "c" the omission errors. Given DC is a measure of aggregate precision, it obscures differences in the individual measurements of CE and OE. Therefore, CB has limitations if CE and OE are not equally significant, in which case the accuracy analysis should be directed to the largest specific error [38].

The reference image corresponded to about 25% of the study area (19,486.3664 Km²) obtained from the visual interpretation of TM, ETM+, and OLI images on the following dates: 10/10/2001, 10/05/2002, 09/22/2003, 10/02/2004, 09/19/2005, 09/22/2006, 09/09/2007, 09/27/2008, 09/30/2009, 09/09/2010, 09/12/2011, 09/30/2012, 10/03/2013, and 09/28/2014. In 2012, we used Landsat 7 ETM+ images (even with the presence of errors) because it was the only sensor in operation of the Landsat program [92], the scan-line issues were masked and disregarded in that year's accuracy analysis.

The non-parametric McNemar's test [93] assessed the independence of the results obtained by pair-wise comparisons of the classifications [94]. The McNemar test calculates the chi-square distribution (x^2) considering the matrix elements of Table 4 in the following Equation:

$$x^2 = \frac{(f_{12} - f_{21})^2}{f_{12} + f_{21}} \tag{7}$$

Table 3.4. McNemar test between two classifications.

	Classification 2		
	Correct	Incorrect	Total
Classification 1			
Correct	f_{11}	f_{12}	$f_{11}+f_{12}$
Incorrect	f_{21}	f_{22}	$f_{21}+f_{22}$
Total	$f_{11}+f_{21}$	$f_{12}+f_{22}$	$f_{11}+f_{12}+f_{21}+f_{22}$

The McNemar test analysis considered 4000 random samples for each year between 2001 and 2014. The significance assessment compared the value of x^2 obtained with the tabulated value, indicating the null hypothesis when the x^2 value was less than 5% of significance (3.841), or rejection of the null hypothesis when the x^2 value was higher.

The validation of the MCD45 [36], MCD64 [26], and Fire CCI [62,63] products used the same data set to facilitate comparison with the proposed methodologies. The MCD45 uses an algorithm that identifies burned areas daily, eliminating false events such as cloud shadows. The MCD64 identifies persistent changes in the time series of vegetation indices and includes the localization of active fire to define boundary values for the burned area and unburned area. The Fire CCI product combines active fire pixel information and spectral changes of the MERIS sensor time series. These products are available in monthly data with 500 meters of resolution, where each pixel can indicate the exact day of the burn on Julian days (1–365), unburned area, cloud area, or water area [31,62]**.**

3.8. Analysis of the Spatial Relationships between Land Use/Land Cover Classes and Burned Area

Land use dynamics is a crucial factor to understand the spatial pattern of fires. In this spatial analysis, we used the land use/land cover mapping produced by the Amazon Surveillance System (SIVAM) [55] and deforestation provided by the National Institute for Space Research by Project for Monitoring Deforestation in the Legal Amazon (PRODES) [54]. In the SIVAM mapping, land use/land cover classes considered those established by the Brazilian Institute of Geography and Statistics [55]: Ombrophylous Forests, Seasonal Forests, Campinarana, Savanna, Secondary Vegetation, Annual Deforestation, and Water. As the PRODES methodology considers one year beginning in August, we used Landsat images to update deforestation by the end of each year from 2001 to 2014, resulting in annual land cover maps. The intersection of information allowed us to evaluate the interactions between deforestation, land use, and fire. Moreover, we assessed the influence of the BR 163 highway on the occurrence of fires, calculating the percentage of burned area in a buffer zone with distance intervals of 20km from the highway.

4. Results

4.1. Determination of the Best Threshold Value

The use of both the seasonal differencing and the zero-mean normalization improves the overall accuracy of the original images (Table 3.5). The zero-mean normalization obtained better precision results (overall accuracy) than the Z-score normalization (increasing false positives) and seasonal differencing (lower overall accuracy).

The BAIM presented the best accuracy index from the original data and the difference index (Table 3.5). The normalized NIR band by Z-score or by the mean presented the best fit for the burn area detection, with higher overall accuracy values than all the spectral indices evaluated. The BAIM, NIR band, GEMI, and MIRBI normalized by the mean had similar overall accuracy, while the NBR and its variation NBR2 presented the fifth-best performance, despite being a widely-used index for the mapping of burned areas. The NDVI showed the worst value for overall accuracy.

The annual difference already implies the loss of one year of the time series [83].Moreover, the use of fixed intervals without the image selection by quality causes the reduction of the validation area due to the presence of clouds in the differenced images (Table 3.2). Although the seasonal differences highlight the burned areas, there is confusion between newly cleared areas with or without burning and omission of pixels burned in consecutive years.
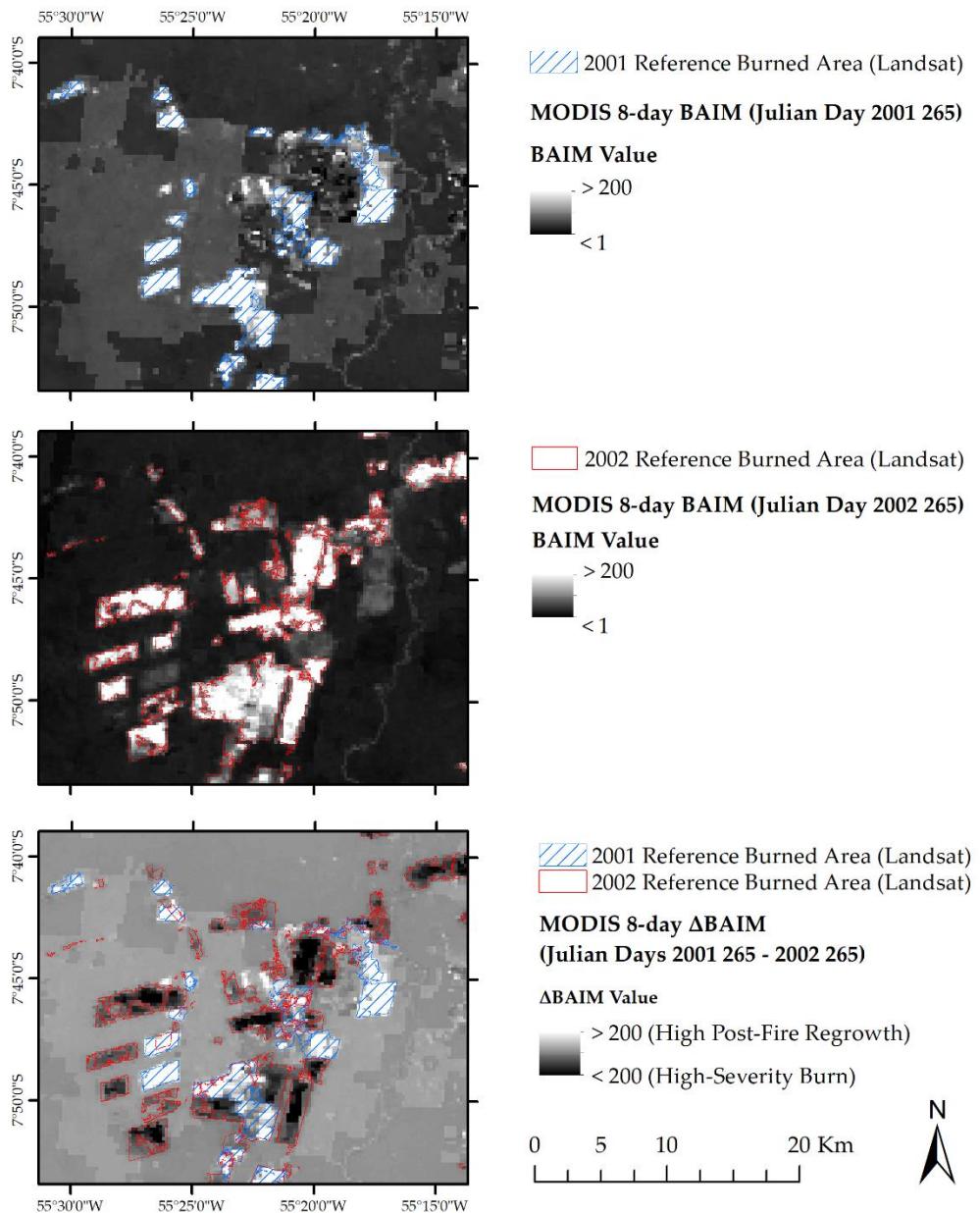
Table 3.5. Average of best thresholds and overall accuracy (OA) for different tested procedures in the years of 2001, 2002, 2004, 2005, 2008, and 2010.

	BAIM	Band 2	GEMI	MIRBI	NBR	NBR2	NDVI
Original Data							
Threshold	17.48	0.206	0.560	1.312	0.148	0.230	0.480
OA	97.1%	97.0%	97.0%	97.0%	96.3%	96.7%	96.0%
Seasonal Difference (Δ = Pre−fire − Post−fire)							
	ΔBAIM	ΔBand 2	ΔGEMI	ΔMIRBI	ΔNBR	ΔNBR2	ΔNDVI
Threshold	−31.2	0.04	0.11	−0.25	0.22	0.12	0.22
OA	98.7%	98.2%	98.3%	98%	98.2%	98.4%	98.3%
Seasonal Difference (Δ = Pre−fire − Post−fire) with selected images by quality next to birthday							
	ΔBAIM	ΔBand 2	ΔGEMI	ΔMIRBI	ΔNBR	ΔNBR2	ΔNDVI
Threshold	−28.32	0.041	0.156	−0.406	0.278	0.138	0.172
OA	97.2%	97.1%	97.0%	97.0%	96.7%	96.5%	96.5%
Z-score normalization							
	BAIM	Band 2	GEMI	MIRBI	NBR	NBR2	NDVI
Threshold	1.235	−1.744	−1.825	1.430	−1.925	−1.428	−1.918
OA	97.1%	97.4%	97.2%	97.0%	96.5%	96.5%	96.0%
Zero−mean normalization							
	BAIM	Band 2	GEMI	MIRBI	NBR	NBR2	NDVI
Threshold	11	−0.109	−0.200	0.250	−0.284	−0.160	−0.203
OA	97.8%	97.9%	97.7%	97.3%	96.9%	96.9%	96.8%

The lower accuracy of the seasonal difference method compared to the normalization method was due to the following factors: (a) Pixel quality, recurrent fires, and continuous deforestation. Pixel quality is one of the main limitations of seasonal difference in the tropical region due to intense cloud cover. The selection of high-quality pixels in two consecutive years is unlikely in most of the Amazon region, requiring algorithms for the selection of images close to the anniversary or temporal composition methods. In contrast, the normalization method does

not depend on pixel quality in consecutive years, since it uses the entire time series available, facilitating the delimitation of fires in regions with high cloud presence.
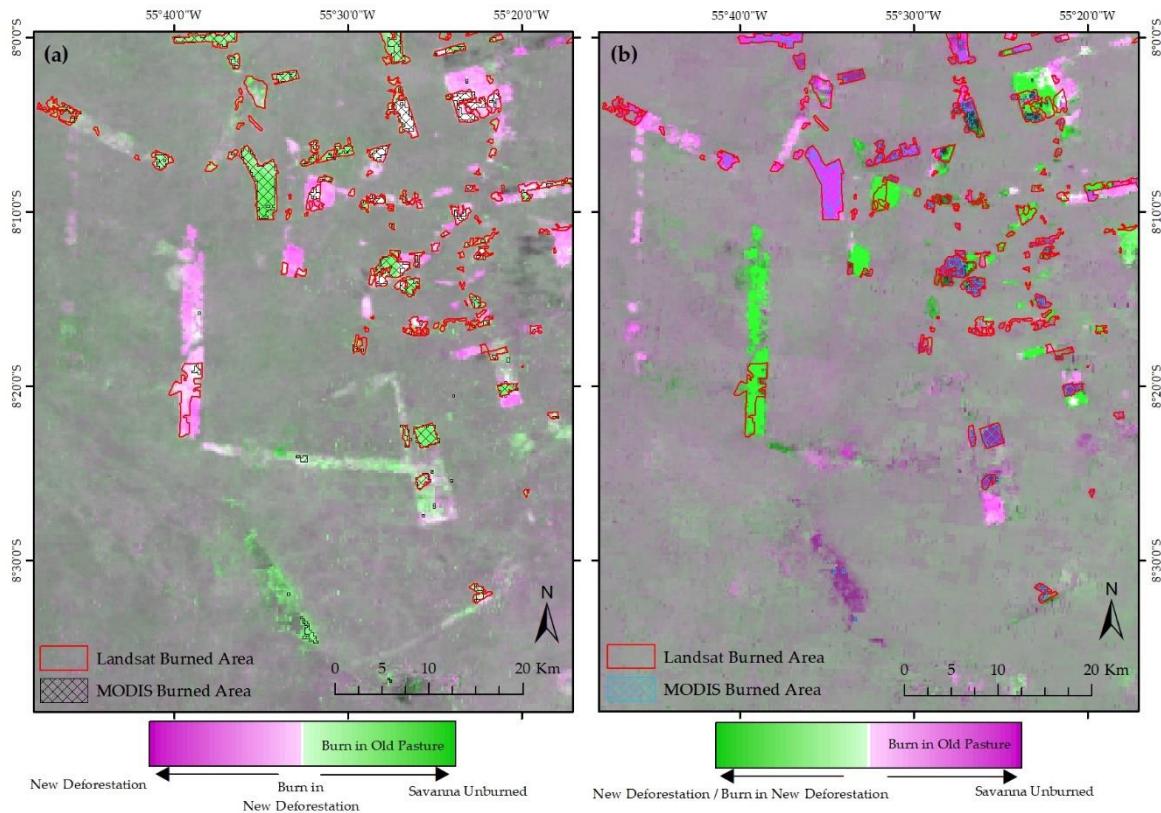
The seasonal difference in areas with high fire recurrence tends to omit burned areas in consecutive years or regenerating regions due to the decrease in the difference values (Figure 3.9). The continuous deforestation of the tropical regions generates areas burned in new deforestation with different values of the fires in old deforestation, preventing the use of a single threshold value. Differently, the normalization method allows the grouping of burned areas in new and old deforestation from only one threshold value.

Figure 3.9. Comparison of the burned area vector detected by visual interpretation from Landsat images and the response of the Burnt Area Index (BAIM) and ΔBAIM indices in the MODIS images.

Figure 3.10 compares the application zero-mean normalization and the seasonal difference in the BAIM image. The RGB composition of the 2005 and 2006 dates (R-2005/G-2006/B-2005) highlights the changes between the two methods. The RGB combination of zero-mean images showed deforested areas of 2006 in magenta color, burned deforestation areas in white, with

burned areas in old deforestation in green (Figure 3.10a). In this case, a single threshold identifies most of the fires in the white and green areas. The seasonal difference method has inverse values in relation to the zero-mean normalization method, where deforested areas in 2005 are in greens and "burned areas" in 2006 are in magenta (Figure 3.10b). However, burned deforestation areas also have green tones, mixing with deforested areas and preventing their separation by a single threshold.

Figure 3.10. Detection of burned areas in the years 2005 and 2006 using: (**a**) BAIM with zero-mean normalization; and (**b**) ΔBAIM. Comparison of the burned areas extracted by visual interpretation of the Landsat images and by the automated method in the MODIS images.

4.2. Validation and Data Comparison

The MODIS mapping validation indicated that the NIR band normalized by the mean achieved the best result (Dice coefficient of 0.647) (Table 3.6). The zero-mean normalization obtained higher accuracy than the other methods in most of the tests performed. Z-Score normalization presented a significant improvement in the detection of burned areas in Band 2, GEMI, and MIRBI. The seasonal differencing with image selection by quality next to birthday improved the classification of all indexes, exhibiting better performance than the Z-Score normalization in the BAIM, GEMI, NBR, NBR2, and NDVI indices, and higher than the zero-mean normalization for the NBR index. The seasonal differencing using image selection showed the lowest commission error rate, and with the zero-mean normalization or Z-score had the smallest error of omission.
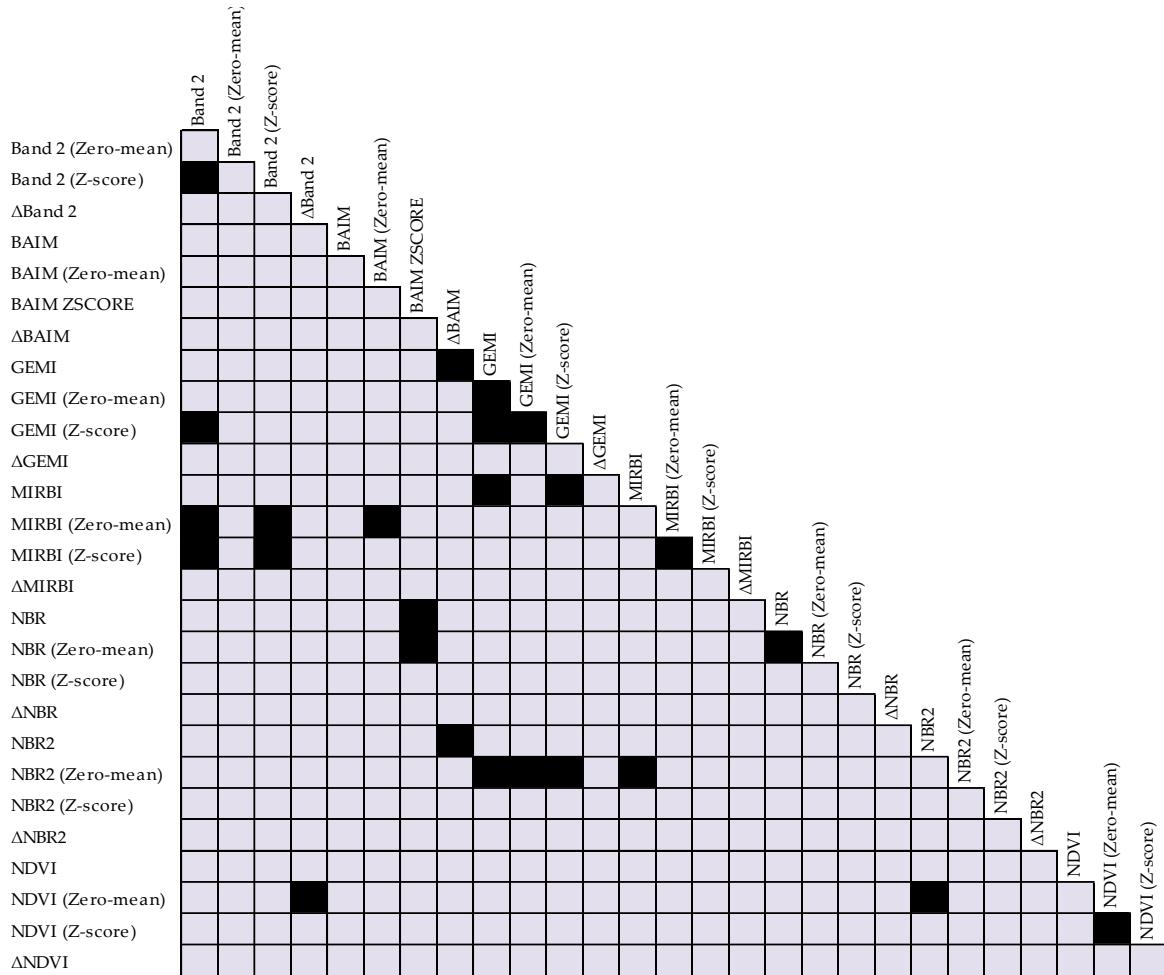
Table 3.6. Accuracy indices of the burned areas using MODIS times series in the study area. "DC" is the Dice coefficient and "OA" is the overall accuracy.

Original Data							
	BAIM	Band 2	GEMI	MIRBI	NBR	NBR2	NDVI
DC	0.588	0.527	0.337	0.326	0.422	0.430	0.399
OA	98.56%	98.71%	98.36%	98.31%	98.30%	97.71%	96.81%
Commission Errors	48.02%	34.21%	20.75%	27.44%	34.40%	61.99%	46.06%
Omission Errors	38.20%	53.75%	79.96%	76.95%	62.60%	45.49%	38.02%
Seasonal Difference (Pre-fire − Post-fire) with fixed interval							
	ΔBAIM	ΔBand 2	ΔGEMI	ΔMIRBI	ΔNBR	ΔNBR2	ΔNDVI
DC	0.506	0.485	0.384	0.334	0.428	0.412	0.400
OA	98.15%	97.87%	97.11%	96.59%	97.51%	97.50%	97.15%
Commission Errors	29.82%	71.67%	40.71%	42. 37%	51.22%	54.21%	69.47%
Omission Errors	62.60%	42.85%	73. 57%	74.02%	61.23%	62.01%	59.41%
Seasonal Difference (Pre-fire − Post-fire) with selected images							
	ΔBAIM	ΔBand 2	ΔGEMI	ΔMIRBI	ΔNBR	ΔNBR2	ΔNDVI
DC	0.592	0.606	0.481	0.357	0.537	0.487	0.425
OA	98.69%	98.74%	98.57%	98.49%	98.62%	98.52%	97.23%
Commission Errors	14.86%	32.30%	17.98%	25.56%	23.14%	35.46%	40.22%
Omission Errors	48.43%	38.71%	64.98%	76.45%	57.50%	58.50%	46.72%
Z-score normalization							
	BAIM	Band 2	GEMI	MIRBI	NBR	NBR2	NDVI
DC	0.591	0.618	0.476	0.501	0.429	0.452	0.397
OA	98.38%	98.80%	98.54%	98.44%	98.69%	97.73%	96.38%
Commission Errors	45.42%	38.97%	34.16%	35.80%	45.77%	47.23%	56.81%
Omission Errors	39.36%	38.70%	62.58%	55.90%	45.45%	45.74%	45.59%
Zero-mean normalization							
	BAIM	Band 2	GEMI	MIRBI	NBR	NBR2	NDVI
DC	0.625	0.647	0.566	0.539	0.508	0.503	0.479
OA	98.36%	98.99%	98.44%	98.59%	98.66%	98.31%	97.54%
Commission Errors	38.01%	32.41%	28.29%	33.21%	35.55%	46.61%	48.60%
Omission Errors	31.64%	34.75%	55.20%	49.60%	42.69%	42.48%	30.96%

The McNemar test confirmed the statistical independence between most of the classification methods, presenting values of $x^2 > 3.841$ (Figure 3.11). The most accurate method (Band 2 with zero-mean normalization) was statistically different from the other classifications. The procedures with the highest degree of agreement between them were those derived from the GEMI, MIRBI, and NBR2 indices, while the methods based on Band 2, BAIM, and Seasonal Difference were independent.

Considering the same reference data (Landsat-TM, ETM +, and OLI Images), the burned area products (MCD45, MCD65, and FIRE CCI) presented less than 25% of commission errors, like the seasonal difference method, but due to the high error rate of omission, the Dice coefficient was lower than all the methods used. The MCD45 and FIRE CCI products had a Dice coefficient lower than 0.11 and omission errors higher than 90%. The MCD64 product obtained the Dice coefficient of 0.24 in detriment of the reduction of the omission errors, surpassing the products MCD45 and FIRE_CCI (Table 3.7). The MODIS products still need improvements [24], validations in Africa using Landsat images obtained 34% commission errors and 59% omission errors [86], and globally containing a commission error of 46% and omission error of 72%, where specific biomass showed more satisfactory results than others such as Borealis Forestry and Tropical and subtropical Savanna [38]. The imprecision of the proposed method occurred in small burn areas due to the spatial resolution difference between the sensors used for validation, showing commission errors in forest and savanna areas. The proposed method had a lower commission
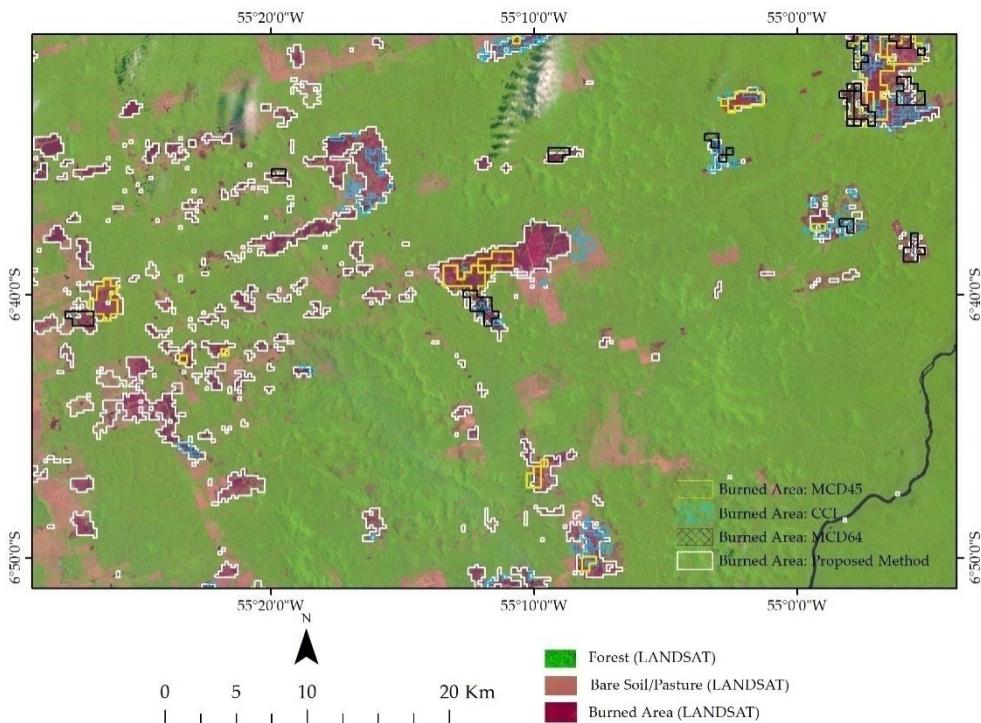
error rate than MODIS / MERIS products, which focused on the resolution difference with the validation image (Figure 3.12).

Figure 3.11. McNemar's test from the original image and the methods of normalization (zero-mean and Z-score) and seasonal differencing (selected images). The black markings indicate the statistical equivalence of the two methods with chi-square < 3.841.

Table 3.7. Dice coefficient and overall accuracy of the burned areas for MCD45/MCD64/FIRE CCI data in the study area during 2001-2014 period.

Burned Area Product	Overall accuracy	Dice Coefficient	Commission Errors	Omission Errors
MCD45	98.58%	0.11	24.34%	93.55%
MCD64	98.61%	0.24	23.83%	84.51%
FIRE_CCI	98.48%	0.09	24.89%	94.67%

Figure 3.12. Comparison of burned area mappings from the proposed method, MCD45, MCD64, and FIRE CCI products and Landsat TM image.

4.3. Mapping Validation by Land Cover Type

The accuracy analysis of the burned area mapping by different land cover used the result of higher accuracy (NIR band and zero-mean normalization). The overall accuracy was higher than 98% in all classes, due to the high proportion of unburned area correctly identified. The Campinarana and Deforestation classes presented the highest Dice coefficients (0.778 and 0.755, respectively), and lower commission and omission errors. Burnings in the Ombrophilous Forest obtained low commission errors, but significant errors of omission. Burnings in savanna vegetation and seasonal forests presented the highest rates of commission and omission errors, respectively (Table 3.8).

Table 3.8. Estimated accuracy of burned area for each land use/cover classes. The water and secondary vegetation were not evaluated by the low level of representation of fires in the selected area.

Land Cover	Overall Accuracy	Dice Coefficient	Commission Errors	Omission Errors
Campinarana	99.25%	0.778	9.71%	27.60%
Deforestation/Pasture	99.19%	0.755	18.57%	34.76%
Ombrophilous Forest	98.68%	0.506	23.40%	49.62%
Savanna	98.62%	0.466	59.25%	37.42%
Seasonal Forest	98.57%	0.371	23.23%	76.85%

4.4. Land Use/Land Cover Classes and Burned Area Patterns

Fire events and deforestation showed a high correlation (Table 3.9). Deforestation had the highest fire representativeness in the years studied, representing more than 70% of the total area burned annually. This attested to the anthropogenic influence on current burning patterns, both

in deforestation and in agricultural management. In the study area, the Ombrophylous Forest had intense deforestation, decreasing from 70% in 2000 to 59% in 2014, which resulted in a high number of burnings in the years 2004, 2006, and 2010. More than 16% of deforested areas burned in 2004, while less than 2% burned in 2013. The other types of vegetation (Savanna, Seasonal Forests, and Secondary Vegetation) presented a low proportion of annual burned area, with average values smaller than 1% of the affected areas.

Table 3.9. Annual burned area (km² and percentage within each class) from MODIS daily images for the following classes of land use and land cover: Campinarana (CP), Deforestation/Pasture (D/P), Ombrophilous Forest (OF), Savanna (S), Seasonal Forest (SF), and Secondary Vegetation (SV).
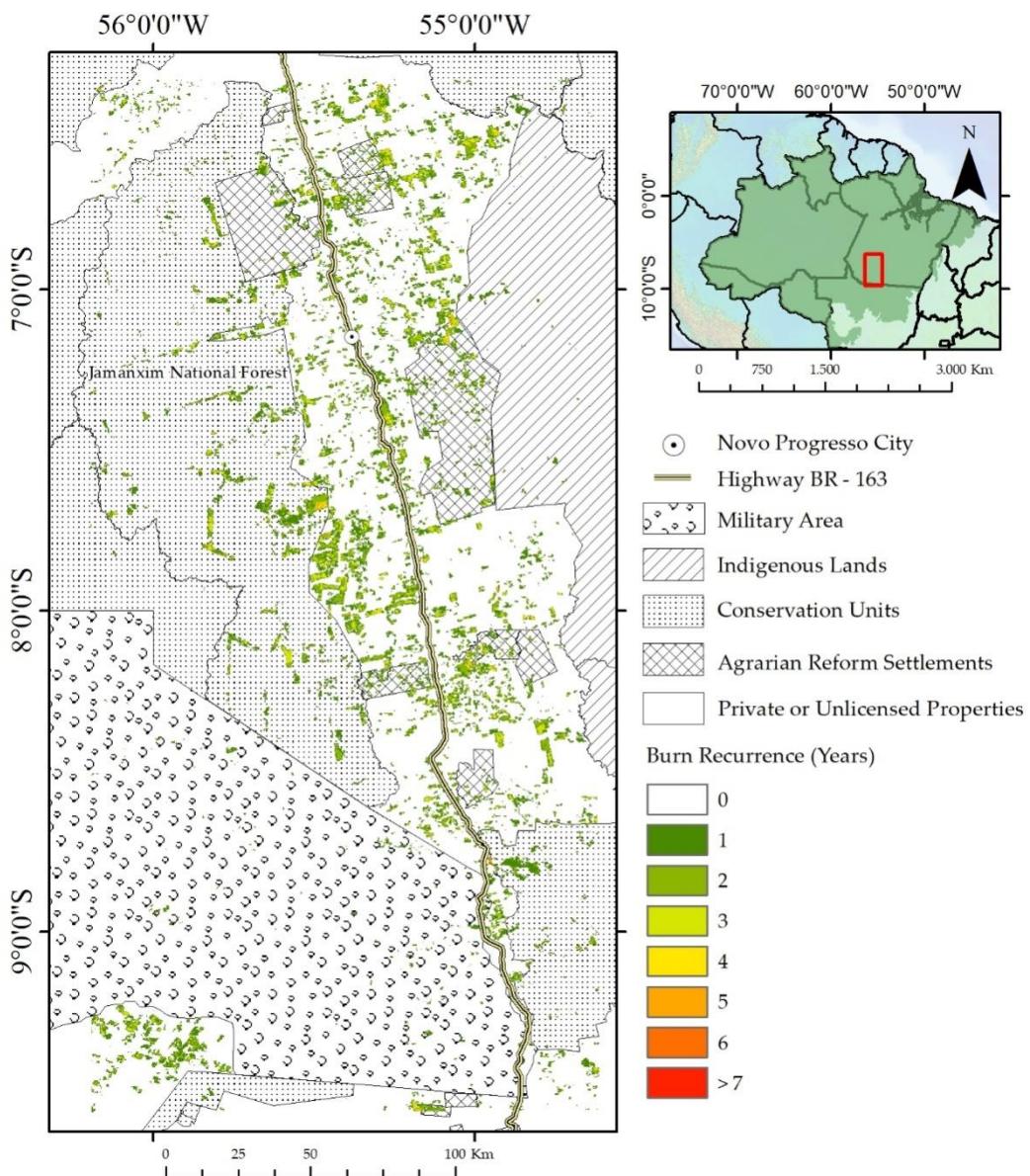
Area (Km²)						
Year	CP	D/P	OF	S	SF	SV
2001	14.16 (0.5%)	280.66 (6.9%)	49.56 (0.1%)	2.55 (0.03%)	12.18 (0.2%)	0.28 (0.1%)
2002	12.84 (0.4%)	773.68 (14.4%)	84.08 (0.2%)	14.61 (0.18%)	12.77 (0.2%)	0.78 (0.2%)
2003	26.82 (0.9%)	497.05 (8.2%)	92.58 (0.2%)	9.06 (0.11%)	18.24 (0.3%)	1.05 (0.3%)
2004	51.60 (1.7%)	1203.22 (16.8%)	235.74 (0.5%)	15.58 (0.19%)	20.14 (0.3%)	0.12 (0.0%)
2005	33.10 (1.1%)	771.25 (9.9%)	111.60 (0.2%)	15.38 (0.19%)	23.97 (0.4%)	0.86 (0.3%)
2006	26.85 (0.9%)	781.16 (9.4%)	244.92 (0.5%)	22.15 (0.28%)	70.80 (1.1%)	1.52 (0.5%)
2007	18.24 (0.6%)	677.03 (7.6%)	143.28 (0.3%)	5.21 (0.06%)	22.24 (0.3%)	0.20 (0.1%)
2008	41.48 (1.4%)	625.33 (6.6%)	130.02 (0.3%)	28.77 (0.36%)	44.52 (0.7%)	1.37 (0.4%)
2009	15.19 (0.5%)	233.87 (2.3%)	121.21 (0.3%)	4.53 (0.06%)	52.62 (0.8%)	0.43 (0.1%)
2010	7.21 (0.2%)	749.36 (7.2%)	196.83 (0.4%)	11.10 (0.14%)	23.60 (0.4%)	1.62 (0.5%)
2011	23.66 (0.8%)	214.61 (2.0%)	90.71 (0.2%)	5.95 (0.07%)	15.54 (0.2%)	0.66 (0.2%)
2012	4.49 (0.1%)	395.61 (3.5%)	87.07 (0.2%)	2.78 (0.03%)	13.08 (0.2%)	0.40 (0.1%)
2013	10.77 (0.4%)	166.01 (1.4%)	47.75 (0.1%)	3.30 (0.04%)	6.06 (0.1%)	0.25 (0.1%)
2014	5.65 (0.2%)	748.24 (6.2%)	102.40 (0.2%)	3.18 (0.04%)	16.60 (0.3%)	2.06 (0.6%)

The highest occurrence of burned areas was concentrated near the BR-163 highway, especially in the buffer zone up to 40km (Table 3.10). More than 85% of the forest area showed no fires. In the 14 years examined, the burned area was slightly more than 11% of the study area (Figure 3.13). Most of the area burned only once or twice during the study period (7% and 3%). Approximately 1% of the pixels burned in more than three years in the time series, concerning the agricultural areas. The indigenous territories and the military base showed a low incidence of fires in the temporal series, in contrast, the Jamanxim National Forest (highly degraded conservation unit) exhibited a high frequency of fires. The private or unlicensed properties (without the direct intervention of public authorities) totaled 24,358.8 square kilometers of the

study area, and corresponded to the highest burning rates, followed by the settlement projects (Figure 3.13).

Table 3.10. Burned area percentage in buffer zones with 20km distance intervals from the BR-163 highway.

Distance	20 km	40 km	60 km	80 km	100 km	120 km	140 km	160 km
Burned Area (%)	12.5%	10.1%	3.7%	1.6%	0.9%	2.7%	2.5%	0.7%

Figure 3.13. Map of the fire recurrence (14 Years).

5. Discussion

Consistent with other research, seasonal differences and standardization techniques improved the burned area mapping [47,83,95]. However, seasonal differencing considering continuous data in time has the following limitations [83]: (a) The subtraction operation highlights the noise present in the two images (pre- and post-fire); (b) Fire detection is susceptible

to interference of phenological variations, oscillation of cropping cycles, and land use changes. Therefore, the main difficulty of the seasonal difference is to ensure that other changes independent of the fire event are not confused with burned areas, such as deforestation or atmospheric variations. The seasonal difference in continuous data over time intensifies this limitation, as opposed to the use of discrete data chosen by the analyst.

Another alternative is the use of time series standardized by pixel, which has been used to identify burned areas in the savanna region of Central Brazil [83]. This procedure converts the data set to Z-Score values (with the mean of zero and standard deviation of one), facilitating the determination of a threshold value of the burned areas from a reference image. This technique does not alter the relative values of the temporal signature and avoids the errors described by the seasonal difference. However, the application of this method to forest areas generated false positives mainly related to the presence of cloud shadows not detected by the MODIS sensor quality mask due to the resolution difference between the products. The MODIS cloud mask has a 1-km resolution, while the images of this research had 250- and 500-m resolutions. The time series of spectral indexes in forest areas shows low standard deviation in comparison to the other targets, always having a photosynthetically active behavior with little change over time. Therefore, the Z-score normalization that has the standard deviation as the denominator causes an overestimation of the normalized forest values, differently from what occurs in the vegetation with high seasonal variation such as the savannah. An alternative proposed in this research was the use of zero-mean normalization, with only the subtraction by the mean, without the division by the standard deviation. This normalization approach allowed an adaptation of the method [83] for these vegetation types, and more accurate results in the detection of burned areas. The main advantage of the zero-mean normalization is that it equalizes the values of the burned area in the different scenarios of the Amazon region (forest, pasture, and deforestation), facilitating their detection from the single threshold.

Except for the NBR index, all the data tested (band of Near Infrared, BAIM, GEMI, MIRBI, NBR2, and NDVI) presented better accuracy using zero-mean normalization than the other procedures (original image, seasonal differencing, seasonal differencing with the selected images, and Z-score), attesting to the superiority of the zero-mean in detriment of the z-score normalization for the mapping of burning areas in forest regions. The NBR index presents a higher accuracy using the seasonal difference with the selected images.

Within the normalization procedures, the input data that had the best Dice coefficient were two: (a) BAIM in the original image and seasonal difference with fixed interval; and (b) Infrared band in the seasonal differencing with selected images, Z-score, and zero-mean normalization methods. Therefore, the best result used the infrared band and zero-mean normalization. Pleniou *et al*. [96] and Alonso-Canas [63] emphasized the ability to separate the burned areas from the near infrared. Although the NBR and dNBR indices are widely used in the literature for the detection of burned areas and fire severity [27,97], there are limitations in the study area due to the intense dynamics of deforestation. Roy *et al.* [97] warned about the ineffectiveness of the NBR index to measure the severity of burning in tropical forests.

Some limitations persist in the mapping of small areas burned due to MODIS spatial resolution, as verified by other authors [81,98]. The burned areas on small farms and agrarian reform settlements result in an underestimation of the total area burned. Moreover, the daily images may present better results than the MODIS products from the multitemporal compositing techniques [66,99]. Future research efforts could use high spatial and temporal resolution satellite data, which should reduce the omission of undetected small fires.

The comparison between the MCD45, MCD64, and FIRE CCI products and the reference burned area mapping demonstrated proved unfeasible for use in the Amazon region due to the low detection of burned areas. Libonati *et al.* [100] also highlighted a high percentage of omission errors in the MCD45 product. Even with MCD64 product enhancements, the omission errors may exceed 60% [35]. Despite the limitations of the burned area products in the Amazon, these were

developed for the world surpassing in many cases other techniques of burned-area detection. The spatial resolution of 500 meters from MODIS and 300 meters from FIRE CCI products influenced the difference between the two methods.

The methodology used presents better fire detection capacity in pasture/deforestation areas and Campinarana vegetation. Deforested regions were the most affected by fires, where it is used at regular intervals for pasture maintenance, combating invasive plants, pests, and improving low soil productivity [13]. The lack of access to alternative agricultural management is also an essential factor to explain the high rates of fires in the region [101]. Locations with a single occurrence of burning in the time series are often fires in the native forest that originated externally in agricultural areas and became out of control. In this context, fragmented forests are more vulnerable to fires because of the increased border with agrarian regions [2,8].

The Novo Progresso region is located between a conservation unit and Indigenous Parks that are essential barriers to deforestation and fires [7,102]. However, the Jamanxim National Forest is among the most deforested and burnt protected areas of the Brazilian Amazon due to the proximity of the Cuiabá-Santarém highway. Currently, the Brazilian Congress is negotiating a 26% reduction proposal in the Jamanxim National Forest area to allow the construction of a railroad for the transport of grain from Mato Grosso by the port of Mirituba, Pará. This railway will undoubtedly cause impacts increasing the occurrence of deforestation and fires.

Although the most widespread methods for detecting burned areas are based on specific thresholds of spectral indices, the temporal normalization per pixel should be evaluated in the future with other methods. Instead of considering spectral indices, several studies use spectral mixing techniques to highlight burned areas. [85,103,104]. Thus, the temporal normalization techniques for the pixel can be further tested in the time series of fraction images. Another approach used is the supervised classification, either by pixel or object-based, which depends on the collection of samples of the different targets present in the scene [105,106]. Thus, the supervised classification on normalized data per pixel should be tested.

6. Conclusions

This study evaluated different procedures for the mapping of burned areas in the Amazon Forest, considering different image processing in the MODIS time series, such as seasonal difference, normalization (Z-score, zero-mean normalization, and without normalization), spectral indices and bands (BAIM, GEMI, MIRBI, NBR, NBR2, NDVI, and NIR band). The zero-mean normalization and seasonal difference showed improvements in burned area detection in comparison with the original images. Although the seasonal difference method was widely used in other biomes, the zero-mean normalization achieved better accuracy, confirmed by the McNemar statistical test. The use of the NIR band presented the best results in burned area detection. The zero-mean normalization allowed comparison of the burning behaviors of different environments in an integrated way, defining a single threshold value for the different vegetal formations. This approach to time series normalization per pixel is an innovation in the processing of remotely sensed data for detection of burned areas that must be improved for other environments and monitoring studies. In addition to the methodology presented, greater accuracy in the detection of burned areas in Campinarana and pastures, burned areas occur predominantly in deforested areas, which account for more than 70% of annually burned areas. The adopted methodology presented an overall accuracy (98.99%) greater than the burned area products (MCD45, MCD64, and FIRE CCI), and low errors of omission, despite having higher commission errors. The improvement of the monitoring of burned areas in the Amazon enables better environmental management and the estimations of their impacts.

References

1. Morton, D.C.; Defries, R.S.; Randerson, J.T.; Giglio, L.; Schroeder, W.; van der Werf, G.R. Agricultural intensification increases deforestation fire activity in Amazonia. *Glob. Chang. Biol.* **2008**, *14*, 2262–2275,

doi:10.1111/j.1365-2486.2008.01652.x.

2. Cochrane, M.A. Synergistic interactions between habitat fragmentation and fire in evergreen tropical forests. *Conserv. Biol.* **2001**, *15*, 1515–1521, doi:10.1046/j.1523-1739.2001.01091.x.

3. Pivello, V.R. The use of fire in the cerrado and Amazonian rainforests of Brazil: Past and present. *Fire Ecol.* **2011**, *7*, 24–39, doi:10.4996/fireecology.0701024.

4. Silvestrini, R.A.; Soares-Filho, B.S.; Nepstad, D.; Coe, M.; Rodrigues, H.; Assunção, R. Simulating fire regimes in the Amazon in response to climate change and deforestation. *Ecol. Appl.* **2011**, *21*, 1573–1590, doi:10.1890/10-0827.1.

5. Cano-Crespo, A.; Oliveira, P.J.C.; Boit, A.; Cardoso, M.; Thonicke, K. Forest edge burning in the Brazilian Amazon promoted by escaping fires from managed pastures. *J. Geophys. Res. G Biogeosci.* **2015**, *120*, 2095–2107, doi:10.1002/2015JG002914.

6. Nepstad, D.; Carvalho, G.; Barros, A.C.; Alencar, A.; Capobianco, J.P.; Bishop, J.; Moutinho, P.; Lefebvre, P.; Silva, U.L.; Prins, E. Road paving, fire regime feedbacks, and the future of Amazon forests. *For. Ecol. Manag.* **2001**, *154*, 395–407, doi:10.1016/S0378-1127(01)00511-4.

7. Nepstad, D.; Schwartzman, S.; Bamberger, B.; Santilli, M.; Ray, D.; Schlesinger, P.; Lefebvre, P.; Alencar, A.; Prinz, E.; Fiske, G.; et al. Inhibition of Amazon deforestation and fire by parks and indigenous lands. *Conserv. Biol.* **2006**, *20*, 65–73, doi:10.1111/j.1523-1739.2006.00351.x.

8. Cochrane, M.A.; Laurance, W.F. Fire as a large-scale edge effect in Amazonian forests. *J. Trop. Ecol.* **2002**, *18*, 311–325, doi:10.1017/S0266467402002237.

9. Alencar, A.A.; Brando, P.M.; Asner, G.P.; Putz, F.E. Landscape fragmentation, severe drought, and the new Amazon forest fire regime. *Ecol. Appl.* **2015**, *25*, 1493–1505, doi:10.1017/CBO9781107415324.004.

10. van Marle, M.J.E.; Field, R.D.; van der Werf, G.R.; Estrada de Wagt, I.A.; Houghton, R.A.; Rizzo, L.V.; Artaxo, P.; Tsigaridis, K. Fire and deforestation dynamics in Amazonia (1973-2014). *Glob. Biogeochem. Cycles* **2016**, 24–38, doi:10.1002/2016GB005445.

11. Cochrane, M.A.; Schulze, M.D. Fire as a recurrent event in tropical forests of the eastern Amazon: Effects on forest structure, biomass, and species composition. *Biotropica* **1999**, *31*, 2–16, doi:10.2307/2663955.

12. Chuvieco, E.; Aguado, I.; Jurdao, S.; Pettinari, M.L.; Yebra, M.; Salas, J.; Hantson, S.; de la Riva, J.; Ibarra, P.; Rodrigues, M.; et al. Integrating geospatial information into fire risk assessment. *Int. J. Wildl. Fire* **2014**, *23*, 606–619.

13. Nepstad, D.C.; Verissimo, A.; Alencar, A.; Nobre, C.; Lima, E.; Lefebvre, P.; Schlesinger, P.; Potter, C.; Moutinho, P.; Mendoza, E.; et al. Large-scale impoverishment of Amazonian forests by logging and fire. *Nature* **1999**, *398*, 505–508, doi:10.1038/19066.

14. Righi, C.A.; de Alencastro Graça, P.M.L.; Cerri, C.C.; Feigl, B.J.; Fearnside, P.M. Biomass burning in Brazil's Amazonian "arc of deforestation": Burning efficiency and charcoal formation in a fire after mechanized clearing at Feliz Natal, Mato Grosso. *For. Ecol. Manag.* **2009**, *258*, 2535–2546, doi:10.1016/j.foreco.2009.09.010.

15. Lima, A.; Silva, T.S.F.; de Aragão, L.E.O.eC.; de Feitas, R.M.; Adami, M.; Formaggio, A.R.; Shimabukuro, Y.E. Land use and land cover changes determine the spatial relationship between fire and deforestation in the Brazilian Amazon. *Appl. Geogr.* **2012**, *34*, 239–246, doi:10.1016/j.apgeog.2011.10.013.

16. Laurance, W.F.; Bruce Williamson, G. Positive feedbacks among forest fragmentation, drought, and climate change in the Amazon. *Conserv. Biol.* **2001**, *15*, 1529–1535, doi:10.1046/j.1523-1739.2001.01093.x.

17. Phillips, O.L.; van der Heijden, G.; Lewis, S.L.; López-González, G.; Aragão, L.E.O.C.; Lloyd, J.; Malhi, Y.; Monteagudo, A.; Almeida, S.; Dávila, E.A.; et al. Drought-mortality relationships for tropical forests. *New Phytol.* **2010**, *187*, 631–646, doi:10.1111/j.1469-8137.2010.03359.x.

18. Nepstad, D.; Lefebvre, P.; Da Silva, U.L.; Tomasella, J.; Schlesinger, P.; Solórzano, L.; Moutinho, P.; Ray, D.; Benito, J.G. Amazon drought and its implications for forest flammability and tree growth: A basin-wide analysis. *Glob. Chang. Biol.* **2004**, *10*, 704–717, doi:10.1111/j.1529-8817.2003.00772.x.

19. Alencar, A.; Nepstad, D.; Del Carmen Vera Diaz, M. Forest understory fire in the Brazilian Amazon in ENSO and non-ENSO years: Area burned and committed carbon emissions. *Earth Interact.* **2006**, *10*, doi:10.1175/EI150.1.

20. Aragão, L.E.O.C.; Malhi, Y.; Roman-Cuesta, R.M.; Saatchi, S.; Anderson, L.O.; Shimabukuro,

Y.E.Spatial patterns and fire response of recent Amazonian droughts. *Geophys. Res. Lett.* **2007**, *34*, 1–5, doi:10.1029/2006GL028946.

21. Gutiérrez-Velez, V.H.; Uriarte, M.; Defries, R.; Pinedo-Vasquez, M.; Fernandes, K.; Ceccato, P.; Baethgen, W.; Padoch, C. Land cover change interacts with drought severity to change fire regimes in Western Amazonia. *Ecol. Appl.* **2014**, *24*, 1323–1340, doi:10.1890/13-2101.1.

22. Asner, G.P. Cloud cover in Landsat observations of the Brazilian Amazon. *Int. J. Remote Sens.* **2001**, *22*, 3855–3862, doi:10.1080/01431160010006926.

23. Lentile, L.B.; Holden, A.Z.A.; Smith, A.M.S.; Falkowski, M.J.; Hudak, A.T.; Morgan, P.; Lewis, S.A.; Gessler, P.E.; Benson, N.C. Remote sensing techniques to assess active fire characteristics and post-fire effects. *Int. J. Wildl. Fire* **2006**, *15*, 319–345, doi:10.1071/WF05097.

24. Mouillot, F.; Schultz, M.G.; Yue, C.; Cadule, P.; Tansey, K.; Ciais, P.; Chuvieco, E. Ten years of global burned area products from spaceborne remote sensing—A review: Analysis of user needs and recommendations for future developments. *Int. J. Appl. Earth Obs. Geoinf.* **2014**, *26*, 64–79, doi:10.1016/j.jag.2013.05.014.

25. Huesca, M.; Litago, J.; Merino-de-Miguel, S.; Cicuendez-López-Ocaña, V.; Palacios-Orueta, A. Modeling and forecasting MODIS-based Fire Potential Index on a pixel basis using time series models. *Int. J. Appl. Earth Obs. Geoinf.* **2014**, *26*, 363–376, doi:10.1016/j.jag.2013.09.003.

26. Giglio, L.; Loboda, T.; Roy, D.P.; Quayle, B.; Justice, C.O. An active-fire based burned area mapping algorithm for the MODIS sensor. *Remote Sens. Environ.* **2009**, *113*, 408–420, doi:10.1016/j.rse.2008.10.006.

27. Bastarrika, A.; Chuvieco, E.; Martin, M.P. Automatic burned land mapping from MODIS time series images: Assessment in Mediterranean ecosystems. *IEEE Trans. Geosci. Remote Sens.* **2011**, *49*, 3401–3413, doi:10.1109/TGRS.2011.2128327.

28. Hardtke, L.A.; Blanco, P.D.; del Valle, H.F.; Metternicht, G.I.; Sione, W.F. Automated mapping of burned areas in semi-arid ecosystems using modis time-series imagery. *ISPRS Int. Arch. Photogramm. Remote Sens. Spat. Inf. Sci.* **2015**, *XL-7/W3*, 811–814, doi:10.5194/isprsarchives-XL-7-W3-811-2015.

29. Giglio, L.; Csiszar, I.; Justice, C.O. Global distribution and seasonality of active fires as observed with the Terra and Aqua Moderate Resolution Imaging Spectroradiometer (MODIS) sensors. *J. Geophys. Res. Biogeosci.* **2006**, *111*, 1–12, doi:10.1029/2005JG000142.

30. Justice, C.O.; Giglio, L.; Korontzi, S.; Owens, J.; Morisette, J.T.; Roy, D.; Descloitres, J.; Alleaume, S.; Petitcolin, F.; Kaufman, Y. The MODIS fire products. *Remote Sens. Environ.* **2002**, *83*, 244–262, doi:10.1016/S0034-4257(02)00076-7.

31. Roy, D.P.; Jin, Y.; Lewis, P.E.; Justice, C.O. Prototyping a global algorithm for systematic fire-affected area mapping using MODIS time series data. *Remote Sens. Environ.* **2005**, *97*, 137–162, doi:10.1016/j.rse.2005.04.007.

32. Vivchar, A.V.; Moiseenko, K.B.; Pankratova, N.V. Estimates of carbon monoxide emissions from wildfires in northern Eurasia for airquality assessment and climate modeling. *Izv. Atmos. Ocean. Phys.* **2010**, *46*, 281–293, doi:10.1134/S0001433810030023.

33. Vivchar, A. Wildfires in Russia in 2000–2008: Estimates of burnt areas using the satellite MODIS MCD45 data. *Remote Sens. Lett.* **2011**, *2*, 81–90, doi:10.1080/01431161.2010.499138.

34. Safronov, A.N.; Fokeeva, E.V.; Rakitin, V.S.; Grechko, E.I.; Shumsky, R.A. Severe wildfires near Moscow, Russia in 2010: Modeling of carbon monoxide pollution and comparisons with observations. *Remote Sens.* **2015**, *7*, 395–429, doi:10.3390/rs70100395.

35. Padilla, M.; Stehman, S.V.; Ramo, R.; Corti, D.; Hantson, S.; Oliva, P.; Alonso-Canas, I.; Bradley, A.V.; Tansey, K.; Mota, B.; et al. Comparing the accuracies of remote sensing global burned area products using stratified random sampling and estimation. *Remote Sens. Environ.* **2015**, *160*, 114–121, doi:10.1016/j.rse.2015.01.005.

36. Roy, D.P.; Boschetti, L.; Justice, C.O.; Ju, J. The collection 5 MODIS burned area product - Global evaluation by comparison with the MODIS active fire product. *Remote Sens. Environ.* **2008**, *112*, 3690–3707, doi:10.1016/j.rse.2008.05.013.

37. Anaya, J.A.; Chuvieco, E. Accuracy Assessment of Burned Area Products in the Orinoco Basin. *Photogramm. Eng. Remote Sens.* **2012**, *7*, 53–60, doi:10.14358/PERS.78.1.53.

38. Padilla, M.; Stehman, S.V.; Chuvieco, E. Validation of the 2008 MODIS-MCD45 global burned area product using stratified random sampling. *Remote Sens. Environ.* **2014**, *144*, 187–196,

doi:10.1016/j.rse.2014.01.008.

39. Da Silva Cardozo, F.; Pereira, G.; Shimabukuro, Y.E.; Moraes, E.C. Validation of MODIS MCD45A1 product to identify burned areas in Acre State—Amazon forest. *Int. Geosci. Remote Sens. Symp.* **2012**, 6741–6744, doi:10.1109/IGARSS.2012.6352558.

40. Key, C.H.; Benson, N.C. Measuring and Remote Sensing of Burn Severity. In Proceedings of the U.S. Geological Survey Wildland Fire Workshop, Los Alamos, NM, USA, 31 October–3 November 2002.

41. Rouse, J.W.; Haas, R.H.; Schell, J.A.; Deering, D.W.; Harlan, J.C. *Monitoring the Vernal Advancement and Retrogradation (Green Wave Effect) of Natural Vegetation*. In: NASA/GSFC, Final Report, Greenbelt, MD, USA, 1974.

42. Kasischke, E.S.; French, N.H.F.; Harrel, P.; Christensen, N.L.; Ustin, S.L.; Barry, D. Monitoring of wildfires in boreal forest using large are AVHRR-NDVI composite image data. *Remote Sens. Environ.* **1993**, *45*, 61–71, doi:10.1016/0034-4257(93)90082-9.

43. Martín, M.P.; Gómez, I.; Chuvieco, E. Burnt Area Index (BAIM) for burned area discrimination at regional scale using MODIS data. *For. Ecol. Manag.* **2006**, *234*, S221, doi:10.1016/j.foreco.2006.08.248.

44. Pinty, B.; Verstraete, M.M. GEMI: A non-linear index to monitoring global vegetation from satellite. *Vegetation* **1992**, *101*, 15–20.

45. Trigg, S.; Flasse, S. An evaluation of different bi-spectral spaces for discriminating burned shrub-savannah. *Int. J. Remote Sens.* **2001**, *22*, 2641–2647, doi:10.1080/01431160110053185.

46. Key, C.H.; Benson, N.C.*Landscape Assessment: Sampling and Analysis Methods*;USDA For. Serv. Gen. Tech. Rep. RMRS-GTR-164-CD; USDA Forest Service: Washington, D.C., USA,2006; pp. 1–55, doi:10.1002/app.1994.070541203.

47. Loboda, T.; O'Neal, K.J.; Csiszar, I. Regionally adaptable dNBR-based algorithm for burned area mapping from MODIS data. *Remote Sens. Environ.* **2007**, *109*, 429–442, doi:10.1016/j.rse.2007.01.017.

48. Veraverbeke, S.; Lhermitte, S.; Verstraeten, W.W.; Goossens, R. The temporal dimension of differenced Normalized Burn Ratio (dNBR) fire/burn severity studies: The case of the large 2007 Peloponnese wildfires in Greece. *Remote Sens. Environ.* **2010**, *114*, 2548–2563, doi:10.1016/j.rse.2010.05.029.

49. Lhermitte, S.; Verbesselt, J.; Verstraeten, W.W.; Veraverbeke, S.; Coppin, P. Assessing intra-annual vegetation regrowth after fire using the pixel based regeneration index. *ISPRS J. Photogramm. Remote Sens.* **2011**, *66*, 17–27, doi:10.1016/j.isprsjprs.2010.08.004.

50. Diaz-Delgado, R.; Salvador, R.; Pons, X. Monitoring of plant community regeneration after fire by remote sensing. In *Fire Management and LandscapeEcology*; Traboud, L., Ed.; International Association of Wildland Fire: Fairfield, WA, USA, 1998; pp. 315–324.

51. Instituto Brasileiro de Geografia e Estatística (IBGE) Mapa de Climas do Brasil.Available online: http://portaldemapas.ibge.gov.br (accessed on 23 October 2015).

52. Instituto Nacional de Meteorologia (Inmet) Normais Climatológicas do Brasil. Available online: http://www.inmet.gov.br (accessed on 23 October 2015).

53. Instituto Nacional de Pesquisas Espaciais (INPE) Portal do Monitoramento de Queimadas e Incêndios. Available online: http://queimadas.cptec.inpe.br (accessed on 22 June 2015).

54. Instituto Nacional de Pesquisas Espaciais (INPE) Monitoramento da Floresta Amazônica Brasileira por Satélite—Projeto PRODES. Available online: http://www.obt.inpe.br/prodes (accessed on 25 October 2015).

55. Instituto Brasileiro de Geografia e Estatística (IBGE) Vegetação: Estado do Pará. Available online: http://portaldemapas.ibge.gov.br (accessed on 23 October 2015).

56. Instituto Chico Mendes de Conservação da Biodiversidade (ICMBIO) Geoprocessamento. Available online: http://www.icmbio.gov.br (accessed on 25 October 2015).

57. Fundação Nacional do Índio (FUNAI) Mapas. Available online: http://mapas2.funai.gov.br (accessed on 24 October 2015).

58. Instituto Nacional de Colonização e Reforma Agrária (INCRA) Acervo Fundiário. Available online: http://acervofundiario.incra.gov.br (accessed on 25 October 2015).

59. Instituto do Homem e Meio Ambiente da Amazônia (IMAZON) Mapas - Áreas Protegidas da Amazônia Legal. Available online: http://imazon.org.br (accessed on 25 October 2015).

60. Zimmerman, B.; Peres, C.A.; Malcolm, J.R.; Turner, T. Conservation and development alliances with the Kayapó of south-eastern Amazonia, a tropical forest indigenous people. *Environ. Conserv.* **2001**, *28*,

10–22, doi:10.1017/S0376892901000029.

61. Fearnside, P.M. Brazil's Cuiabá- Santarém (BR-163) Highway: The environmental cost of paving a soybean corridor through the Amazon. *Environ. Manag.* **2007**, *39*, 601–614, doi:10.1007/s00267-006-0149-2.

62. Chuvieco, E.; Pettinari, M.L.; Heil, A.; Storm, T. *ESA Climate Change Initiative – Fire Disturbance: D1.2 Product Specification Report, Version 6.1*; University of Alcala, Spain, 2016.

63. Alonso-Canas, I.; Chuvieco, E. Global burned area mapping from ENVISAT-MERIS and MODIS active fire data. *Remote Sens. Environ.* **2015**, *163*, 140–152, doi:10.1016/j.rse.2015.03.011.

64. Justice, C.O.; Townshend, J.R.G.; Vermote, E.F.; Masuoka, E.; Wolfe, R.E.; Saleous, N.; Roy, D.P.; Morisette, J.T. An overview of MODIS Land data processing and product status. *Remote Sens. Environ.* **2002**, *83*, 3–15, doi:10.1016/S0034-4257(02)00084-6.

65. Vermote, E.F.*MOD09A1 MODIS Surface Reflectance 8-Day L3 Global 500m SIN Grid V006*; NASA LP DAAC, Sioux Falls, SD, USA, 2016, doi:10.5067/MODIS/MOD09A1.006.

66. Chuvieco, E.; Ventura, G.; Martín, M.P.; Gómez, I. Assessment of multitemporal compositing techniques of MODIS and AVHRR images for burned land mapping. *Remote Sens. Environ.* **2005**, *94*, 450–462, doi:10.1016/j.rse.2004.11.006.

67. Morton, D.C.; Nagol, J.; Carabajal, C.C.; Rosette, J.; Palace, M.; Cook, B.D.; Vermote, E.F.; Harding, D.J.; North, P.R.J. Amazon forests maintain consistent canopy structure and greenness during the dry season. *Nature* **2014**, *506*, 1–16, doi:10.1038/nature13006.

68. Maier, S.W. Changes in surface reflectance from wildfires on the Australian continent measured by MODIS. *Int. J. Remote Sens.* **2010**, *31*, 3161–3176, doi:10.1080/01431160903154408.

69. Pereira, J.M.C.; Sa, A.C.L.; Souza, A.M.O.; Silva, J.M.N.; Santos, T.N.; Carreiras, J.M. Spectral characterization and discrimination of burnt areas. In *Remote Sensing of Large Wildfires in the European Mediterranean Basin*; Springer: Berlin, Germany, 1999; pp. 123–138.

70. Forkel, M.; Carvalhais, N.; Verbesselt, J.; Mahecha, M.D.; Neigh, C.S.R.; Reichstein, M. Trend Change detection in NDVI time series: Effects of inter-annual variability and methodology. *Remote Sens.* **2013**, *5*, 2113–2144, doi:10.3390/rs5052113.

71. Kolden, C.; Roganf, J. Mapping Wildfire Burn Severity in the Arctic Tundra from Downsampled MODIS Data. *Arct. Antarct Alp. Res.* **2013**, *45*, 64–76, doi:10.1657/1938-4246-45.1.64.

72. Godwin, D.R.; Kobziar, L.N. Comparison of burn severities of consecutive large-scale fires in Florida sand pine scrubusing satellite imagery analysis. *Fire Ecol.* **2011**, *7*, 99–113, doi:10.4996/fireecology.0702099.

73. Chen, X.; Vogelmann, J.E.; Rollins, M.; Ohlen, D.; Key, C.H.; Yang, L.; Huang, C.; Shi, H. Detecting post-fire burn severity and vegetation recovery using multitemporal remote sensing spectral indices and field-collected composite burn index data in a ponderosa pine forest. *Int. J. Remote Sens.* **2011**, *32*, 7905–7927, doi:10.1080/01431161.2010.524678.

74. Zidane, I.; Lhissou, R.; Bouli, A.; Mabrouki, M. An improved algorithm for mapping burnt areas in the Mediterranean forest landscape of Morocco. *J. For. Res.* **2018**, doi:10.1007/s11676-018-0669-7.

75. Holden, Z.A.; Morgan, P.; Smith, A.M.S.; Vierling, L. Beyond Landsat: A comparison of four satellite sensors for detecting burn severity in ponderosa pine forests of the Gila Wilderness, NM, USA. *Int. J. Wildl. Fire* **2010**, *19*, 449–458, doi:10.1071/WF07106.

76. Hislop, S.; Jones, S.; Soto-Berelov, M.; Skidmore, A.; Haywood, A.; Nguyen, T.H. Using landsat spectral indices in time-series to assess wildfire disturbance and recovery. *Remote Sens.* **2018**, *10*, 1–17, doi:10.3390/rs10030460.

77. Dempewolf, J.; Trigg, S.; DeFries, R.S.; Eby, S. Burned-Area Mapping of the Serengeti–Mara Region Using MODIS Reflectance Data. *IEEE Geosci. Remote Sens. Lett.* **2007**, *4*, 312–316, doi:10.1109/LGRS.2007.894140.

78. McCarley, T.R.; Smith, A.M.S.; Kolden, C.A.; Kreitler, J. Evaluating the Mid-Infrared Bi-spectral Index for improved assessment of low-severity fire effects in a conifer forest. *Int. J. Wildl. Fire* **2018**, *27*, 407, doi:10.1071/WF17137.

79. García, M.J.L.; Caselles, V. Mapping burns and natural reforestation using thematic Mapper data. *Geocarto Int.* **1991**, *6*, 31–37, doi:10.1080/10106049109354290.

80. Pereira, J.M.C. Remote sensing of burned areas in tropical savannas. *Int. J. Wildl. Fire* **2003**, *12*, 259,

doi:10.1071/WF03028.

81. Cardozo, S.; Pereira, G.; Shimabukuro, Y.E.; Moraes, E.C. Avaliação Das Áreas Queimadas No Estado De Rondônia. *Rev. Bras. Cartogr.* **2014**, *66*, 705–716.

82. Shimabukuro, Y.E.; Duarte, V.; Arai, E.; Freitas, R.M.; Lima, A.; Valeriano, D.M.; Brown, I.F.; Maldonado, M.L.R. Fraction images derived from Terra Modis data for mapping burnt areas in Brazilian Amazonia. *Int. J. Remote Sens.* **2009**, *30*, 1537–1546, doi:10.1080/01431160802509058.

83. de Carvalho Júnior, O.A.; Guimarães, R.F.; Silva, C.; Gomes, R.A.T. Standardized Time-Series and Interannual Phenological Deviation: New Techniques for Burned-Area Detection Using Long-Term MODIS-NBR Dataset. *Remote Sens.* **2015**, *7*, 6950–6985, doi:10.3390/rs70606950.

84. Lhermitte, S.; Verbesselt, J.; Verstraeten, W.W.; Coppin, P. A Pixel Based Regeneration Index using Time Series Similarity and Spatial Context. *Photogramm. Eng. Remote Sens.* **2010**, *76*, 673–682, doi:10.14358/PERS.76.6.673.

85. Veraverbeke, S.; Somers, B.; Gitas, I.; Katagis, T.; Polychronaki, A.; Goossens, R. Spectral mixture analysis to assess post-fire vegetation regeneration using Landsat Thematic Mapper imagery: Accounting for soil brightness variation. *Int. J. Appl. Earth Obs. Geoinf.* **2012**, *14*, 1–11, doi:10.1016/j.jag.2011.08.004.

86. Roy, D.P.; Boschetti, L. Southern Africa validation of the MODIS, L3JRC, and GlobCarbon burned-area products. *IEEE Trans. Geosci. Remote Sens.* **2009**, *47*, 1032–1044, doi:10.1109/TGRS.2008.2009000.

87. Eva, H.; Lambin, E.F. Fires and land-cover change in the tropics:a remote sensing analysis at the landscape scale. *J. Biogeogr.* **2000**, *27*, 765–776, doi:10.1046/j.1365-2699.2000.00441.x.

88. Parrini, F.; Owen-Smith, N. The importance of post-fire regrowth for sable antelope in a Southern African savanna. *Afr. J. Ecol.* **2010**, *48*, 526–534, doi:10.1111/j.1365-2028.2009.01143.x.

89. Padilla, M.; Stehman, S.V.; Litago, J.; Chuvieco, E. Assessing the temporal stability of the accuracy of a time series of burned area products. *Remote Sens.* **2014**, *6*, 2050–2068, doi:10.3390/rs6032050.

90. Congalton, R.G. A review of assessing the accuracy of classifications of remotely sensed data. *Remote Sens. Environ.* **1991**, *37*, 35–46, doi:10.1016/0034-4257(91)90048-B.

91. Fleiss, J.L.; Levin, B.; Paik, M.C.*Statistical Methods for Rates and Proportions*; Wiley Series in Probability and Statistics; John Wiley & Sons, Inc.: Hoboken, NJ, USA, 2003.

92. Arvidson, T.; Goward, S.N.; Gasch, J.; Williams, D. Landsat-7 long-term acquisition plan: Development and validation. *Photogramm. Eng. Remote Sens.* **2006**, *72*, 1137–1146, doi:10.14358/pers.72.10.1137.

93. McNemar, Q. Note on the sampling error of the difference between correlated proportions or percentages. *Psychometrika* **1947**, *12*, 153–157, doi:10.1007/BF02295996.

94. Foody, G.M. Thematic map comparison: Evaluating the statistical significance of differences in classification accuracy. *Photogramm. Eng. Remote Sens.* **2004**, *70*, 627–633, doi:0099-1112/04/7005–0627/\$3.00/0.

95. Quintano, C.; Fernández-Manso, A.; Fernández-Manso, O. Combination of Landsat and Sentinel-2 MSI data for initial assessing of burn severity. *Int. J. Appl. Earth Obs. Geoinf.* **2018**, *64*, 221–225, doi:10.1016/j.jag.2017.09.014.

96. Pleniou, M.; Koutsias, N. Sensitivity of spectral reflectance values to different burn and vegetation ratios: A multi-scale approach applied in a fire affected area. *ISPRS J. Photogramm. Remote Sens.***2013**, *79*, 199–210, doi:10.1016/j.isprsjprs.2013.02.016.

97. Roy, D.P.; Boschetti, L.; Trigg, S.N. Remote sensing of fire severity: Assessing the performance of the normalized burn ratio. *IEEE Geosci. Remote Sens. Lett.* **2006**, *3*, 112–116, doi:10.1109/LGRS.2005.858485.

98. Quintano, C.; Fernández-Manso, A.; Stein, A.; Bijker, W. Estimation of area burned by forest fires in Mediterranean countries: A remote sensing data mining perspective. *For. Ecol. Manag.* **2011**, *262*, 1597–1607, doi:10.1016/j.foreco.2011.07.010.

99. Chen, Y.; Morton, D.C.; Jin, Y.; Collatz, G.J.; Kasibhatla, P.S.; van der Werf, G.R.; DeFries, R.S.; Randerson, J.T.; Gollatz, G.J.; Kasibhatla, P.S.; et al. Long-term trends and interannual variability of forest, savanna and agricultural fires in South America. *Carbon Manag.* **2013**, *4*, 617–638, doi:10.4155/cmt.13.61.

100. Libonati, R.; DaCamara, C.C.; Setzer, A.W.; Morelli, F.; Melchiori, A.E. An algorithm for burned area detection in the Brazilian Cerrado using 4 μm MODIS imagery. *Remote Sens.* **2015**, *7*, 15782–15803, doi:10.3390/rs71115782.

101. De Mendonça, M.J.C.; Vera Diaz, M.D.C.; Nepstad, D.; Seroa Da Motta, R.; Alencar, A.; Gomes, J.C.; Ortiz, R.A. The economic cost of the use of fire in the Amazon. *Ecol. Econ.* **2004**, *49*, 89–105, doi:10.1016/j.ecolecon.2003.11.011.

102. Nelson, A.; Chomitz, K.M. Effectiveness of strict vs. multiple use protected areas in reducing tropical forest fires: A global analysis using matching methods. *PLoS ONE* **2011**, *6*, doi:10.1371/journal.pone.0022722.

103. Quintano, C.; Fernández-Manso, A.; Fernández-Manso, O.; Shimabukuro, Y.E. Mapping burned areas in Mediterranean countries using spectral mixture analysis from a uni-temporal perspective. *Int. J. Remote Sens.* **2006**, *27*, 645–662, doi:10.1080/01431160500212195.

104. Quintano, C.; Fernández-Manso, A.; Roberts, D.A. Multiple Endmember Spectral Mixture Analysis (MESMA) to map burn severity levels from Landsat images in Mediterranean countries. *Remote Sens. Environ.* **2013**, *136*, 76–88, doi:10.1016/j.rse.2013.04.017.

105. Cao, X.; Chen, J.; Matsushita, B.; Imura, H.; Wang, L. An automatic method for burn scar mapping using support vector machines. *Int. J. Remote Sens.* **2009**, *30*, 577–594, doi:10.1080/01431160802220219.

106. Dragozi, E.; Gitas, I.; Stavrakoudis, D.; Theocharis, J. Burned Area Mapping Using Support Vector Machines and the FuzCoC Feature Selection Method on VHR IKONOS Imagery. *Remote Sens.* **2014**, *6*, 12005–12036, doi:10.3390/rs61212005.

CAPÍTULO 4. Comparison of post-fire dynamics in Brazilian savanna and tropical forest from remote sensing time series[3]

Níckolas Castro Santana[1], Osmar Abílio de Carvalho Júnior[1]

[1]Department of Geography, University of Brasília, Brasília, Brazil

Abstract

The monitoring of fire-related changes is essential to understand the vegetation dynamics in the medium and long term. The evaluation of the effects of fire recurrences on vegetation in the Amazon and Cerrado used MODIS time series of albedo, enhanced vegetation index (EVI), gross primary productivity (GPP), and surface temperature. The annual aggregated time series (AAT) method identified the slope trend of each pixel in the period 2001-2016 and its statistical significance. The temporal trends of EVI, GPP, and surface temperature were determined by the total fire recurrence, indicating that the vegetation cannot recover its original status in scenarios of high fire recurrence. Areas with degraded vegetation, together with high fire recurrence, may increase up to 0.15 Kelvin/Year at surface temperature and decrease up to -0.004 EVI/year in the vegetation index. Although savannas are more resistant to fire, the alteration of their structure and degradation leads to the higher intensity of fire effects. In the Amazon area, the protection of forests in conservation units and indigenous lands allowed the exclusion of fire in these sensitive areas, which resulted in positive vegetation index trends.

Keywords: Fire recurrence; Amazon; Cerrado; vegetation biophysics

Introduction

Fire is a natural agent present in tropical biomes, especially in savannas with intermediate primary productivity (Bowman *et al.* 2011). The regions with high primary productivity, such as tropical forests, present a low natural fire occurrence because of their high humidity, but the anthropic action aiming at agricultural production causes fires in the dry period (Cochrane 2003). Consequently, fire activity increased by human actions, mainly in the conversion and management of pasture and agriculture areas (Pivello 2011). Moreover, fire management in agriculture causes accidental fires that generally do not obey the same natural regime.

---

[3] Artigo submetido ao periódico *International Journal of Wildland Fire.*

Fires cause changes in surface albedo, nutrient cycling, energy exchanges between the surface and the atmosphere, ecological processes, and climate (Kasischke *et al.* 1995; Chambers *et al.* 2005; Wittkuhn *et al.* 2017; Archibald *et al.* 2018). The albedo change from the burning is due to the vegetation cover by the ash, which directly influences the surface energy balance. Fire may increase the surface albedo in forest and decrease in the savanna (Beringer *et al.* 2003; Dintwe *et al.* 2017). Fire intensifies the air and soil heat fluxes, increasing the surface temperature immediately after the fire. The temperature is directly correlated with the fire severity, biomass converted to ash, and exposed soil area (Veraverbeke *et al.* 2012).

Another important parameter of vegetation dynamic is gross primary productivity (GPP), one of the main components in the carbon biogeochemical cycle, since it represents carbon exchanges between terrestrial ecosystems and the atmosphere. Large-scale changes in GPP by burning have a direct impact on carbon flux and consequently on the planet's climate (Gao *et al.* 2013; Huang *et al.* 2013; Danelichen *et al.* 2015). Finally, the fires modify the structure, composition, distribution and diversity of terrestrial biomes (Bond *et al.* 2005; Pausas and Ribeiro 2017), which influence the regeneration rates and the phenological pattern.
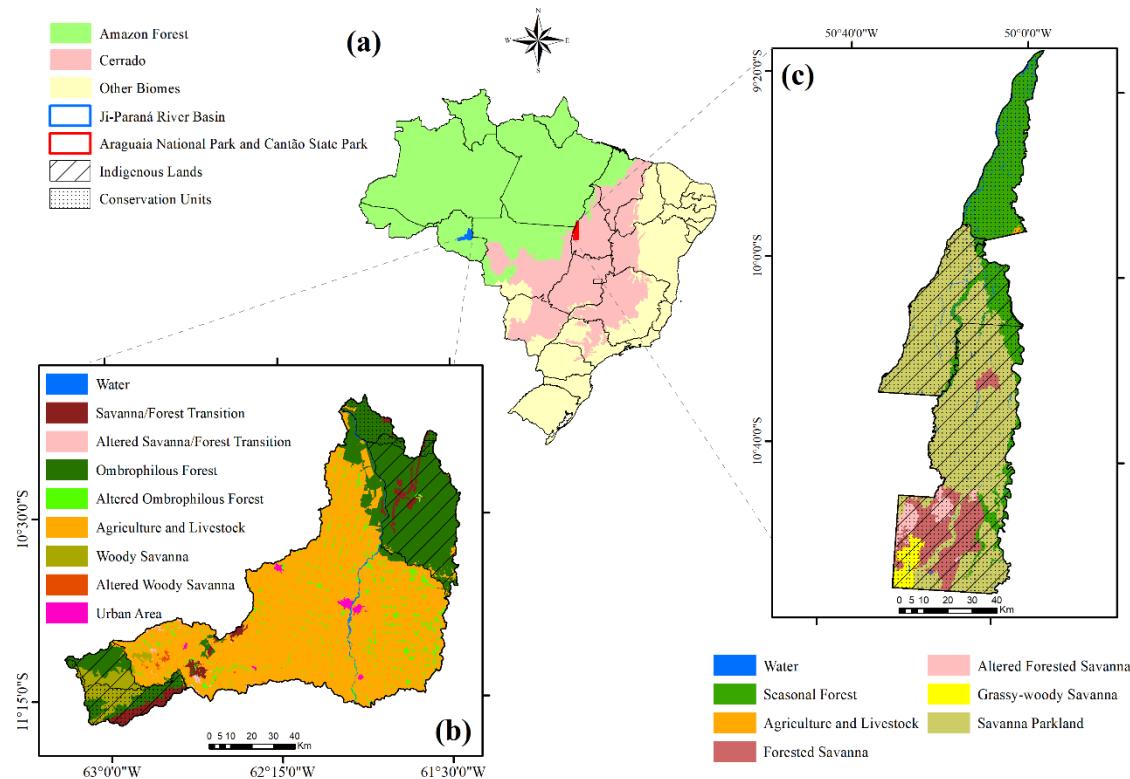
The fire effect studies on the environmental parameters have two approaches: (a) the quantification of fire influence on net productivity and radiation balance from measurements immediately after the occurrence of fire (Chambers *et al.* 2005)or by flux towers that provides a nearly continuous dataset over a long-term experiment (Beringer *et al.* 2003; Dintwe *et al.* 2017); and (b) quantification of biophysical changes from remote sensing time series (van Leeuwen 2008; Veraverbeke *et al.* 2012; Li *et al.* 2018). Despite the diversity of studies, there are few that sought to compare the mid-term fire influence between forest-savanna, such as in the Amazon and Cerrado, as well as the application of remote sensing products as alternatives to areas where no flux towers are available.

This study intended to investigate the post-fire impact in Amazon and Cerrado environments from remote sensing time series for the parameters of albedo, enhanced vegetation index (EVI), GPP, and surface temperature. We used the time series trend analysis in several products derived from MODIS sensor (Moderate Resolution Imaging Spectroradiometer) during the period 2001-2016 in the Amazon (Ji-Paraná river basin) and Cerrado (Cantão State Park and Araguaia National Park).

Materials and Methods

Study Area

The research comprises two areas located in the Cerrado and Amazonian biomes, which allowed to compare the fire effect in distinct environments (**Figure 4.1a**). These regions are subject to the high incidence of fire, despite the climatic and vegetation differences (Cardozo *et al.* 2014). The land cover and land use data were from the Project for the Conservation and Sustainable Use of Brazilian Biological Diversity (PROBIO) (MMA 2007) and the Project for the Satellite-Based Monitoring of Brazilian Biome Deforestation (PMDBBS) (MMA and IBAMA 2008).

Figure 4.1. Location of the study areas and the land use/cover in Brazil (a), Ji-Paraná River Basin (JPRB) (b); and Araguaia National Park and Cantão State Park (ANP-CSP) (c).

The study area in the Amazonian biome is the Ji-Paraná River Basin (JPRB) located in the State of Rondônia, covering an area of 12,200 km². The area has the following classes: (a) savanna/forest transition; (b) altered savanna/forest transition; (c) ombrophilous forest (mainly in conservation units and indigenous lands); (d) altered ombrophilous forest; (e) anthropic use (agriculture and livestock); (f) woody savanna;

and (g) altered woody savanna (**Figure 4.1b**). The choice for the area of JPRB was due to the representativeness of different land uses and fire regimes. In the Amazon, fire generally occurs in pasture-dominated areas, such as in the JPRB.

The study area of the Cerrado biome includes the Araguaia National Park (ANP) (5,555.00 km²) and the Cantão State Park (CSP) (1,004.00 km²), belonging to the State of Tocantins. The ANP-CSP area has the following classes: (a) seasonal forest; (b) agriculture and livestock; (c) forested savanna; (d) altered forested savanna; (e) grassy-woody savanna; and (f) savanna parkland (**Figure 4.1c**). Fire in the Cerrado occurs primarily in areas where there is a greater proportion of preserved vegetation, so the selected area of the ANP-CSP expresses the general fire pattern in the biome.

The two areas have a common pattern with overlapping of fully protected conservation unit (severe land use restrictions) and indigenous lands, generating a multi-managed environment. In this research, we divided the natural vegetation into preserved vegetation and altered vegetation due to high fragmentation or selective cutting.

MODIS Dataset

The MODIS sensor onboard of the Terra and Aqua satellites, developed by the National Aeronautics and Space Administration (NASA), aims to continuously monitor the Earth's surface, with 36 spectral bands ranging from 0.4 μm to 14.4 μm in three different spatial resolutions (250, 500 and 1000 meters) (Justice *et al.* 2002). The products used from the Terra satellite were: (a) MOD13Q1, which provides the Enhanced Vegetation Index (EVI) at 250m spatial resolution and 16-day composite; (b) MOD09Q1, surface reflectance (bands 1 and 2) at 250m spatial resolution and in 8-day composite; (c) MOD09A1, surface reflectance (bands 1 to 7) at 500m spatial resolution and 8-day composite; (d) MOD11A2, surface temperature at 1km spatial resolution and 8-day composite; and (e) MOD17A2, GPP at 500m spatial resolution and 8 day composite. Data acquisition used the NASA website (https://search.earthdata.nasa.gov/). The definition of the surface albedo (α_s) used the MOD09Q1 and MOD09A1 products according to the equation (Liang 2001):

$$\alpha_s = 0{,}160_{p1} + 0{,}291_{p2} + 0{,}243_{p3} + 0{,}116_{p4} + 0{,}112_{p5} + 0{,}081_{p7} - 0{,}0015$$

Where p_i is the surface reflectance of the MODIS bands (1-7), except band 6.

The MODIS data are from the 2001-2016 period, with the elimination of poor-quality pixels. In the data compatibilization, we resampled the products with 500 and

1,000 m spatial resolution to 250 m by the nearest neighbor interpolation method and the 8-day composite to 16 days from the mean value.

The Saviztky-Golay filter (Savitzky and Golay 1964) was applied in the time series to reduce noise. This filter has been widely used in time series analysis of remote sensing and is based on local polynomial regression for noise removal, allowing the retention of the waveform and the natural characteristics of the vegetation, both seasonal and persistent changes (Chen *et al.* 2004; Schafer 2011; Carvalho Júnior *et al.* 2015).

Burned Area

The delimitation of the burned areas used a semi-automatic methodology, by applying threshold values in Near Infrared time series (band 2) normalized by the mean or by the Z-Score (Carvalho Júnior *et al.* 2015; Santana *et al.* 2018). The near infrared band presents greater separability between burned and unburned areas (Maier 2010; Santana *et al.* 2018). The best-threshold definition used five Landsat scenes (TM, ETM+ and OLI) for both the Amazon and Cerrado areas (**Table 4.1**). Data validation used visual inspection in each year of the series (2001-2016) and Landsat images.

Table 4.1. Landsat database used to define the best threshold for mapping of burned areas.

Amazon Forest			Cerrado		
Scenes	Image date	Sensor	Scenes	Image date	Sensor
223-67 223-68	01/10/2002	ETM+	231-67 231-68	20/09/2001	ETM+
	01/10/2005	TM		18/09/2003	TM
	21/09/2007	TM		13/09/2007	TM
	10/10/2014	OLI		21/09/2010	TM
	27/09/2015	OLI		16/09/2014	OLI

Temporal Trend
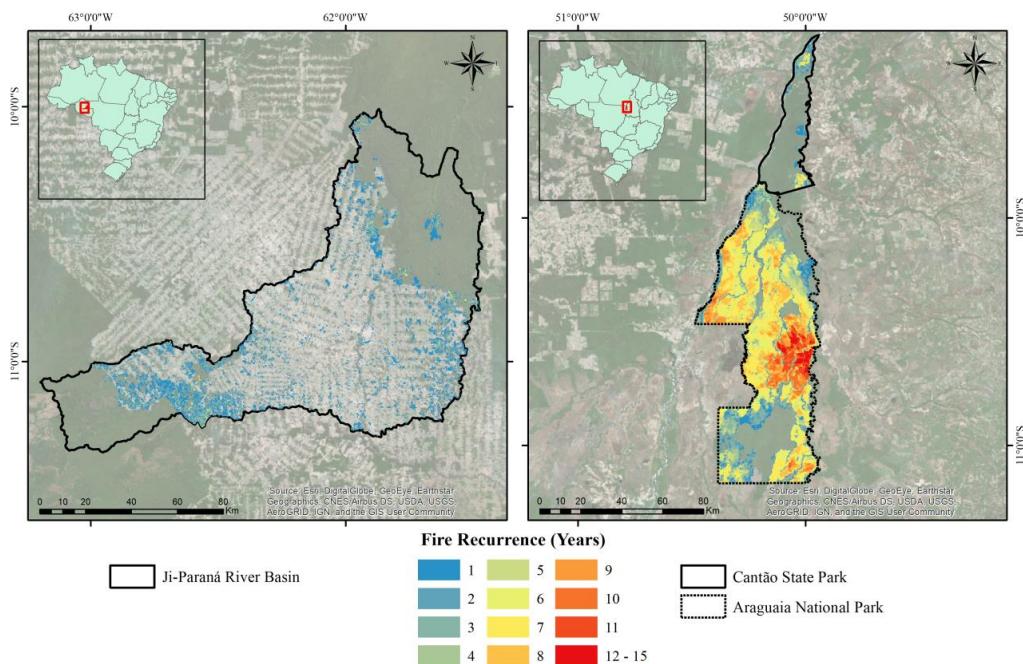
Trend change detection in period 2001-2016 for the different parameters used the method of annual aggregated time series (AAT) (Forkel *et al.* 2013), available in the Land Surface Phenology and Trend Analysis package (http://greenbrown.r-forge.r-project.org/). The ATT method estimates the trend of each pixel and the predictable significance of each temporal segment using the Mann-Kendall test (Mann 1945; Kendall 1955). The annual average is the basis for detecting structural changes or significant breakpoints in a regression analysis, which requires data with at least 4 years (Bai and Perron 2003). The result per pixel indicates the annual magnitude of increase or decrease and if that value is significant. The correlation of trends with fire recurrence and soil use

class allowed to evaluate the effect of fire in the determination of the temporal pattern of vegetation.

Results

Fire Recurrence

In the JPRB region, the area burned at least once, in the period 2001-2016, was of 1400 km² (12%) (**Figure 4.2; Table 4.2**). Most of the fires occurred in areas converted to pasture, while forest areas presented few influences of fire. The ANP-CSP area burned about 4400 km ² (68%) between 2001 and 2016, concentrating on the savanna phytophysiognomies, and just as in the JPRB, forest areas were less affected by fire.

Figure 4.2. Fire Recurrence in JPRB and ANP-CSP, in the period 2001-2016.

Table 4.2. Area burned (Km²) by fire recurrence class in the 2001-2016 period.

Study Area	Fire Recurrence (Km²/Years)					
	0	1 - 3	4 - 6	7 - 9	10 - 12	>12
JPRB	10774.4 (88%)	1373.9 (11%)	47.6 (0,4%)	4.2 (0%)	0.5 (0%)	0.0 (0%)
ANP-CSP	2126.8 (32%)	877.4 (13%)	1551.0 (23%)	1651.9 (25%)	337.1 (5%)	14.0 (0.2%)

The spatial patterns of fire were distinct in the two biomes. The JPRB region has high vegetation fragmentation, consequently the burn scars are small and with low connectivity. Furthermore, JPRB has a low fire recurrence, where most of the burned

areas (11% of the total area) presented between one and three fire events in the analyzed time series (**Table 4.2**).

The ANP-CSP region, with high connectivity of native vegetation, had an area burned more significant than the JPRB region. The fire recurrence was high, containing in most of the area burned (25% of the total area) from seven to nine fire events in the period, concentrated in savanna vegetation.
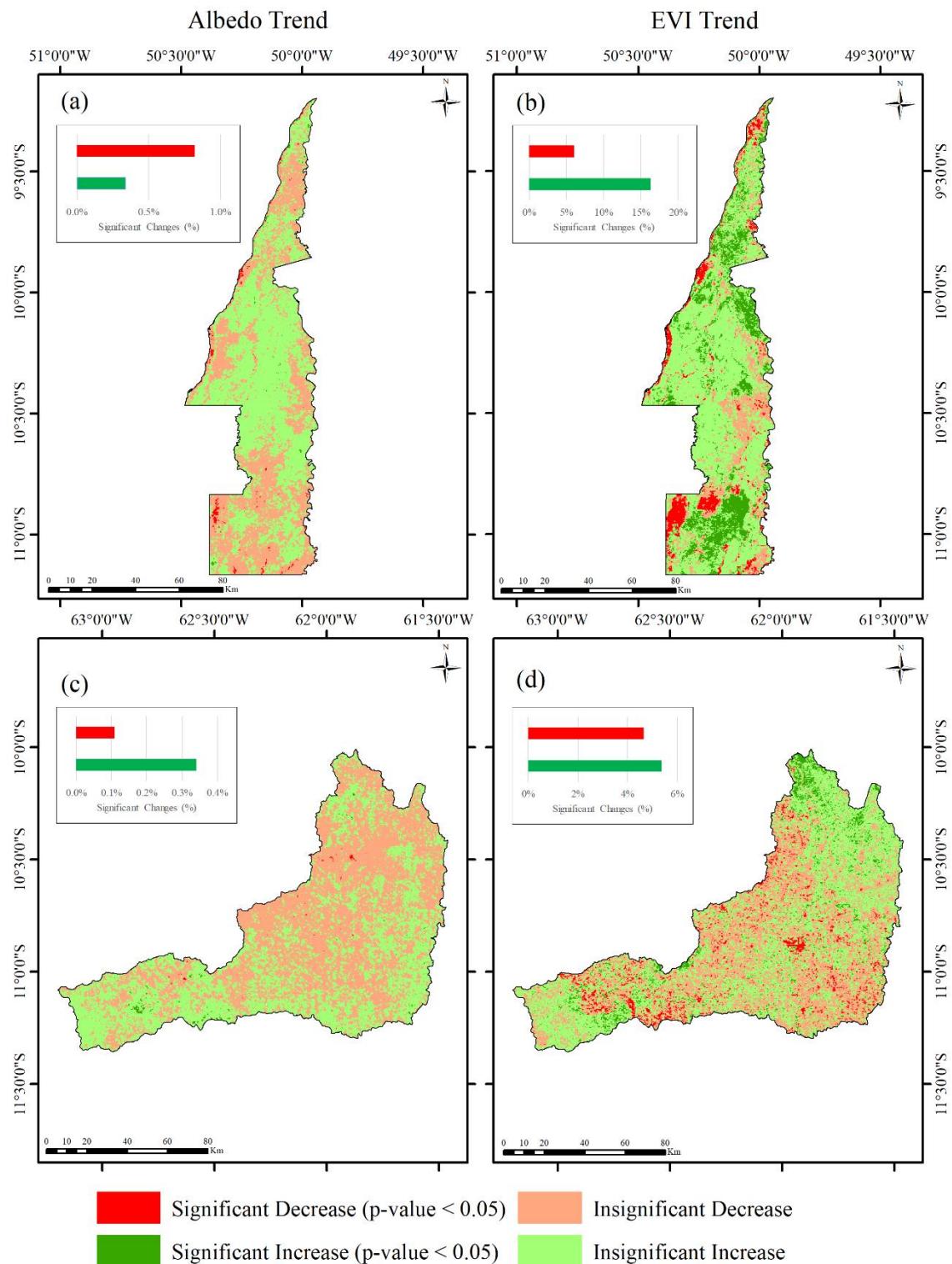
Vegetation dynamics

The vegetation trend analysis indicated different spatial patterns in the variables of albedo, EVI, GPP, and surface temperature (**Figure4.3 and 4.4**). Positive inclinations indicate the increase in the value of variables, while negative indicate the decline. The alterations of the albedo and GPP presented low spatial representativeness, whereas the alterations of the EVI and of the superficial temperature were more representative in the analyzed period.
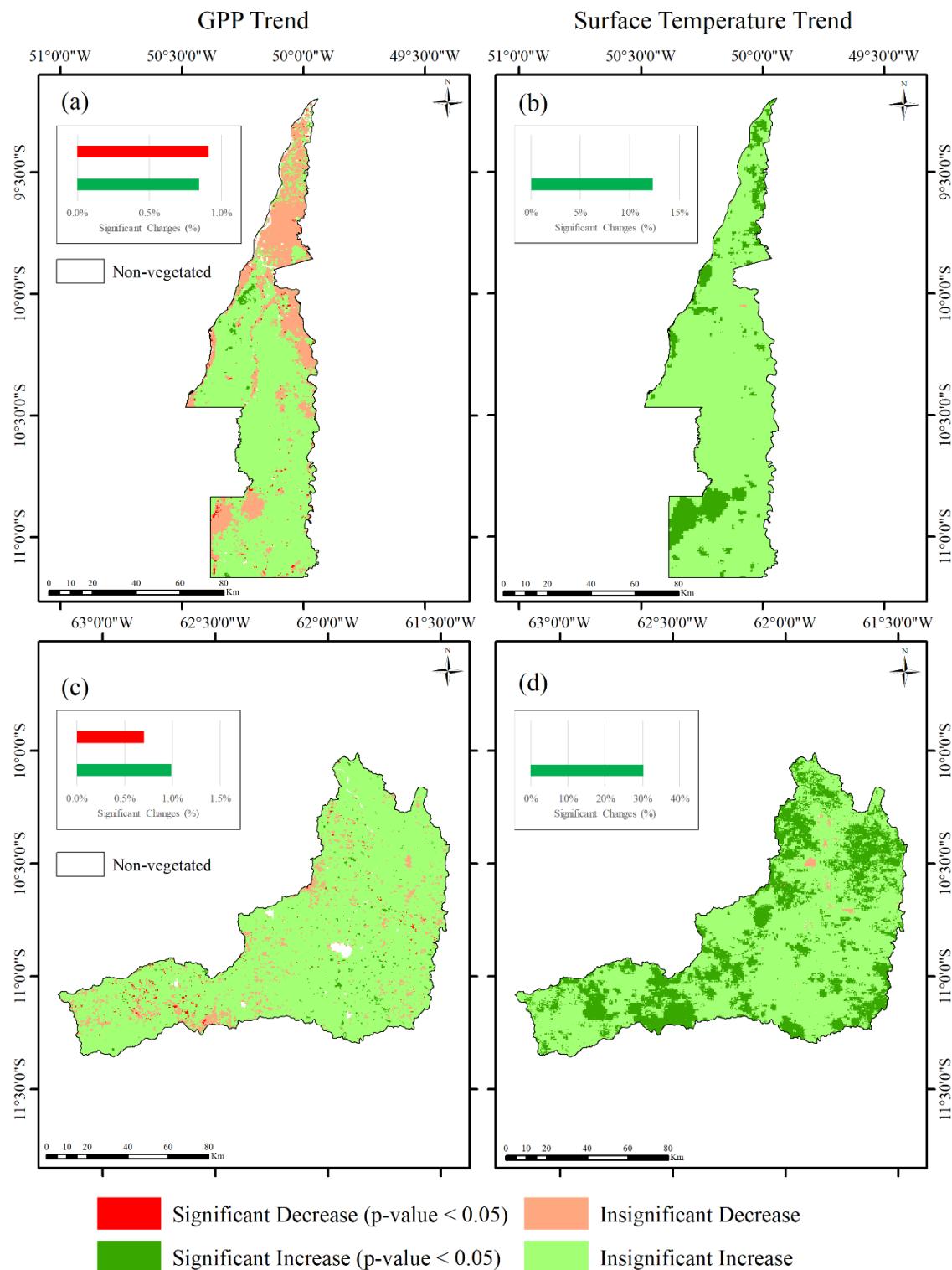
The albedo was the variable with the lowest significant statistical change (p-value <0.05) in the period for both areas: Amazon (<0.5% of the area with significant changes) and Cerrado (<1.2% of the surface with significant changes) (**Figure4.3a, c**). The highest significant increase of albedo was in the JPRB area, while the ANP-CSP area had the largest significant decrease.

Several points showed significant EVI trends (**Figure4.3b e d**). In the JPRB basin, significant negative EVI trends localized in the region with greater deforestation and vegetation fragmentation, while positive trends occurred in conservation units and indigenous lands with little altered vegetation. In the ANP-CSP area, significant negative EVI trends focused on areas with intense vegetation degradation, as well as mobile river banks. In contrast, the positive EVI trends are mainly located in forests.

In both study areas, GPP showed small change in the time series with less than 2% of the total area (**Figure4.4a, c**). Surface temperature was the most significant variable in the JPRB area (> 30% of the area with significant positive changes). In contrast, the ANP-CSP area had 10% of the total area with significant positive changes (**Figure4.4b, d**). The surface temperature variable did not present significant negative changes.

Figure 4.3. Spatial distribution of the trend per pixel, in the period 2001-2016, of the Albedo in the JPRB (a) and ANP-CSP (c), and the Enhanced Vegetation Index in the JPRB (b) and the ANP-CSP (d).

Figure 4.4. Spatial distribution of the trend per pixel, in the period 2001-2016, of the gross primary productivity in the JPRB (a) and ANP-CSP (c), and the surface temperature in the JPRB (b) and the ANP-CSP (d).

Biophysical changes and recurrence of fire
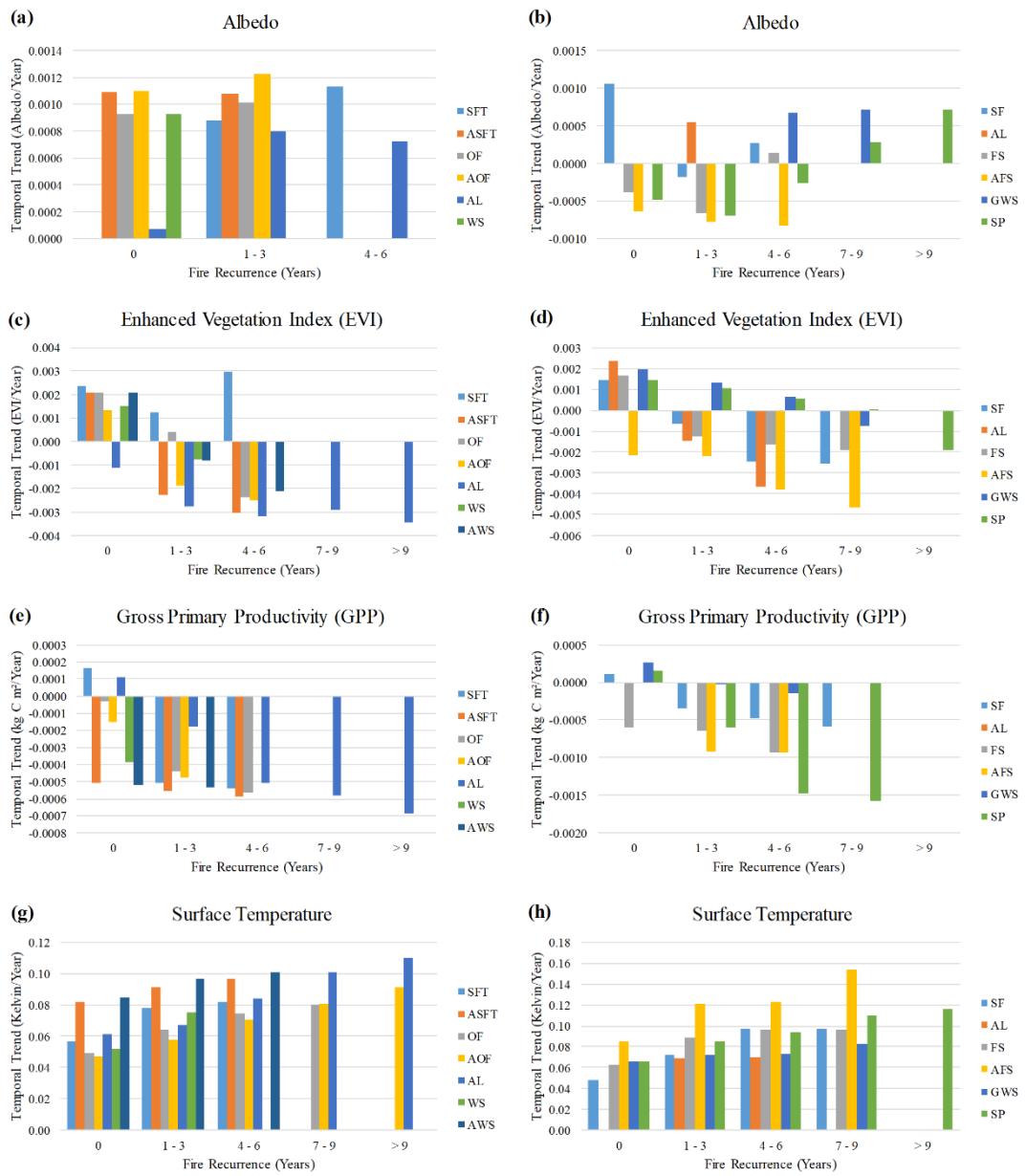
Figure 4.5 shows the variation of biophysical variables with fire recurrence. In the study areas, the albedo showed a low percentage of changes and the locals with significant changes did not have similar fire recurrence behaviors (**Figure 4.5a, b**). In the JPRB area, the savanna/forest transition and altered ombrophilous forest showed an integrated increased of albedo and fire recurrence. On the contrary, wooded savanna and altered forested savanna in the ANP-CSP areas presented a decrease of the albedo with increased fire recurrence.

In most of the phytophysiognomies analyzed, pixels with significant changes in EVI and GPP showed marked reductions in the trend with increased fire recurrence (**Figure4.5c, d, e, f**). In the JPRB area, the EVI trend was lower in the altered savanna/ forest transition and pasture (-0.003 EVI/ year), while the trend in the ANP-CSP area was lower in the altered woody savanna (-0.004 EVI/ year). The GPP in the JPRB area has change pattern like EVI with a lower tendency for the pasture (-0.0007 kg C m²/ year) and altered savanna/forest transition (-0.0005 kg C m²/ year). In the ANP-CSP area, GPP changes intensified with the highest fire recurrence in the savanna parkland areas (-0.0015 kg C m²/ year).

The increase in fire recurrence showed a direct effect on the significant positive trend of surface temperature in all types of land cover in the two study areas (**Figure 4.5g, h**). The most significant increases were in pasture areas of the JPRB area (+ 0.1 Kelvin/ year) and altered vegetation of both areas, especially in the altered woody savanna of the ANP-CSP area (+ 0.14 Kelvin/ year).

Discussion

Spatial analysis of fire recurrence shows a distinct effect considering land use/land cover and biophysical variables. The comparison between the area of study in the Amazon (not adapted to fire) and the study area in the Cerrado (adapted to fire events of low recurrence) showed that both vegetations are highly sensitive to fire events with high recurrence despite their different adaptations (Chuvieco *et al.* 2014). The main changes occurred in the altered vegetation of the Cerrado, which has a lower percentage of protected areas than the Amazon (Klink and Machado 2005). In the case of the Amazonian biome, the protected areas in the JPRB were essential for the maintenance of biophysical parameters. Especially the indigenous lands present a low incidence of fires, allowing greater preservation of vegetation (Nelson and Chomitz 2011).

Figure 4.5. Mean temporal trend by type of land use and fire recurrence: of the albedo in the JPRB (a) and ANP-CSP (b); EVI in JPRB (c) and ANP-CSP (d); GPP in JPRB (e) and ANP-CSP (f); and surface temperature in JPRB (g) and ANP-CSP (h). The classes of land use established in the JPRB area were: Savanna/Forest Transition (SFT), Altered Savanna/Forest Transition (ASFT), Ombrophilous Forest (OF), Altered Ombrophilous Forest (AOF), Agriculture and Livestock (AL), Woody Savanna (WS) and Altered Woody Savanna (AWS); and in the ANP-CSP area were: Seasonal Forest (SF), Agriculture and Livestock (AL), Forested Savanna (FS), Altered Forested Savanna (AFS), Grassy-woody Savanna (GWS) and Savanna Parkland (SP).

Land cover governs changes in the post-fire albedo, where forest areas can increase the albedo, and grass and savanna areas may decrease due to different rates of

vegetation regeneration (Dintwe *et al.* 2017). However, post-fire albedo changes do not remain long-term on the surface because of ash removal and vegetation recovery (Tsuyuzaki *et al.* 2009; Veraverbeke *et al.* 2012). In the altered vegetation of the studied areas, the albedo changes acquire a medium-term evolution with the intensification of the fire recurrence.

Several studies analyzed the fire action through time series of vegetation indexes (van Leeuwen 2008; Veraverbeke *et al.* 2012; Ireland and Petropoulos 2015). In this research, the EVI index allowed to quantify vegetation changes and to correlate with fire recurrence. In both study areas, EVI had an increase in protected forest areas and a decrease in altered vegetation. The recurrence of fire by anthropic action was the main cause for the decrease of the EVI during the 15 years, proving that even the savanna vegetation, which is adapted to fire, has fragility to the anthropic perturbation (Bowman *et al.* 2011).

The GPP is one of the main variables of the global carbon cycle, being correlated with climate change and fire activities (Zscheischler *et al.* 2014). The study areas had negative GPP trend in the vegetation with high fire recurrence. Although GPP generally has a high correlation with EVI (Li *et al.* 2018), the study areas did not have this behavior due to the predominance of non-significant GPP trend, indicating the rapid recovery of photosynthetic processes after fire (Huang *et al.* 2013), although its phenological structure represented by EVI has not been fully recovered.

The surface temperature changes were the most significant in the study areas, increasing the temperature with fire recurrence, especially in altered vegetation (pastures and degraded vegetation). The increase in surface temperature occurs immediately after the fire event, but over time these effects are attenuated (Veraverbeke *et al.* 2012). However, the results demonstrate that surface temperature changes were consistent throughout the time series, establishing a new pattern on surfaces highly affected by fire.

The results demonstrate the effectiveness of the AAT method to evaluate vegetation changes from temporal series with moderate spatial resolution images such as MODIS. However, for the identification of long-term changes, there is a need to longer time series, as well as higher spatial and spectral resolution images can provide more detailed information on these changes.

Conclusions

This research presents the behavior of four biophysical variables during 15 years in different scenarios of fire recurrence in the areas of the Ji-Paraná River Basin, in the Amazon, and in the Araguaia National Park and Cantão State Park, in the Cerrado. The results show that (a) post-fire vegetation changes are strictly correlated with the land cover type, conditioning the acceleration or delay of its recovery;(b) the increase in fire recurrence caused significant trend change with medium-term variability especially in EVI and surface temperature; and (c) the vegetation degradation (selective cutting and fragmentation practices) generated significant trends. The high fire recurrence influenced the temporal trend of vegetation in both study sites, which reinforces the need for an adequate national fire policy to maintain the vegetation structure.

References

Archibald S, Lehmann CER, Belcher CM, Bond WJ, Bradstock RA, Daniau AL, Dexter KG, Forrestel EJ, Greve M, He T, Higgins SI, Hoffmann WA, Lamont BB, McGlinn DJ, Moncrieff GR, Osborne CP, Pausas JG, Price O, Ripley BS, Rogers BM, Schwilk DW, Simon MF, Turetsky MR, Van Der Werf GR, Zanne AE (2018) Biological and geophysical feedbacks with fire in the Earth system. *Environmental Research Letters* **13**, 1–18. doi:10.1088/1748-9326/aa9ead.

Bai J, Perron P (2003) Computation and analysis of multiple structural change models. *Journal of Applied Econometrics* **18**, 1–22. doi:10.1002/jae.659.

Beringer J, Hutley LB, Tapper NJ, Coutts A, Kerley A, O'Grady AP (2003) Fire impacts on surface heat, moisture and carbon fluxes from a tropical savanna in northern Australia. *International Journal of Wildland Fire* **12**, 333–340. doi:10.1071/WF03023.

Bond WJ, Woodward F. I, Midgley GF (2005) The Global Distribtuion of Ecosystems in a world without Fire. *New Phytologist* **165**, 525–538. doi:10.1111/j.1469-8137.2004.01252.x.

Bowman DMJS, Balch J, Artaxo P, Bond WJ, Cochrane MA, D'Antonio CM, Defries R, Johnston FH, Keeley JE, Krawchuk MA, Kull CA, Mack M, Moritz MA, Pyne S, Roos CI, Scott AC, Sodhi NS, Swetnam TW (2011) The human dimension of fire regimes on Earth. *Journal of Biogeography* **38**, 2223–2236. doi:10.1111/j.1365-2699.2011.02595.x.

Cardozo S, Pereira G, Shimabukuro YE, Moraes EC (2014) Avaliação Das Áreas Queimadas No Estado De Rondônia. *Revista Brasileira de Cartografia* **v.66/3**, 705–716.

Carvalho Júnior OA de, Guimarães RF, Silva C, Gomes RAT (2015) Standardized Time-Series and Interannual Phenological Deviation: New Techniques for Burned-Area Detection Using Long-Term MODIS-NBR Dataset. *Remote Sensing* **7**, 6950–6985. doi:10.3390/rs70606950.

Chambers SD, Beringer J, Randerson JT, Chapin IS (2005) Fire effects on net radiation and energy partitioning: Contrasting responses of tundra and boreal forest

ecosystems. *Journal of Geophysical Research D: Atmospheres* **110**, 1–9. doi:10.1029/2004JD005299.

Chen J, Jönsson P, Tamura M, Gu Z, Matsushita B, Eklundh L (2004) A simple method for reconstructing a high-quality NDVI time-series data set based on the Savitzky-Golay filter. *Remote Sensing of Environment* **91**, 332–344. doi:10.1016/j.rse.2004.03.014.

Chuvieco E, Martínez S, Román MV, Hantson S, Pettinari ML (2014) Integration of ecological and socio-economic factors to assess global vulnerability to wildfire. *Global Ecology and Biogeography* **23**, 245–258. doi:10.1111/geb.12095.

Cochrane MA (2003) Fire science for rainforests. *Nature* **421**, 913–919. doi:10.1038/nature01437.

Danelichen VHM, Biudes MS, Velasque MCS, Machado NG, Gomes RSR, Vourlitis GL, Nogueira JS (2015) Estimating of gross primary production in an Amazon-Cerrado transitional forest using MODIS and Landsat imagery. *Anais da Academia Brasileira de Ciências* **87**, 1545–1564. doi:10.1590/0001-3765201520140457.

Dintwe K, Okin GS, Xue Y (2017) Fire-induced albedo change and surface radiative forcing in sub-Saharan Africa savanna ecosystems: Implications for the energy balance. *Journal of Geophysical Research* **122**, 6186–6201. doi:10.1002/2016JD026318.

Forkel M, Carvalhais N, Verbesselt J, Mahecha MD, Neigh CSR, Reichstein M (2013) Trend Change detection in NDVI time series: Effects of inter-annual variability and methodology. *Remote Sensing* **5**, 2113–2144. doi:10.3390/rs5052113.

Gao Y, Zhou X, Wang Q, Wang C, Zhan Z, Chen L, Yan J, Qu R (2013) Vegetation net primary productivity and its response to climate change during 2001-2008 in the Tibetan Plateau. *Science of the Total Environment* **444**, 356–362. doi:10.1016/j.scitotenv.2012.12.014.

Huang S, Liu H, Dahal D, Jin S, Welp LR, Liu J, Liu S (2013) Modeling spatially explicit fire impact on gross primary production in interior Alaska using satellite images coupled with eddy covariance. *Remote Sensing of Environment* **135**, 178–188. doi:10.1016/j.rse.2013.04.003.

Ireland G, Petropoulos GP (2015) Exploring the relationships between post-fire vegetation regeneration dynamics, topography and burn severity: A case study from the Montane Cordillera Ecozones of Western Canada. *Applied Geography* **56**, 232–248. doi:10.1016/j.apgeog.2014.11.016.

Justice CO, Townshend JRG, Vermote EF, Masuoka E, Wolfe RE, Saleous N, Roy DP, Morisette JT (2002) An overview of MODIS Land data processing and product status. *Remote Sensing of Environment* **83**, 3–15. doi:10.1016/S0034-4257(02)00084-6.

Kasischke ES, Christensen NL, Stocks BJ (1995) Fire, Global Warming, and the Carbon Balance of Boreal Forests. *Ecological Applications* **5**, 437–451. doi:10.2307/1942034.

Kendall MG (1955) 'Rank correlation methods, 2nd ed.' (Hafner Publishing Co.: Oxford, England)

Klink CA, Machado RB (2005) Conservation of the Brazilian Cerrado. *Conservation Biology* **19**, 707–713. doi:10.1111/j.1523-1739.2005.00702.x.

van Leeuwen WJD (2008) Monitoring the Effects of Forest Restoration Treatments on Post-Fire Vegetation Recovery with MODIS Multitemporal Data. *Sensors* **8**, 2017–2042. doi:10.3390/s8032017.

Li X, Zhang H, Yang G, Ding Y, Zhao J (2018) Post-Fire Vegetation Succession and Surface Energy Fluxes Derived from Remote Sensing. *Remote Sensing* **10**, 1000–

1019. doi:10.3390/rs10071000.

Liang S (2001) Narrowband to broadband conversions of land surface albedo I Algorithms. *Remote Sensing of Environment* **76**, 213–238. doi:10.1016/S0034-4257(00)00205-4.

Maier SW (2010) Changes in surface reflectance from wildfires on the Australian continent measured by MODIS. *International Journal of Remote Sensing* **31**, 3161–3176. doi:10.1080/01431160903154408.

Mann HB (1945) Nonparametric Tests Against Trend. *Econometrica* **13**, 245–259. doi:10.2307/1907187.

Ministério do Meio Ambiente (MMA) (2007) Mapeamento da Cobertura Vegetal do Bioma Cerrado, Edital Probio 02/ 2004, Projeto Executivo B.02.02.109, Relatório Final. Available at http://mapas.mma.gov.br/ [Verified 05 April 2019]

Ministério do Meio Ambiente (MMA), Instituto Brasileiro do Meio Ambiente e dos Recursos Naturais Renováveis (IBAMA) (2008) Projeto de Monitoramento do Desmatamento dos Biomas Brasileiros por Satélite - PMDBBS.Available at https://siscom.ibama.gov.br/monitora_biomas/ [Verified 05 April 2019]

Nelson A, Chomitz KM (2011) Effectiveness of strict vs. multiple use protected areas in reducing tropical forest fires: A global analysis using matching methods. *PLoS ONE* **6**, 1–14. doi:10.1371/journal.pone.0022722.

Pausas JG, Ribeiro E (2017) Fire and plant diversity at the global scale. *Global Ecology and Biogeography* **26**, 889–897. doi:10.1111/geb.12596.

Pivello VR (2011) The use of fire in the cerrado and Amazonian rainforests of Brazil: Past and present. *Fire Ecology***7**, 24–39. doi:10.4996/fireecology.0701024.

Santana NC, de Carvalho Júnior OA, Gomes RAT, Guimarães RF (2018) Burned-Area Detection in Amazonian Environments Using Standardized Time Series Per Pixel in MODIS Data. *Remote Sensing* **10**, 1904–1931. doi:10.3390/rs10121904.

Savitzky A, Golay MJE (1964) Smoothing and Differentiation of Data by Simplified Least Squares Procedures. *Analytical Chemistry* **36**, 1627–1639. doi:10.1021/ac60214a047.

Schafer RW (2011) What is a savitzky-golay filter? *IEEE Signal Processing Magazine* **28**, 111–117. doi:10.1109/MSP.2011.941097.

Tsuyuzaki S, Kushida K, Kodama Y (2009) Recovery of surface albedo and plant cover after wildfire in a Picea mariana forest in interior Alaska. *Climatic Change* **93**, 517–525. doi:10.1007/s10584-008-9505-y.

Veraverbeke S, Verstraeten WW, Lhermitte S, Van De Kerchove R, Goossens R (2012) Assessment of post-fire changes in land surface temperature and surface albedo, and their relation with fireburn severity using multitemporal MODIS imagery. *International Journal of Wildland Fire* **21**, 243–256. doi:10.1071/WF10075.

Wittkuhn RS, Lamont BB, He T (2017) Combustion temperatures and nutrient transfers when grasstrees burn. *Forest Ecology and Management* **399**, 179–187. doi:10.1016/j.foreco.2017.05.037.

Zscheischler J, Mahecha MD, Von Buttlar J, Harmeling S, Jung M, Rammig A, Randerson JT, Schölkopf B, Seneviratne SI, Tomelleri E, Zaehle S, Reichstein M (2014) A few extreme events dominate global interannual variability in gross primary production. *Environmental Research Letters* **9**, 1–13. doi:10.1088/1748-9326/9/3/035001.

CONCLUSÕES

O regime do fogo natural tem sido alterado no Brasil, com a implantação de novos usos do solo, especialmente nas áreas da Amazônia. O desmatamento e pecuária são os principais agentes de alteração do padrão do fogo. No Cerrado, a recorrência do fogo tem sido ampliada acima do limite de regeneração da vegetação, o tornando frágil a novos eventos de incêndios. Os dados derivados de sensores orbitais são algumas das principais fontes de informações sobre a superfície terrestre, incluindo-se a vegetação e o fogo. Nesse sentido, se faz importante a ampliação de metodologias de trabalho com essas fontes de dados para um melhor conhecimento da superfície terrestre.

Os resultados desta tese permitiram aprofundar o conhecimento sobre a aplicação de séries temporais de sensoriamento remoto no estudo da dinâmica do fogo no Brasil. O trabalho apresentou exemplos de metodologias que podem servir de subsídios para análises temporais com o objetivo de aperfeiçoar o monitoramento e gestão de áreas florestais.

Como base geral, o estudo se utilizou de produtos MODIS em três escalas espaço-temporais distintas: (a) no período de 2001 a 2015 em todo o território nacional, neste caso os produtos utilizados foram os de área queimada; (b) no período de 2000 a 2014 foram utilizadas séries temporais de reflectância, no visível e infravermelho, no município de Novo Progresso, Pará; e (c) no período de 2001 a 2016, com séries temporais de albedo, produtividade primária bruta, temperatura superficial e índice de vegetação, na bacia do rio Ji-paraná, em Rondônia, e no conjunto dos Parques Nacional do Araguaia e Estadual do Cantão, no Tocantins. Os produtos atuais de mapeamento de queimadas a nível global apresentaram limitações no Brasil, principalmente nos biomas de florestas tropicais e nos pampas, com altas taxas de erros de omissão. Apesar desta limitação, os produtos MODIS são a principal fonte de informação de áreas queimadas a nível regional e global. A utilização destes produtos permitiu identificar a distribuição espacial do fogo de acordo com as características da vegetação e do clima: (a) limitação do fogo nas áreas semiáridas, devido à baixa disponibilidade de combustíveis; (b) limitação do fogo nas áreas sem estiagem, devido à alta umidade; e (c) domínio do fogo nos biomas com moderada umidade, onde há alta produção de combustíveis nos períodos úmidos e períodos de seca propícios para a ocorrência do fogo.

A aplicação de diferentes metodologias para a identificação de áreas queimadas em produtos de sensoriamento remoto permitiu observar: (a) O canal do infravermelho

próximo com normalização pela média possuí alta capacidade de distinção entre áreas queimadas de outros alvos, tanto em fitofisionomias florestais, quanto savânicas; (b) A aplicação de índices espectrais como o BAIM melhora a separabilidade de áreas queimadas em relação às imagens originais, mas com a aplicação da normalização ou da diferença sazonal, a banda do Infravermelho Próximo é superior; (c) Técnicas de diferença sazonal apresentaram resultados inferiores em comparação com a normalização; (d) A aplicação de normalização em séries temporais auxilia na distinção de alvos com resposta espectral semelhante a queimada, mas com curvas temporais distintas como a água.

Séries temporais do sensor MODIS foram utilizadas para quantificar as alterações da vegetação exposta ao fogo, tanto na Amazônia, quanto no Cerrado. Em casos de incêndios de alta recorrência, aliados com a degradação antrópica, observou-se a fragilidade em ambos os biomas. As alterações na tendência temporal de EVI, produtividade primária bruta e temperatura superficial foram consistentes com o padrão de recorrência do fogo, sendo sua direção, positiva ou negativa, influenciada principalmente pelo nível de conservação da vegetação. As alterações na vegetação do Cerrado foram mais expressivas em comparação com a Amazônia, salientando a necessidade de novas práticas de manejo do fogo.

Quanto a revisita das questões de pesquisa pode-se destacar:

1. Qual a aplicabilidade de modelos globais de mapeamento de áreas queimadas nos diferentes biomas brasileiros?

Os produtos globais de mapeamento de áreas queimadas apresentam acurácia distinta em cada bioma brasileiro. Em comum todos apresentaram altas taxas de erros de omissão, relacionadas principalmente com a baixa resolução espacial do sensor, de 250 metros, assim como o tipo de metodologia empregada em cada algoritmo. O melhor produto, MCD64, apresentou cerca de 50% de áreas com erros de comissão, e 64% de áreas com erros de omissão, em média para todo o país.

2. Qual a potencialidade de produtos globais de área queimada para a descrição do regime do fogo no Brasil?

Apesar do produto MCD64 apresentar altas taxas de erros de omissão, foi possível destacar o padrão histórico de ocorrência do fogo no Brasil. Puderam-se observar as áreas de maior ocorrência do fogo, a sua freqüência, seu período de médio de retorno e as classes cobertura da terra mais afetadas. Apesar da baixa acurácia do

produto, ele ainda é útil em análises regionais e globais, especialmente pela longa série temporal de dados.

3. Qual é um método eficaz de mapeamento de áreas queimadas em séries temporais que suporte a detecção de cicatrizes nas regiões tropicais?

    Para responder a esta pergunta foram avaliados diversos métodos e índices espectrais para mapeamento de queimadas. Apesar do resultado positivo de alguns métodos indicados pela literatura, como a diferença sazonal ou o índice Normalized Burn Ratio (NBR), o método de normalização pela média, em séries temporais do infravermelho próximo, foi o mais adequado para a detecção de cicatrizes de queimadas na área de floresta tropical. Pôde-se avaliar a acurácia de cada método, e a sua validade estatística, além de explorar a sua aplicação para a descrição da dinâmica do fogo na região analisada.

4. Qual a potencialidade de dados orbitais na quantificação dos efeitos do fogo sobre parâmetros biofísicos da vegetação de savana e de floresta tropical?

    Os resultados permitiram quantificar a influência do fogo, sobre quatro parâmetros biofísicos da vegetação, atestando a potencialidade do uso de séries temporais orbitais. As séries orbitais permitiram avaliar a tendência temporal positiva ou negativa de cada variável, além da influência do fogo no aceleramento desse processo. Cabe-se salientar, que a série de 15 anos utilizada, é pequena para confirmar mudanças de longo-prazo, mas pode indicar o padrão a curto ou médio-prazo da vegetação. Há ainda a limitação natural destes dados quanto a quantificação dos diferentes parâmetros analisados, sendo especialmente recomendável para áreas onde dados de estações terrestres não estão disponíveis.

Os resultados deste trabalho indicam a possibilidade de novos estudos e aprofundamento destas temáticas. A baixa resolução espacial do sensor MODIS, principal base do trabalho, é um fator relevante em todas as análises, especialmente em regiões onde os fragmentos de queimadas são pequenos. Portanto novos sensores com maior resolução espacial e espectral podem retratar com maior confiabilidade o regime do fogo nestas regiões. Outros métodos de mapeamento de áreas queimadas não foram englobados neste estudo, como por exemplo, as técnicas de mistura e classificação espectral, sendo importante que trabalhos futuros comparem os métodos descritos neste trabalho para avaliar as suas dependências ou independências estatísticas. Por fim, cabe-se identificar a importância de novos métodos de mapeamento de áreas queimadas, e dos seus danos na vegetação, como base para modelos gerais de emissão de gases ou da

estrutura da vegetação, além de servirem como instrumentos de suporte para os gestores do meio ambiente.